SBI/IFUSP
BASE: 04
SYS Nº: 1080388

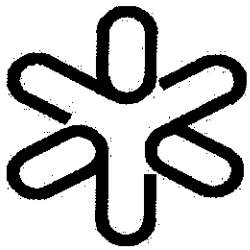

Instituto de Física
Universidade de São Paulo

Fundamental Symmetry Violation in Nuclei

Feshbach, H.; Kerman, A.K.

Center for Theoretical Physics, Laboratory for Nuclear science and Department of Physics, Massachusetts Institute of Technology, Cambridge, Massachusetts, U.S.A

Hussein, M.S.; Vorov, O.K.

Instituto de Física, Universidade de São Paulo, São Paulo, Brasil

Publicação IF - 1381/99

Fundamental symmetry violation in nuclei

H. Feshbach[1] *, M.S. Hussein[2] †, A.K. Kerman[1] *, and O.K. Vorov[2] ‡

[1] *Center for Theoretical Physics*

Laboratory for Nuclear Science and Department of Physics

Massachusetts Institute of Technology

Cambridge, MA 02139-4307

[2] *Instituto de Fisica,*

Universidade de Sao Paulo ,

Caixa Postal 66318, 5315-970

Sao Paulo, SP, Brasil

(July 1999)

*This work is supported in part by funds provided by the U.S. Department of Energy (D.O.E.) under contract #DE-FC02-94ER40818.

†Supported in part by the CNPq and FAPESP

‡Supported by FAPESP

Abstract

Fundamental symmetry violation effects in various nuclear phenomena are considered and their microscopic origins are discussed. We use the Unified Theory of Nuclear Reactions to investigate symmetry violation effects in neutron scattering at low energies. Both Parity nonconservation and Time-reversal symmetry breaking are considered. The observation of sign correlations in the longitudinal asymmetry of polarized neutron scattering from ^{232}Th at epithermal energies is analyzed. We provide quantitative explanation of the magnitude of PNC effects in nuclear compound states and give relation between observable Time reversal violation effects and the magnitude of microscopic subnuclear TRSB forces. The PNC effects are considered for neutron-rich nuclei where the halo phenomenon seems to enhance it by an order of magnitude when compared to stable nuclei.

Contents

I. INTRODUCTION

The electron-neutrino, i.e. the leptonic, manifestations of the standard model have been much studied. No deviation from theory has been found. The standard model also predicts a weak interaction between nucleons and more generally between hyperons and nucleons. It is the hadronic aspect of the standard model with which we shall be concerned in this paper.

The observation of parity non conserving process is the tool with which one probes the weak interaction between hadrons. Parity conservation has been directly studied in nucleon-nucleon scattering. It has been studied by the observation of the mixing of a small magnetic dipole component of the opposite parity. In an electromagnetic decay, say of the electric dipole variety, the recipient level will have a parity opposite to the decaying level. The small component can also be responsible for a decay. However its radiation will be that of a magnetic dipole so that the limited gamma ray will be a coherent mixture of electric and magnetic dipole radiation. This fact can be observed by determining the circular polarization of the emitted radiation. If it exists, parity is not conserved. This effect is a consequence of the interference between the electric and magnetic dipole components and is thus linear in the weak interaction strength. From the experiment one can obtain the magnitude of the matrix element of the weak interaction. At a pion Compton wavelength the ratio of the weak to strong nucleon-nucleon interaction is of the order of 10^{-7}. If the strong force has the magnitude of 10 MeV, the weak force has the magnitude of 1 eV. This is an extremely small force. Amplification is essential if it is to be brought within reach of observation [1].

Amplification is obtained if two levels of differing parity are approximately degenerate

for then the mixing of those two levels will be especially strong. Such near degeneracy can be found in several nuclei and as a consequence the ratio of weak to strong matrix elements can be raised from 10^{-7} to roughly (it varies with nuclei) 10^{-4}. This effect has been observed in a wide variety of nuclei.

The recently discovered symmetry breaking exhibited in the formation of compound nuclear levels by epithermal neutrons provides new insights into the nature of the weak interaction and the structure of the compound nucleus. When very slow neutrons bombard a heavy target nucleus a compound nucleus with excitation energy of about 6–7 MeV is formed. Generally a high density of resonances is seen. Because of the low neutron kinetic energy only s and p waves are involved and the compound nuclear levels which are excited are correspondingly constrained. We shall refer to these levels as s and p levels. They have opposite parity. Parity nonconservation occurs when, because of the weak interactions, the s and p levels mix. Such mixing is enhanced in the compound nucleus because of the close spacing of the s and p levels. An additional enhancement occurs if several levels belonging to the same doorway states are involved.

Similar remarks may be made about time reversal. There will be levels of differing time reversal properties, odd or even. Mixing these will lead to time reversal symmetry breaking. Needless to say the weak force stands on its own as an important vehicle with whose help several properties of the strongly interacting system can be studied.

The very close spacing of the s and p levels, together with the huge complexity of the compound nuclear wave function introduce an enhancement factor that would amplify the signature of parity or time reversal nonconservation. This makes the use of the compound nucleus to study fundamental symmetry violation a natural undertaking.

Further, owing to the complexity of the compound nuclear wave function, it is expected that the measured quantity, the longitudinal asymmetry at a given resonance, to be random in sign. The large value of the asymmetry and its randomness have been nicely verified in a number of nuclei. Only one exception, ^{232}Th, has presented a challenge. Here the randomness is not complete. Instead, the average value of the asymmetry was found to be large and positive. This has become known as the sign correlation problem. Several reviews on parity violation in the compound nucleus have been published [2-6]. A most recent review by Mitchell, Bowman and Weidenmuller [5] concentrates on the statistical features of the TRIPLE data.

In so far as parity nonconservation (PNC) is used to further test the compound nucleus model, and more importantly, to set measurement standards for the future investigation of time reversal symmetry breaking (TRSB) tests, it is important to have at hand a unified reaction theory which can address the statistical and nonstatistical aspects of symmetry violation. The purpose of this paper is to supply this theory.

Of course, besides PNC and TRSB, there is another discrete symmetry that is also broken in the nucleus, namely isospin. The force that is responsible for the breakdown in the EM one, several order of magnitude larger than the weak force which is our main interest. Though some of the reaction theory techniques used here are similar to the one developed in this review, we shall not dwell upon this issue in the following.

The paper is organized as follows: In Section II, a summary of the experimental results of the TRIPLE group is given. In Section III, a full development of the reaction theory needed to study symmetry violation is presented. Here, the hierarchy of complexities (optical potential, 2 particle-1 hole doorways, 3 particle-2 hole hallways, etc.) is exhibited in the

formulation. In Section IV the data on PNC in the compound nucleus are analyzed using the result of Section III. The sign correlation effect in ^{232}Th is traced to the 2p-1h doorway states which are taken to be responsible for the PNC. This is discussed in Section V. The rms value of weak matrix element exctracted from the data is also discussed in Section V. In Section VI the optical model description of PNC is developed and applied to the TRIPLE data. In Section VII the strength of the PNC matrix element is calculated for neutron-rich (exotic) nuclei, and compared with that of stable nuclei. In Section VIII, the TRSB is considered both in the isolated resonance and the overlapping resonances, statistical, cases. Finally, in Section IX, concluding remarks are made.

II. SUMMARY OF THE EXPERIMENTAL RESULTS FROM THE TRIPLE COLLABORATION

In this section we give a brief review of the experimental result of the TRIPLE collaboration [7-16]. The undertaking of the TRIPLE group followed the earlier discovery [17] at Dubna of the very large parity violation in the scattering of slow polarized neutrons from heavy target nuclei.

Measurement of the PNC longitudinal asymmetries were done for the following targets: $^{107+109}$Ag, ^{113}Cd, ^{115}In, ^{127}I, ^{232}Th and ^{238}U. For the epithermal energies considered here the dominant partial wave is $l = 0$ (s-wave). Several p-wave resonances are populated as well with much smaller cross section. It is the mixing of these $p - waves$ with nearby s-waves owing to PNC that is extracted from the longitudinal asymmetry

$$P_i = \frac{\sigma_i^{(+)} - \sigma_i^{(-)}}{\sigma_i^{(+)} + \sigma_i^{(-)}} \quad , \tag{2.1}$$

where the index i refers to the p-wave resonance being probed and $\sigma^{+(-)}$ refers to the total p-wave cross-section with positive (negative) helicities. If one uses the usual sum-over-resonances form for the scattering amplitude and with the use of the optical theorem, one may write for P_i the following expression, assuming the p-resonance is mixed with one s-resonance

$$P_i = 2\frac{\langle i|V_{PNC}|j\rangle}{E_{s_j} - E_{p_i}}\sqrt{\frac{\Gamma_{s_i}}{\Gamma_{p_i}}} \quad \equiv \quad 2\frac{V_{ij}}{\Delta E_{ij}}\sqrt{\frac{\Gamma_{s_i}}{\Gamma_{p_i}}} \tag{2.2}$$

where Γ_{p_i} and Γ_{s_j} are the neutron decay amplitudes of $p - wave$ and $s - wave$ resonances respectively. Since the compound states $|i\rangle$ and $|j\rangle$ are very complicated, one expects the

matrix element $\langle i|V_{PNC}|j\rangle$ to involve a much reduced overlap and then a smaller value when compared to single particle matrix element. The reduction factor is roughly $\sqrt{D}$ where D is the average spacing between resonances [17],[18], see also [3] for review. On the other hand, the energy difference $E_{sj} - E_{p_i}$ becomes smaller as the excitation energy is increased and it goes as D. Writing $E_{s_j} - E_{p_{pi}} \simeq \Delta\ D$, and $V_{ij} \equiv \langle i|V_{PNC}|j\rangle \simeq \sqrt{D}\ (V_{PNC})$, where (V_{PNC}) designates average single particle value of the PNC matrix element, we find [17b]

$$P_i = 2\frac{1}{\sqrt{D}}\frac{(V_{PNC})}{\Delta}\sqrt{\frac{\Gamma_{s_j}}{\Gamma_{p_i}}} \quad . \tag{2.3}$$

Further, expressing Γ_{s_j} and Γ_{p_i} in terms of their respective reduced widths, $\Gamma_{s_j} = \overset{(o)}{\gamma}{}^2_{s_j}$, $\Gamma_{p_i} = \overset{\circ}{\gamma}{}^2_{p_j}\ (kR)^2$, where the factor $(kR)^2$ accounts for the effect of the $\ell = 1$ centrifugal barrier, we have finally

$$P_i = \left[\frac{1}{\sqrt{D}}\right]\left[\frac{1}{kR}\right]\left[2\frac{(V_{PNC})}{\Delta}\frac{\overset{\circ}{\gamma}_{s_j}}{\overset{\circ}{\gamma}_{p_i}}\right] \quad . \tag{2.4}$$

The first factor in Eq. (2.4) is the dynamical enhancement factor which can be as large as 10^2. The second factor is roughly 10^3 for epithermal neutrons scattered off heavy targets. The first factor grows with excitation energy while the second decreases. Further, there is an important oscillatory behavior of the reduced resonance amplitudes with the mass number. This is exemplified by the strength unction, $\left\langle\frac{\overset{\circ}{\gamma}{}^2}{D}\right\rangle$ as a function of A, shown in Fig. (1) for $s-$and $p-$ waves. The factor $\frac{\overset{\circ}{\gamma}_{s_j}}{\overset{\circ}{\gamma}_{pi}}$ in Eq. (2.4) is equal to $\sqrt{\frac{S_o}{S_1}}$ and accordingly, one would expect a good target choice would be such as to have a minimum in S_1 and a maximum in S_o ($A \sim 160$). However, a minimum in p-wave scattering implies a smaller cross-section thus making the measurement more difficult. Thus a more judicious choice has be made such that S_1 is large enough to make the p-wave cross-section easily measurable and yet maintaining $\sqrt{\frac{S_o}{S_1}}$ as large as possible.

Having dwelled upon the physical parameters in the longitudinal asymmetry which would help make the optimal choice of neutron energy and target mass we turn now to the experimental results, obtained using an experimental set up as shown in Fig.2 (for details see, e.g., Ref.[5]). A typical measurement of the helicity dependence of the neutron cross section at a p-resonance is shown in Fig.3 for ^{238}U.

The results for P_i are shown in Table I, for the targets indicated. It has been shown by the TRIPLE group [7-16] that the P_i data for all targets except ^{232}Th are consistent with an average value of P_i equal to zero, in accordance with the statistical nature of the compound nucleus. As an example we show in Fig.4 P_i vs. E_n for n+^{238}U for $0 < E_n < 3$eV.

The analyses were performed using a generalized form Eq. (2),

$$P_i = \sum_j \left(\frac{2}{E_j - E_i} \sqrt{\frac{\Gamma_j}{\Gamma_i}} \right) V_{i_j} \equiv \sum_j A_{i_j} V_{i_j} \quad . \tag{2.5}$$

Thus since $\bar{V}_{i_j} = 0$, $\bar{P} = 0$. This is confirmed for $^{107+109}$Ag,^{113}Cd, ^{115}In, ^{127}I and ^{238}U. The rms value of V_{i_j}, defined by

$$M^2 \equiv \langle |V_{i_j}|^2 \rangle \quad , \tag{2.6}$$

was found to be $M \simeq 1meV$, which corresponds to a PNC spreading width $\Gamma^{\downarrow}_{PNC} = 2\pi \frac{M^2}{D}$ of the order of 1.35 $\times 10^{-7} eV$. Table II summarizes the results for several target.

The ^{232}Th case warrants special care. In Figure 5 we show the p-wave asymmetries for n+^{232}Th at $0 < E_n < 300$eV. Here the average value of P_i is large and positive, in the resonance region, $\bar{P}_i \cong 0.08$. The contribution of the background here is almost three orders of magnitude smaller [8], consistent with zero value for $\langle P_{nonres} \rangle$. Statistical analysis done in this case yielded value for the rms value of the PNC matrix element M, and the corresponding PNC spreading width $\Gamma^{\downarrow}_{PNC}$ which is of the same order of magnitude as in the

other cases that have been already mentioned. More recent data on this system indicated that $\langle P \rangle$ dips into negative values at $E_n \geq eV$ [19]. So far only one point was measured in this region. It would be of great importance to extend the measurement to higher energies to verify the average trend of $\bar{P}$.

In order to understand the origin of the non-zero value of $\langle P_i \rangle$ for Thorium, we shall apply in the following sections the hierarchy-of-complexity description of section III. We shall show that the origin of the non-statistical behavior in P_i can be traced to simple p-wave 2p-1h doorway states which are parity mixed with nearby s-wave 2p-1h doorways.

Further, we shall demonstrate that a more appropriate quantity to analize is the cross-section difference, $\Delta\sigma_i \equiv \sigma_i^{(+)} - \sigma_i^{(-)} \simeq 2\sigma_i P_i$. The reason being that the average $\langle \Delta\sigma_i \rangle$ can be directly compared to optical model calculation. Further, in cases where the σ's are small and difficult to measure, as is the case at higher neutron energies, one would be bound to be content with the analysis of $\Delta\sigma$.

To conclude, the experimental findings of the TRIPLE Collaboration can be summarized as follows

1. The longitudinal asymmetries, P_p, for p-wave resonance scattering of epithermal neutrons from several targets are large.

2. The average longitudinal asymmetry, $\langle P \rangle$, is roughly zero for all cases studied except in ^{232}Th where it is found to be positive and significant (~ 0.08).

3. The average longitudinal asymmetries of all cases studied in the off-resonance region are practically zero.

4. The PNC spreading width is found to be weakly dependent on the mass number of the compound nucleus involved ($\Gamma^{\downarrow} \sim A^{1/3}$) with average value of $\sim 10^{-7} eV$ [20].

III. SYMMETRY VIOLATION WITHIN REACTION THEORY

At very low energies one expects the population of widely spaced, isolated, resonances in the compound nucleus. To describe the scattering problem, we use the unified theory of nuclear reactions of Feshbach [21] together with the optical background representation (OBR) method developed by Kawai, Kerman and McVoy [22]. We also allow for the existence of a single doorway to test its influence. Further, we allow the Hamiltonian of the system to be a general one, containing both PNC and TRSB terms.

The many-body Schrdinger equation describing the n + Target system can be written as usual, within the Feshbach formalism:

$$(E - PHP)P\Psi = PHQQ\Psi$$
$$(E - QHQ)Q\Psi = PHPP\Psi, \tag{3.1}$$

where P projects onto the elastic channel, as well as the 2p-1h doorway state, and Q onto the compound states. We consider all the subspace Hamiltonians to contain a symmetry conserving part H_s, and symmetry violating part, H_v. The second equation in (3.1) can be formally solved for $Q\Psi$, and when the solution is inserted into Eq.(3.1), we obtain:

$$(E - PHP - PHQG_QQHP)P\Psi = 0$$
$$G_Q = \frac{1}{E - QHQ}. \tag{3.2}$$

We now perform the OBR on Eq.(3.2). We do this by writing:

$$G_Q = \bar{G}_Q + (G_Q - \bar{G}_Q) \tag{3.3}$$

where $\bar{G}_Q$ is the energy-averaged compound propagator which is given by

$$\bar{G}_Q = \frac{1}{E - QHQ + iI/2} \tag{3.4}$$

with I denoting the energy interval that contains many compound resonances but still smaller than the width of the doorway.

Equation (3.2) can be written as :

$$G_Q = \bar{G}_Q + \bar{G}_Q^{1/2}(iI/2)G_Q\bar{G}_Q^{1/2} \tag{3.5}$$

and thus we can write formally:

$$\begin{aligned}
&\left(E - PHP - PHQ\bar{G}_QQHP\right)P\Psi \\
&= PHQ\bar{G}_Q^{1/2}\left(\frac{iI}{2}\right)^{1/2}G_Q\left(\frac{iI}{2}\right)^{1/2}\bar{G}_Q^{1/2}QHP \quad P\Psi \\
&\equiv PVQG_QQVP \quad P\Psi; \\
&PVQ \equiv PHQ\bar{G}_Q^{1/2}\left(\frac{iI}{2}\right)^{1/2}
\end{aligned} \tag{3.6}$$

We then obtain the desired solution:

$$\begin{aligned}
P\Psi &= \overline{P\Psi} + G_{Opt}^{(+)}PVQ\frac{1}{E - QHQ - QVPG_{Opt}^{(+)}PVQ}QVP \quad P\Psi \\
&\equiv \overline{P\Psi} + P\Psi^{fl}
\end{aligned} \tag{3.7}$$

The energy average of the second term on the RHS of Eq. (3.7) is identically zero by construction. The solution $\overline{P\Psi}$ is the optical model wave function and $G_{Opt}^{(+)}$ is:

$$G_{Opt}^{(+)} = (E - PHP - PHQ\bar{G}_QQHP + i\varepsilon)^{-1} \tag{3.8}$$

The S-matrix element for the transition $a \to b$ is directly obtained from the asymptotic form of $P\Psi$:

$$S_{ab} = \bar{S}_{ab} - i\sum_q \frac{\tilde{\gamma}_{qa}\gamma_{qb}}{E - \varepsilon_q} \tag{3.9}$$

where $\bar{S}_{ab}$ is the optical + doorway S-matrix while the γ's are given by:

$$\gamma_{qa} = \sqrt{2\pi}\langle\tilde{q}|H_{QP}|\Psi_a^{(+)}\rangle \tag{3.10}$$

$$\tilde{\gamma}_{qa} = \sqrt{2\pi}\langle\Psi_a^{(-)}|H_{PQ}|q\rangle \tag{3.11}$$

In the above equations $|\Psi_a^{(+)}\rangle$ is the optical + doorway solution ($P\Psi^{(+)}$) and the complex energies, ε and vectors $|q\rangle$ and $\langle\tilde{q}|$ are the solutions of the equations:

$$(QHQ + QVPG_{Opt}^{(+)}PVQ)|q\rangle = \varepsilon_q|q\rangle \tag{3.12}$$

$$(QHQ^+ + (QVPG_{Opt}^{(+)}PVQ)^+)|\tilde{q}\rangle = \varepsilon_q^*|\tilde{q}\rangle \tag{3.13}$$

We set $\varepsilon_q = E_q - i\Gamma_q/2$.

Equation (3.9) is the starting point for discussing symmetry violation in nuclei. For PNC, $\tilde{\gamma} = \gamma$. However, γ depends on the helicity of the impinging neutron. Here one attaches to γ the helicity label, $\gamma^{(\pm)}$. For TRSB, $\tilde{\gamma} \neq \gamma$ and one has to define and calculate the observables sensitive to the difference $(\tilde{\gamma} - \gamma)$. This is left out to Section VIII.

In discussing Eq.(3.9) one has assumed that all the compound nucleus states can be treated on the same footing. However, if simple $2p - 1h$ doorway states are present and should be considered explicitly, the formalism above can be easily generalized. For this purpose a further splitting of the projection operator Q is required $Q = D + q$, where D is the doorway projectors. If P is assumed to be coupled to the genuine compound states projected off by q, only through D, one can obtain easily the necessary modifications in the physical observables [21,23]. Depending on convenience, one may take D to be part of a new P projector, namely $P' = P + D$ and q.

Assuming that the doorway state is contained in P', allows the γ_{qa}' s to have the following structure:

$$\gamma_{qa} = \gamma_{qD} C_{Da} \tag{3.14}$$

where the coefficients C_{Da} are random in sign and average to zero over many resonances. Further, the same doorway state would cause correlation among channels to which it is coupled to. A full account of the formalism with ideas of intermediate structure and doorways has been given long time ago [24] and has been reviewed recently by Feshbach [21]. Thus we shall not repeat this formalism here, but point out in the next section the qualitative effect the doorway state has on the scattering observables.

In the following, we discuss the application of the reaction theory to PNC and TRSB. For this purpose, it is useful to write the scattering amplitude that is obtained from S_{ab}, Eq.(3.3), for a given partial wave

$$f_{ab} = \bar{f}_{ab} - \frac{1}{2k} \sum_q \frac{\tilde{\gamma}_{qa}\gamma_{qb}}{E - E_q - i\Gamma_q/2}. \tag{3.15}$$

The total cross-section, $\sigma_T^{(a)}$ is directly obtained from f_{aa} through the optical theorem. For very low energy neutrons, $l = 0$ dominates, and we can write

$$\sigma_T^{(a)} = \frac{4\pi}{k} Im f_{aa} = \frac{4\pi}{k} Im \bar{f}_{aa} - \frac{\pi}{k^2} \sum_q \frac{\Gamma_q \tilde{\gamma}_{qa}\gamma_{qa}}{(E - E_q)^2 + \Gamma_q^2/4}. \tag{3.16}$$

IV. PARITY NONCONSERVATION (PNC) IN THE COMPOUND NUCLEUS

From the previous section, The cross-section for positive helicity, $\sigma^{(+)}$, and negative helicity, $\sigma^{(-)}$, for p-wave resonances can be generally written as

$$\sigma_p^{(\pm)} = \frac{4\pi}{k} Im f_p^{(\pm)}(0) \tag{4.1}$$

where $f^{(\pm)}$ is given by

$$f_p^{(\pm)} = \bar{f}_p^{(\pm)} - \frac{1}{2k} \frac{\gamma_p^{(\pm)} \gamma_p^{(\pm)} e^{2i\delta^{(\pm)}}}{E - E_p + i\Gamma_p/2} \tag{4.2}$$

Above, ξ is the factor $2l+1$ for p-waves, $\gamma_p^{(\pm)} = \gamma_p^S + \gamma_p^W$, $\Gamma_p = \left(\gamma_p^S\right)^2$ with $S(W)$ standing for the strong (weak) resonance amplitude. Since $\gamma_p^S \gg \gamma_p^W$, we have

$$f_p^{(\pm)} = \bar{f}_p^{(\pm)} - \frac{1}{2k} \frac{\left(\gamma_p^S\right)^2 \pm 2\gamma_p^W \gamma_p^S}{E - E_p + i\Gamma_p/2} \tag{4.3}$$

Thus, at a p-wave resonance, $E = E_p$, and taking γ_p^S, γ^W to be real,

$$\sigma_p^{(\pm)} \simeq \bar{\sigma}_p^{(\pm)} + \frac{4\pi}{k^2} \frac{\left(\Gamma_p^2 \pm 2\gamma_p^W \gamma_p^S\right)}{\Gamma_p}, \tag{4.4}$$

Eq.(4.4) is the basic formula used to analize PNC in the compound nucleus. If we ignore the contribution of $\left(\bar{\sigma}_p^{(+)} - \bar{\sigma}_p^{(-)}\right)$ [8] then we get

$$P_p = \frac{\sigma_p^{(+)} - \sigma_p^{(-)}}{\sigma_p^{(+)} + \sigma_p^{(-)}} = 2\frac{\gamma_p^W}{\gamma_p^S}. \tag{4.5}$$

for each resonance.

Using first order perturbation theory for the treatment of the PNC interaction, we use the following form for the p-state wave functicn

$$|p'_{1/2}\rangle = |p_{1/2}\rangle + \sum_s \frac{|s_{1/2}\rangle}{E_s - E_p} \langle |s_{1/2}| V_{PNC} |p_{1/2}\rangle \tag{4.6}$$

The state $|p'_{1/2}\rangle$ is what we called $|q\rangle$ in Eq.(1.15). With (4.6), we have for $\gamma^W_{p_{1/2}}$, the following (see Eq.(3.11) for the definition of $\tilde{\gamma}_{qa}$, which is equal to $\gamma_{q,a}$ when time reversal symmetry is not violated)

$$\gamma^W_{p_{1/2}} \equiv \sqrt{2\pi}\sum_s \langle\psi_q^{(-)}|H_{pq}|s_{1/2}\rangle \frac{1}{E_s - E_p}\langle s_{1/2}|V_{PNC}|p_{1/2}\rangle = \tag{4.7}$$

$$= \sum_s \gamma^s_{s_{1/2}} \frac{1}{E_s - E_p} V^{PNC}_{sp} \tag{4.8}$$

Notice that $|s_{1/2}\rangle$ and $|p_{1/2}\rangle$ are complicated compound nucleus states. We shall use the labels ν and μ to designate $|s_{1/2}\rangle$ and $|p_{1/2}\rangle$, respectively.

With (4.8), we obtain the well-known formula for P_μ

$$P_\mu = 2\sum_\nu \frac{1}{E_\nu - E_\mu}\frac{\gamma^S_\nu}{\gamma^S_\mu} V^{PNC}_{\mu,\nu} \tag{4.9}$$

or

$$P_\mu = 2\sum_\nu \frac{1}{D_{\mu,\nu}}\left(\frac{\Gamma^S_\nu}{\Gamma^S_\mu}\right)^{1/2} V^{PNC}_{\mu,\nu} \tag{4.10}$$

where $D_{\mu,\nu} \equiv E_\nu - E_\mu$ and Γ_q is the neutron width of level q.

The statistical theory of the compound nucleus tells us that the Γ_q's obey the Porter-Thomas distribution, the energy spacing of levels with mixed parities the Poisson distribution and the weak matrix element $V^{PNC}_{\mu,\nu}$ is Gaussian distributed with a zero mean value, $\langle V^{PNC}_{\mu,\nu}\rangle = 0$. Accordingly, $\langle P_\mu\rangle = 0$. The average value of P^2_μ can be related to the second moment of the $V^{PNC}_{\mu,\nu}$ distribution, $M^2 = \langle\left(V^{PNC}_{\mu,\nu}\right)^2\rangle$

$$\langle P^2_\mu\rangle = \langle\sum_\nu \frac{1}{D_{\mu,\nu}}\left(\frac{\Gamma_\nu}{\Gamma_\mu}\right)^{1/2}\frac{1}{D_{\mu',\nu}}\left(\frac{\Gamma_{\nu'}}{\Gamma_\mu}\right)^{1/2} V^{PNC}_{\mu\nu}V^{PNC}_{\mu'\nu}\rangle$$

$$= \langle\sum_\mu \frac{1}{D^2_{\mu,\nu}}\left(\frac{\Gamma_\nu}{\Gamma_\mu}\right)\rangle M^2$$

$$\equiv A^2_\mu M^2 \tag{4.11}$$

The quantity A_μ^2 can be calculated for each $p_{1/2}$ resonance. From the experimental data one determines the ensemble average of P_μ^2 and thus from Eq.(4.11), the important quantity M^2 is found. This quantity is directly related to the average weak spreading width of a given p-wave nuclear level

$$\Gamma^{\downarrow} = \langle \frac{2\pi |\langle \mu | V^{PNC} | \nu \rangle|^2}{D_\nu} \rangle \tag{4.12}$$

$$\Gamma^{\downarrow} \simeq 2\pi \frac{M^2}{\bar{D}} = 2\pi M^2 \rho \tag{4.13}$$

with ρ being the density of states of the $s_{1/2}$ levels. Since M goes roughly as $\frac{1}{\rho^{1/2}}$, we expect $\Gamma^{\downarrow}$ to be weakly dependent on excitation energy and as a consequence on the mass number of the nucleus [20a]. The results of the TRIPLE data [7-16] summarized in Section II seems to bear out all of the above properties of the PNC in the compound nucleus except for ^{232}Th, where $\langle P_\mu \rangle$ was found to be large and positive ($\langle P_\mu \rangle \sim 0.08 \pm 0.06$).

V. THE SIGN CORRELATION PROBLEM AND THE ROLE OF $2P$–$1H$ DOORWAY STATES

We discuss in what follows a possible cause of the large and positive value of $\langle P \rangle$ in ^{232}Th. Several theories have been proposed in the recent literature. These range from distant doorways [25], to parity doublets owing to octupole deformation [26,27]. A very good account of the theoretical literature can be found in Ref.[28]. In the following we describe the model of Ref.[29].

A very natural mechanism that could account for this sign correlation is to assume that the compound nuclear process occurs through a *single* dominantly p-wave *local* doorway which contains a small parity violation. For simplicity we start with this extreme hypothesis. Below we will consider the more general case including more doorways. This doorway is relatively simple but statistical combination of two particle-one hole (2p-1h) states in 233Th. In passing we note that it is the dominance of local doorways which may give rise to intermediate structure in the energy dependence of nuclear cross-sections and their statistical nature which gives rise to fluctuations in strength functions from nucleus to nucleus over and above the general optical model trend [23.24]. We stress that our local doorway states [29] are statistical in nature, in contrast to the collective 0^- doorway (giant monopole) states considered by Auerbach and others [25] as responsible for the sign correlation. We assume that parity violation occurs through the coupling of our p-wave doorway to an s-wave doorway, located nearby. Then:

$$\gamma_q = C_{qD}\gamma_{Dp}, \qquad \gamma_q^w = C_{qD}\gamma_{Ds}^w \tag{5.1}$$

where C_{qD} are taken to be random. Taking D to be in the vicinity of the compound

resonances in question, we obtain with the aid of perturbation theory:

$$P = 2\frac{\gamma^w_{Ds}}{\gamma_{Dp}} \tag{5.2}$$

which represents the average value of P, being independent of q. In Eq. (5.2) M^w is a characteristic weak matrix element between p- and s-doorways and ΔE is the corresponding characteristic energy distance between these doorway states given by, e.g.,

$$\Delta E \simeq |\left(E_{D2} - \frac{\Gamma_{D2}}{2}\right) - \left(E_{D1} - \frac{\Gamma_{D1}}{2}\right)| = \left[(E_{D2} - E_{D1})^2 + \frac{(\Gamma_{D1} + \Gamma_{D2})^2}{4}\right]^{1/2} \tag{5.3}$$

In order to estimate the size of (5.2) we take the smooth energy dependence out of the partial width amplitude in the usual fashion, i.e. we define $(1/kR)(\gamma^{(0)}/\gamma^{(0)}_{Dp})$, where $\gamma^{(0)}$ are the reduced widths. Thus:

$$\langle P \rangle = 2\frac{M^w}{\Delta E}\frac{\gamma^{(0)}_{Ds}}{\gamma^{(0)}_{Ds}}\frac{1}{kR} \tag{5.4}$$

which will have a definite sign for a given nucleus as seen in the data.

Properties of simple two particle-one hole states can be deduced from the exiton model, usually employed in pre-equilibrium studies [30]. The density of 2p-1h doorway states coupled to total angular momentum J at an excitation energy E^* in the compound nucleus is given by [31]

$$\rho_{2p-1h}(E^*, J) = \frac{g^3 E^{*2}}{4}\frac{(2J+1)exp[-(j+1/2)/3\sigma^2]}{(27\pi)^{1/2}\sigma^3} \tag{5.5}$$

where g is the average spacing of single particle levels, and σ is the spin cut-off parameter. For the deformed nucleus ^{233}Th, $g \simeq 10MeV^{-1}$, $\sigma \simeq 4.0$, and taking $E^* = 6MeV$, $J = 1/2$, we find $\rho_{2p-1h} \simeq 34MeV^{-1}$. Thus the average spacing, $D_{2p-1h} = (\rho_{2p-1h})^{-1} \simeq 30keV$. For a simple local doorway to dominate the 2p-1h doorways must not be overlapping. Thus we take $\Gamma \simeq D \simeq 30keV$. Then ΔE of Eq. (5.4) becomes roughly $\Delta E \simeq \sqrt{2}\Gamma_D \simeq 50keV$.

Taking for $M^w \simeq 1.0eV$ [1] and $kR \simeq 10^{-3}$ for $E_n \simeq 1eV$, we find that the data ($< P >= 0.08$) require:

$$|\frac{\gamma_{Ds}^{(0)}}{\gamma_{Dp}^{(0)}}| \simeq 4$$

which seems to contradict the fact that p-waves are resonant while s-waves are off resonance. This requires an enhancement which may come about if the particular statistical doorway involved in M^w couples strongly to s and less so to p or if the particular matrix element M^w is larger than average. This will be a statistical phenomenon associated with random properties of the local doorways.

The fluctuation part of P can also be analyzed within the local doorway model. If we consider nearby local doorways which for simplicity we collectively call D', then:

$$\gamma_q = C_{qD}\gamma_{Dp} + C_{qD'}\gamma_{D'p}, \qquad \gamma_q^w = C_{qD}\gamma_{Ds}^w + C_{qD'}\gamma_{D's}^w \tag{5.6}$$

where:

$$C_{qD} < C_{qD'} \tag{5.7}$$

on average. Then:

$$P \simeq \frac{\gamma_{Ds}^w}{\gamma_{Dp}} + \frac{C_{qD'}}{C_{qD}}\left[\frac{\gamma_{D's}^w}{\gamma_{Ds}^w} - \frac{\gamma_{D'p}}{\gamma_{Dp}}\right] \tag{5.8}$$

The variance of P is then given by

$$\nu \equiv \sqrt{\langle P^2\rangle - \langle P\rangle^2} \simeq \sqrt{\langle|\frac{C_{qD'}}{C_{qD}}|^2\rangle}|\frac{\gamma_{D's}^w}{\gamma_{Ds}^w} - \frac{\gamma_{D'p}}{\gamma_{Dp}}| \tag{5.9}$$

From Ref. [2] we find ν to be about unity. Because of (5.7), we find

$$|\frac{\gamma_{D's}^w}{\gamma_{Ds}^w} - \frac{\gamma_{D'p}}{\gamma_{Dp}}| > 1 \tag{5.10}$$

which is entirely reasonable. Thus the fine structure analysis furnishes us with constraining relations involving the weak and strong decay amplitudes of D and D'.

In the above discussion we presented qualitative considerations concerning the role of the simple $2p-1h$ doorway states in the sign correlations seen in the longitudinal asymmetry of epithermal neutrons scattered from ^{232}Th. We emphasised the statistical nature of these simple nuclear states. Further, a typical nucleus which does not show the sign correlation phenomenon, and belong to the same actinide family, ^{238}U, is used to elucidate better the phenomenon. An important physical quantity that enters in the analysis is the density of states of these doorways. In the following we present a detailed quantitative calculation of ρ_{2p-1h} in both ^{233}Th and ^{239}U, using a deformed mean field description of these nuclei. The details of the calculation can be found in a recent preprint [32]. The method used is the microscopic combinatorial approach of [33]. The numerical results for ρ_{2p-1h} are compared with analytical, equi-distant model, formula of Ericson [31].Effects of deformation on the level density has been first studied by Bjornholm, Bohr and Mottelson [34] within the Bethe-Fermi theory. Here we have extended their studies to the calculations of the density of states within the exiton model.

In Ref.[32], a microscopic combinatorial approach is used to calculate the level densities for a given number of excitons (# of excitons = # of particles + # of holes) using a deformed Saxon-Wood shell model. The details of this model are given in Ref.[33]. A part of the residual interaction, namely pairing, was taken into account by applying the BCS theory to each configuration. Both the spin and parity distributions were obtained and the effect of deformations is assessed. Quadrupole and octupole deformations are taken into account.

The result for ρ_{2p-1h} for ^{233}Th and ^{239}U are shown in Fig.(6) for the $j = 1/2$ positive parity levels. The density of negative parity $j = 1/2$ states is in principle the same (see, however, below). In the same figure the results obtained from the Ericson formula for ρ_{2p-1h} of Eq.(5.5) is also shown for comparison. It is clear from the figure that Eq.(5.5) underestimates ρ_{2p-1h} at $E^* \simeq 6.0$ MeV in ^{233}Th and ^{239}U (corresponding to $E_n \sim 1$ eV on ^{23}Th and ^{238}U) by a factor of 3. This stems not so much from the equidistant single particle level approximation of the Ericson formula but rather almost exclusively from deformation [32]. This is clearly seen when a spherical S-W potential is used, Fig.(7). With the above, the average spacing, D, at the above excitation energy is roughly the same for both ^{233}Th and ^{239}U and is about $D \simeq 10$ keV. This is, as expected, three times smaller than the value employed in Ref.[29] and used in the previous section.

An interesting feature of the result concerns the number of positive and negative parity states for a given value of j. In figure (8) we show the fraction, $\frac{(+)}{(+)+(-)}$ of positive parity levels (with respect to all levels) for $j = 1/2$ in ^{239}U (a) and ^{233}Th (b) vs. excitation energy. The sharp, albeit small magnitude, oscillation around the value 0.5 is very clear. Clearly the fraction of negative parity levels, $\frac{(-)}{(+)+(-)}$, is given by the value in figure (8) subtracted from unity. At $E^* \sim 6$ MeV, the negative parity fraction for ^{239}U is ~ 0.49, while it is 0.51 in ^{233}Th. This translates into $D^{(-)}_{2p-1h}(^{233}Th) \simeq 11$keV and $D^{(-)}_{2p-1h}(^{238}U) \simeq 13$keV. This fact encouraged several authors [26,27] to suggest that the pear-like shape associated with octupole deformation results in parity doublets which when taken explicitly into account can, in principle, lead to positive longitudinal asymmetry. This suggestion, however, was shown to be inconsistent with actual doublet spacings seen in ^{233}Th [35]. Further, and more importantly, recent measurement on ^{238}U [36] has unambiguously demonstrated that this

nucleus also has significant octupole deformation. Thus from the collective point of view ^{233}Th and ^{239}U are very similar.

The presence of a dominant local doorway that gives rise to a large value of $< P >$ is certainly possible in some nuclei. The probability P that $|\gamma^{(0)}_{Ds}/\gamma^{(0)}_{Dp}$ is, say f, can be calculated as follows. Since the local doorways are statistical in nature, the γ^{0}_{Ds} and $\gamma^{(0)}_{Dp}$ are the Gaussian distributed with about the same width. We thus have:

$$P\left(|\frac{\gamma^{(0)}_{Ds}}{\gamma^{(0)}_{Dp}}| = f\right) = \frac{1}{\pi}\int_{-\infty}^{+\infty} dx \int_{-\infty}^{+\infty} dy e^{-(x^2+y^2)}\delta\left(|\frac{x}{y} - f|\right) = \frac{2}{\pi}\frac{1}{1+f^2} \tag{5.11}$$

Thus, within our model, the probability for the occurrence of the phenomenon of large parity violation *with* sign correlation goes as $(1+f^2)^{-1}$, which is small for $f \simeq 4$ which we found in n+^{232}Th. Therefore such a phenomenon is not a global one that is exhibited by nuclei over the periodic table. It happens in ^{232}Th due to a statistical fluctuation among the properties of local doorways. In fact, in all other systems studied by the TRIPLE Group the average value of P was found to be zero and its magnitude smaller so that $f \simeq 1$. This implies that a local dominant 2p-1h doorway state, seemingly so conspicuous in ^{233}Th, does not occur in the other nuclei studied. With no single dominant doorway present, e.g. if two closely spaced doorways are relevant in the energy region of interest, the sign correlation disappears.

Our analysis points to the conclusion that the phenomenon of "sign correlation" is purely a conventional nuclear structure problem, and it is not connected to "exotics". Further, the phenomenon occurs in Th by statistical accident. Before ending we mention that in Th the single particle p-wave is resonant whereas the s-wave is not. Even so, $f \simeq |\gamma^{(0)}_{Ds}/\gamma^{(0)}_{Dp}|$ was found to be about 4. It seems to us that a more favorable case would be to have the p-wave off-resonance and the s-wave on ($A \simeq 170$). This would give rise to a larger f, with

higher probability. Of course, this will be experimentally more difficult because the p-wave resonances in this region may be too narrow.

VI. OPTICAL MODEL DESCRIPTION OF PNC

Our doorway picture emphasizes the role of a local 2p-1h doorway state which is responsible for the weak coupling between the p and s waves. In ^{232}Th, this doorway state is reasonably well separated from other doorways, whereas in, e.g., ^{238}U, where no sign correlation is seen, there are several 2p-1h doorways present in the energy range of interest. In the following we address another question also relevant to the parity non-conserving (PNC) neutron reaction, namely to what extent is the total cross-section difference $\langle \Delta\sigma_q \rangle$ accounted for by an optical model which contains an appropriate one-body PNC. The quantity $\langle \Delta\sigma_q \rangle$ is just $\sigma_q^{(+)} - \sigma_q^{(-)}$ where σ_q is the cross-section at the qth p-resonance and the superscripts $+(-)$ refer to positive (negative) helicity of neutrons.

Before we start our discussion of the optical model analysis, we give first a derivation of the symmetry violating optical potential, based on the theoretical discussion presented in Section III.

The optical model operator can be read off from Eq. (3.6), if we write $H = H_0 + V$, with H_0 being diagonal in channel space and V is the interaction:

$$V_{opt} \equiv PVQ\bar{G}_Q QVP + PVP$$

$$\bar{G}_Q = (E - QHQ + iI)^{-1} \tag{6.1}$$

Writing V as a symmetry conserving piece V_s, plus a symmetry violating piece V_v, we may write, to first order in V_v:

$$V_{opt} = PV_sP + PV_vP + PV_sQ\bar{G}^s_Q QV_sP + P_vQ\bar{G}^s_Q QV_sP + PV_sQ\bar{G}^s_Q QV_vP$$

$$+PV_sQ\bar{G}^s_Q QV_vQ\bar{G}^S_Q QV_sP \tag{6.2}$$

Thus the symmetry violating part of V_{opt} is:

$$V_{opt,v} = PV_sP + PV_vQ\bar{G}^s_QQV_sP + PV_sQ\bar{G}^s_QQV_vP$$
$$= PV_vP + PV_v^D(E)P \tag{6.3}$$

where we have denoted by $V_v^D(E)$ the dispersive component of the symmetry violating part of the optical potential. From the general properties of $\bar{Q}^s_Q$ we may write a dispersion relation for $V_v^D(E)$:

$$ReV_v^D(E) = \frac{P}{\pi}\int \frac{ImV_v^D(Z)}{Z-E}dZ, \tag{6.4}$$

where P stands for the principal value.

So far in the application to data analysis of PNC, the dispersion component has been dropped. As for PV_vP, it is common to use an expression obtained by Michel [37]:

$$PV_vP = \{\vec{\sigma}\cdot\vec{p}, v(r)\} \tag{6.5}$$

Where the symmetrical form insures Hermiticity and the real nature of V_v guarantees evenness under time reversal.

The calculation described below use the form (6.5). It would be interesting to assess the importance of the dispersion part of the PNC interaction $PV_v^D(E)P$. This we leave for a future work. The optical model approach to the longitudinal asymmetry has been considered in [38-41].

The interaction of a neutron with a spin zero target of mass number A is taken to be the sum of complex strong (parity conserving, PC) and weak (parity non-conserving, PNC) potentials.

$$V = V_S(r)) + V_{PNC} \tag{6.6}$$

$$V_S(r) = U(r) + V_{SO}(r)\vec{l}\cdot\vec{S} \tag{6.7}$$

$$V_{PNC} = PV_vP = \vec{\sigma}\cdot\vec{p}\nu(r) + \nu(r)\vec{\sigma}\cdot\vec{p} \tag{6.8}$$

The scattering amplitude which describes the scattering of neutrons from a spin zero target nucleus is generally given by [40]

$$F(\theta) = F_S(\theta) + F_{PNC}(\theta)$$

$$F_S(\theta) = f(\theta) + i\vec{\sigma}\cdot\left(\hat{k}\times\hat{k}'\right).g(\theta) \tag{6.9}$$

and

$$F_{PNC}(\theta) = -\vec{\sigma}\cdot\left(\hat{k}+\hat{k}'\right).h(\theta) \tag{6.10}$$

Partial wave expansion yields

$$f(\hat{k}\cdot\hat{k}') = \frac{1}{k}\sum_l\left[(l+1)t_l^{j=l+1/2} + lt_l^{j=l-1/2}\right]P_l(\hat{k}\cdot\hat{k}')$$

$$g(\hat{k}\cdot\hat{k}') = \frac{1}{k}\sum_l\left[t_l^{j=l+1/2} - t_l^{j=l-1/2}\right]P_l'(\hat{k}\cdot\hat{k}') \tag{6.11}$$

and

$$h(\hat{k}\cdot\hat{k}') = \frac{1}{k}\frac{1}{1+\hat{k}\cdot\hat{k}'}\sum_l\frac{2j+1}{2}t_{l+1,l}^j\left[P_l(\hat{k}\cdot\hat{k}') + P_{l+1}(\hat{k}\cdot\hat{k}')\right]. \tag{6.12}$$

where t_l are the elements of the T-matrix which is taken to be of the general form

$$t^j = \begin{pmatrix} t_{l,l}^j & t_{l,l+1}^j \\ t_{l,l+1}^j & t_{l+1,l+1}^j \end{pmatrix} \tag{6.13}$$

The diagonal terms $t_{l,l}^j$ and $t_{l+1,l+1}^j$ enter in the definition of F_S while $t_{l,l+1}^j$ defines the PNC amplitude, $F_{PNC}(\theta)$, Eq.(6.10).

For the purpose of evaluating the observables it is useful to remind the reader the relation between the $t^j_{l,l'}$'s and the elements of the S-matrix

$$S^j_{l,l'} = \delta_{l,l'} + 2it^j_{l,l'} \tag{6.14}$$

Given the amplitude $F(\theta)$ in spin-space, one may immediately calculate all the spin observables. To do this, we remind that the initial density matrix for an arbitrary polarized beam of spin 1/2 particles incident on a spin-0 target is:

$$\rho_i = \frac{1}{2}\left(1 + \vec{\sigma}\cdot\vec{P}_i\right), \tag{6.15}$$

where $\vec{P}_i$ ($|\vec{P}_i| \leq 1$) is the polarization of the incident beam. The density matrix of the scattered beam can then be written in terms of $F(\theta)$ as:

$$\rho_{sc} = F\rho_i F^+. \tag{6.16}$$

Of course, the total cross-section, σ_T, can be immediately obtained from the optical model theorem, *vis*

$$\sigma_T = \frac{4\pi}{k} ImF(0), \tag{6.17}$$

which can be written as a sum of the total elastic (shape elastic), σ_E and absorption (compound) , σ_{ABS}, cross-sections.

We find

$$\sigma_E = \frac{\pi}{k^2}\sum_j \frac{2j+1}{2}\left[|S^j_{l,l} - 1|^2 + |S^j_{l,l+1}|^2 + |S^j_{l+1,l+1}|^2 + |S^j_{l,l+1}|^2\right] -$$
$$-\vec{\sigma}\cdot\hat{k}\frac{\pi}{k^2}\sum_j \frac{2j+1}{2} 2Re \quad \left[S^{1*}_{l,l+1}\left(S^j_{l,l} - 1 + S^j_{l+1,l+1} + 1\right)\right] \tag{6.18}$$

$$\sigma_{ABS} = \frac{\pi}{k^2}\sum_j \frac{2j+1}{2}\left[1 - |S^j_{l,l}|^2 + 1 - |S^j_{l+1,l+1}|^2\right] +$$
$$+\vec{\sigma}\cdot\hat{k}\frac{\pi}{k^2}\sum_j \frac{2j+1}{2} 2Re \quad \left[S^{j*}_{l,l+1}\left(S^j_{l,l} + S^j_{l+1,l+1}\right)\right] \tag{6.19}$$

$$\sigma_T = \sigma_E + \sigma_{ABS} = \frac{2\pi}{k^2}\sum_j \frac{2j+1}{2}\left[1 - ReS^j_{l,l+1} + 1 - ReS^j_{l+1,l+1}\right] + \\ + \vec{\sigma}\cdot\hat{k}\frac{2\pi}{k^2}\sum_j \frac{2j+1}{2} 2Re\left(S^j_{l,l+1}\right) \tag{6.20}$$

The spin-averaged total cross-section is

$$\bar{\sigma}_T = \frac{2\pi}{k^2}\sum_j \frac{2j+1}{2}\left[1 - ReS^j_{l,l} + 1 - ReS^j_{l+1,l+1}\right]. \tag{6.21}$$

Finally, the spin average, optical, longitudinal asymmetry coefficient, P_{opt}, defined as

$$P_{opt} = \frac{\bar{\sigma}_+ - \bar{\sigma}_-}{2(\bar{\sigma}_{ABS})^2} \tag{6.22}$$

is found to be

$$P_{opt} = \frac{\frac{2\pi}{k^2}\sum_j (2j+1) ReS^j_{l,l+1}}{\bar{\sigma}_{ABS}} \tag{6.23}$$

Secondly, we can evaluate the final spin polarization and rotation. The details are given in Ref.[42].

From Eq.(5) we can calculate the polarized cross-sections $\left(\frac{d\sigma}{d\Omega}\right)$, as:

$$\left(\frac{d\sigma}{d\Omega}\right)_{P_i} = tr\left(\rho_{sc}\right) = \frac{d\sigma}{d\Omega}\left(1 + \vec{P}(\theta))\cdot\vec{P}_i\right) + 4(1+cos\theta)Re(gh^*)(\hat{k}-\hat{k}')\cdot\hat{P}_i \tag{6.24}$$

where we have introduced the **unpolarized** cross-section:

$$\frac{d\sigma}{d\Omega} = |f|^2 + sin^2\theta|g|^2 + 2(1+cos\theta)|h|^2, \tag{6.25}$$

and the polarization vector $\vec{P}(\theta)$:

$$\vec{P}(\theta) = 2\left[\left(\hat{k}\times\hat{k}'\right) Im(fg^*) - \left(\hat{k}+\hat{k}'\right) Re(fh^*) - \left(\hat{k}-\hat{k}'\right)(1+cos\theta)Re(fh^*)\right] / \left(\frac{d\sigma}{d\Omega}\right) \tag{6.26}$$

The final polarization of the beam is calculated from:

$$\vec{P}(\theta) = \frac{tr\left(\vec{\sigma}\rho_{sc}\right)}{tr\left(\rho_{sc}\right)}$$

$$\vec{P}_f(\theta) = \frac{\vec{P}(\theta) + \vec{P}_i - \vec{Q}(\theta) \times \vec{P}_i + \left\{\frac{\left[\vec{r}\left(\vec{r}^* \cdot \vec{P}_i\right) + \vec{r}^*\left(\vec{r} \cdot \vec{P}_i\right) - 2\left(\vec{r} \cdot \vec{r}^*\right)\vec{P}_i\right]}{d\sigma/d\Omega}\right\}}{1 + \vec{P}(\theta) \cdot \vec{P}_i + 2\left(\vec{r}^* \times \vec{r}\right) \cdot \vec{P}_i / \left(\frac{d\sigma}{d\Omega}\right)}, \tag{6.27}$$

$$\vec{r} \equiv \hat{n}g + i\left(\hat{k} + \hat{k}'\right)h. \tag{6.28}$$

In Eq.(6.28) we have introduced the spin rotation vector $\vec{Q}(\theta)$) given by:

$$\vec{Q}(\theta) = \frac{2\left[\left(\hat{k} \times \hat{k}'\right) Re(fg^*) + \left(\hat{k} + \hat{k}'\right) Im(fh^*)\right]}{\frac{d\sigma}{d\Omega}} \tag{6.29}$$

We find from Eqs.(8),(10) and (11)), to leading order in PNC effect that all the PNC spin observables are along the direction of $\hat{k} + \hat{k}'$, i.e., in the scattering plane in contrast ot the PC pieces which are in the direction perpendicular to that plane (along $\hat{n} = \hat{k} \times \hat{k}$)

$$\vec{P}_{f,PNC} \cdot \hat{k} = -\frac{2(1 + cos\theta) Re(fh^*)}{\frac{d\sigma}{d\Omega}}$$

$$\vec{Q}_{PNC} \cdot \hat{k} = \frac{2(1 + cos\theta) Im(fh^*)}{\frac{d\sigma}{d\Omega}} \tag{6.30}$$

Whereas the parity conserving counterparts are given, from Eqs.(10)) and (11), by

$$\vec{P}_{PC} \cdot \hat{n} = 2sin\theta \frac{Im(fg^*)}{\frac{d\sigma}{d\Omega}}$$

$$\vec{Q}_{PC} \cdot \hat{n} = 2sin\theta \frac{Re(fg^*)}{\frac{d\sigma}{d\Omega}} \tag{6.31}$$

Ate sufficiently high energies, the parity conserving amplitudes, $f(\theta)$ and $g(\theta)$ are given by

$$f(\theta) = \frac{1}{2ik}\left(s_0^{1/2} - 1\right),$$

$$g(\theta) = \frac{1}{2ik}\left(s_1^{3/2} - s_1^{1/2}\right), \tag{6.32}$$

while the PNC amplitude, $h(\theta)$) is given by [42]

$$h(\theta) \simeq \frac{1}{2ik} s_{10}^{1/2}, \tag{6.33}$$

where $s_0^{1/2}$ refers to s_L^J and the non-diagonal amplitude $s_{10}^{1/2}$ is proportional to the PNC interaction.

Using the above expressions, we find

$$
\begin{aligned}
P_{opt} &= \frac{2Res_{10}^{1/2}}{(1-|s_{00}|^2)+(1-|s_{11}|^2)} \\
\vec{P}_{PNC}\cdot\vec{k} &= -2(1+cos\theta)\frac{Re\left[\left(s_0^{1/2}-1\right)s_{10}^{1/2*}\right]^2}{|s_0^{1/2}-1|^2} \\
\vec{Q}_{PNC}\cdot\vec{k} &= 2(1+cos\theta)\frac{Im\left[\left(s_0^{1/2}-1\right)s_{10}^{1/2*}\right]^2}{|s_0^{1/2}-1|^2} \\
\vec{P}_{PC}\cdot\vec{n} &= 2sin\theta\frac{Im\left[\left(s_0^{1/2}-1\right)\left(s_1^{3/2}-s_1^{1/2}\right)^*\right]}{|s_0^{1/2}-1|^2} \\
\vec{Q}_{PC}\cdot\vec{n} &= 2sin\theta\frac{Re\left[\left(s_0^{1/2}-1\right)\left(s_1^{3/2}-s_1^{1/2}\right)^*\right]}{|s_0^{1/2}-1|^2}
\end{aligned}
\tag{6.34}
$$

In the following we calculate P_{opt}, P_{PC}, Q_{PC}, P_{PNC} and Q_{PNC} for n+^{232}Th in energy region 10^{-5}MeV, using the Madland-Young [43] (MY) strong optical potential given by

$$
\begin{aligned}
U(r)) &= -V_0 f_r(r) - iW_0 f_I'(r), \\
f_I(r) &= \left(1+exp\left(\frac{r-R_I}{a_I}\right)\right)^{-1} \\
V_0 &= 500.378 - 27.0073\left(\frac{N-Z}{A}\right) - 0.354E_{Lab}(MeV) \\
R_r &= 1.264A^{1/3}fm, \quad a_r = 0.612fm, \\
W_0 &= 9.265 - 12.666\left(\frac{N-Z}{A}\right) - 0.232E_{Lab} + 0.003318E_{Lab}^2(MeV) \\
R_I &= 1.256A^{1/3}, \qquad a_I = 0.553 + 0.0144E_{Lab}(MeV) \\
V_{SO}(r) &= \frac{\hbar}{m_\pi c^2}V_{SO}^{(0)}\frac{1}{r}f_{SO}'(r), \\
V_{SO}^{(0)} &= 6.2MeV, \\
R_{SO} &= 1.02A^{1/3}fm, \\
a_{SO} &= 00.75fm.
\end{aligned}
\tag{6.35}
$$

This potential is appropriate for treating low energy neutron scattering from actinide nuclei.

As for the Michel-typePNC interaction V_{PNC}, we use the form (6.5) with the following general shape for the formfactor $\nu(r))$

$$\nu(r)) = \frac{1}{2}\varepsilon_7 \hbar c 10^{-7} \left[1 + exp\left(\frac{r - r_0 A^{1/3}}{a}\right)\right]^{-7} ,$$
$$r_0 = 1.25fm, \qquad a = 0.6fm \quad , \tag{6.36}$$

and ε_7 is of the order of unity.

Optical model calculation of the longitudinal asymmetry.

In the following, we use the formalism developed above in conjunction with the Madland-Young optical potential and Eq.(6.36) for $\nu(r)$ to calculate the longitudinal asymmetry for ^{232}Th.

The strong potential, Eq.(6.35) gives for the $s-$ and p-wave strength functions S_0, S_1 in ^{232}Th the values (at $E_n = 1eV$):

$$S_0 = \frac{T(s1/2)}{2\pi\sqrt{E_{Lab}(eV)}} = 1.2 \times 10^{-4},$$

$$S_1 = \left[\frac{1}{3}\frac{T(p1/2)}{2\pi\sqrt{E_{Lab}(eV)}} + \frac{2}{3}\frac{T(p3/2)}{2\pi\sqrt{E_{Lab}(eV)}}\right] / \left(\frac{k^2R^2}{1+k^2R^2}\right) = 2.0 \times 10^{-4} \qquad (6.37)$$

where

$$T(s1/2) = 1 - |S_0^{1/2}|^2, \qquad T(p \quad j) = 1 - |S_1^j|^2. \qquad (6.38)$$

In Eq.(6.37) and (6.38) T refers to the transmission coefficient and R in Eq.(6.37) is taken to be $1.25A^{1/3}$ fm. The above values of S_0 and S_1 (both shown vs. A in Fig.(9)) are in reasonable agreement with the experimental ones given, respectively, by $0.84 \pm 0.07 \times 10^{-4}$ and $1.48 \pm 0.07 \times 10^{-4}$. The value of S_1 in Eq.(6.37) could certainly be improved by a convenient fine adjustment of the parameters of the M-Y potential.

The compound nucleus resonances in the n+^{232}Th system start at a neutron Lab. energy of 8 eV. Therefore we have to know the value $P_{opt}(p1/2)/\varepsilon_7$ at this energy. We have calculated $P_{opt}(p1/2)/\varepsilon_7$ as a function of E_n and concluded that it exhibits an $E_n^{-1/2}$ dependence as observed by the TRIPLE group [7-16]. In Fig. (10), we show $P_{opt}(p_{1/2}))$ vs. A at $E_n = 8$eV. At $E_n = 8$ eV we get $P_{opt}(p1/2) = 2.37 \times 10^{-4}(E_n = 8eV, \varepsilon_7 = 1)$. Thus to account for the experimental value of $P(p1/2)$ in the resonance region ($E_n > 8$ eV), which is $8 \pm 6\%$ we

have to take for $\varepsilon_7 = 108 \pm 81$. Qualitatively similar conclusions were reached in Ref.[38] who use a different optical potential. However, the above conclusion is misleading since the optical P_{opt} is obtained from energy averaged cross-sections , while $\langle P_p \rangle$ is calculated from resonance averaged ratios of resonance parameters. In order to make sensible comparison between the TRIPLE data and the optical model, we have to analyze the cross-section difference $\sigma_p^{(+)} - \sigma_p^{(-)}$.

Optical Model Analysis of the TRIPLE Data.

From the optical model point of view, the quantity $< P_q >_q$ is rather cumbersome to analyze. A more natural quantity to discuss is the ratio of energy averages:

$$P_{opt} = \frac{\langle \Delta\sigma \rangle_E}{2\langle \sigma \rangle_E} \equiv \frac{\Delta\sigma_{opt}}{2\sigma_{opt}} \tag{6.39}$$

which will behave differently from $\langle P_q \rangle_E$, where $\langle ... \rangle_E$ implies energy average. It is simple matter to show that:

$$\sigma_{opt} = \sigma_0 + \frac{\pi\Gamma}{2D}\langle \sigma \rangle_q, \tag{6.40}$$

and therefore:

$$\frac{2D}{\pi\Gamma}\Delta\sigma_{opt} = \langle \Delta\sigma \rangle_q + \frac{2D}{\pi\Gamma}\Delta\sigma_0, \tag{6.41}$$

where $\langle \Delta\sigma \rangle_q$ is the cross-section difference at the peak of the resonance (q), averaged over q, and D and Γ are the average spacing and width of the resonances. From the data of Refs. [9,10] we constructed $\Delta\sigma_q$ for n+^{232}Th and n+^{238}U, shown respectively in Figs. (11) and (12). The average, $\langle \Delta\sigma_q \rangle_q$, over the resonances in the energy range $1 < E_n < 400$ eV is (85 ± 12) mb for n+^{232}Th, and (18.2 ± 18.7) mb for n+^{238}U. In performing these averages, involving experimental points with error bars, we followed the procedure of [35]. The data points were scaled by E_n. It is obvious from this analysis that $\langle \Delta\sigma_q \rangle_q$ for n+^{238}U is consistent with a zero value, whereas for n+^{232}Th it is appreciable. To understand this difference in behavior between the two rather similar systems we performed an optical model calculation following the procedure of Refs. [38] and [40]. The results are previously summarized in [45].

In view of Eq.(6.41) the optical model cross-section differences must be multiplied by the factor $(2D/\pi\Gamma)$, before comparing with the experimental $\langle \Delta\sigma_q \rangle_q$ given above. The

value of $2D/\pi\Gamma$ was found to be 297.1 for n+^{232}Th and 197.6 for n +^{238} U. For 232Th, we used $\Gamma_1 = \Gamma_\gamma = 24$ meV and $D_1 = 11.2$ eV. For 238U, we used $\Gamma_1 = \Gamma_\gamma = 23.2$meV and $D_1 = 7.2$eV (the notation Γ_1, D_1 means width and spacing for the p-wave ($l = 1$) resonances). With the exception of the D_1 value for ^{232}Th, these numbers come from the book of Mughabghab on nuclear resonance parameters and thermal cross sections [46]. We obtained the value for D_1 in ^{232}Th by averaging over the spacings of ^{232}Th p-wave resonances below 100 eV. The value of ε_7, which appears in the PNC piece of the optical model potential was set equal to unity. The parity conserving part of the optical model potential is that of Ref. [43], which is appropriate to the actinides.

The results $\frac{2D}{\pi\Gamma}\Delta\sigma_{opt}$ for are shown in Figs. (13) and (14) for the two systems under discussion. The values of $\frac{2D}{\pi\Gamma}\Delta\sigma_{opt}$ at $E_n = 1$ eV is 0.4 mb for n+^{232}Th and 0.68 mb for n+^{238}U at $E_n = 1$ eV. Therefore it is reasonable to conclude that the n+^{238}U system exhibits a "normal" behavior since its $\langle\Delta\sigma_q\rangle_q$ is consistent with the optical value of 0.4 mb: namely PNC transitions whose average is zero and whose resonance background,, is basically the low-energy extrapolated optical model result. On the other hand, the n+^{232}Th system is "abnormal" in the sense that $\langle\Delta\sigma_q\rangle_q = 85$ mb (see above) is more than two orders of magnitude larger than the "scaled" optical model result (scaled in the sense of the factor $2D/\pi\Gamma$. This is certainly related to the fact that $< P_q >_q$ is zero n+^{238}U and relatively large in n +^{232} Th.

We further investigated the behavior of the two systems by examining the p-wave and s-wave optical transmission coefficients and compared them with the corresponding experimental values, namely $2\pi\frac{\Gamma_{0,n}}{D_0}$ and $2\pi\frac{\Gamma_{1n}}{D_1}$ where $\Gamma_{0,n}$(Γ_{1n}) is the s-wave (p-wave) neutron width. The values of $\Gamma_{0,n}$ and Γ_{1n} for ^{232}Th and ^{238}U were taken from Refs. [2] and [46].

Again, the comparison showed the "abnormal" nature of ^{232}Th when compared to ^{238}U. The experimental values of $2\pi\frac{\Gamma_{0,n}}{D_0}$, averaged over the resonances, for n+^{232}Th are slightly lower ($\simeq 20\%$) than the optical transmission coefficients whereas $2\pi\frac{\Gamma_{1n}}{D_1}$ shows conspicuously larger values ($\simeq 30\%$) than the optical transmission in the energy range, $100eV < E_n < 200eV$. This behavior is not shared by $^{n+238}$U.

The existence of a local doorway that is required to explain the sign correlation has clearly important implications on the energy averaged cross-section. Within the energy range where the averaged cross-section is calculated we are assuming that there is only one doorway present, as we emphasized earlier [29]. The contribution to the optical interaction that arises from the doorways is given by [45]:

$$\Delta U^{(\pm)}_{Doorway} = \frac{V_{Dp}(r)[V_{Dp}(r') \pm V^W_{Ds}(r')]}{E - E_D + i\Gamma^{\downarrow}_D/2} \tag{6.42}$$

to first order in the weak force, where $V_{Di}(r)$ is an appropriate form factor representing the doorway coupling to channel i. In (6.42) $\Gamma^{\downarrow}_d$ is the spreading width of the 2p-1h doorway, due to its coupling to the compound nuclear states.

It is clear from Eq. (6.42) that if treated as an optical potential , $\Delta U^{(\pm)}_{doorway}$ will contain a PNC part which is complex:

$$\Delta U^{PNC}_{Doorway} = \frac{2V_{Dp}(r)V^W_{Ds}(r')}{-E + i\Gamma^{\downarrow}_D/2} \tag{6.43}$$

In the optical model calculation of [4], whose results for $\Delta\sigma$ are shown in Figs. (6) and (7), an empirical local energy-dependent optical potential [43], was used to generate distorted waves that are then employed to evaluate the first-order perturbation matrix element:

$$f_{PNC} \propto Im\langle\Psi^{(-)}_s|V^{PNC}|\Psi^{(+)}_p\rangle \tag{6.44}$$

where V^{PNC} is just the MMichel-type interaction, Eq.(6.5). It is clear from the discussion above that the reported OM calculation is incomplete, since, to say the least, U must be complex. Further, the imaginary part to be used in a consistent optical model analysis of the TRIPLE data must arise entirely from the doorway (see Eq. (8.23)). It is, however, conventional to use an empirical complex potential to represent the parity conserving interaction since there are other doorways and, when used at higher energies the averaged potential will contain the contribution of many terms, of the type given in Eq. (6.42). Roughly speaking, the parity conserving (PC) imaginary part will then be given by:

$$Im\Delta U_{Doorway} = -2\pi\overline{V_{Dp}(R)V_{Dp}(r')}\bar{\Gamma}^{\downarrow}_{D}\rho_{D} \tag{6.45}$$

where ρ_D is the 2p-1h density of states. It is usually assumed that when an equivalent local potential is constructed from Eq. (6.45) and extrapolated to low energies, it can be represented by the empirical imaginary potential. On the other hand the PNC interaction to be used must be complex, on account of the local doorway contribution. We believe that the difference between the optical model $\Delta\sigma$ using the real PNC interaction and the data resides in this fact.

We now use the above argument to further pin-down the nature of the local doorway state. We calculate the contribution of the single local doorway to the energy averaged cross-section. This is straightforward, since is separable. We find, taking for an "optical potential", a background real piece plus the parity conserving part of (6.42):

$$\langle\Delta\sigma\rangle_E = \Delta\sigma_0 + \frac{2\pi}{k^2}\frac{\gamma^w_{Ds}\gamma_{Dp}\Gamma_D}{(E^2_D + \Gamma^2_D/4)} \tag{6.46}$$

where Γ_D is the total width of the doorway, $\Gamma_D = \Gamma^{\downarrow}_D + \Gamma^{\uparrow}_D$. The escape width $\Gamma^{\uparrow}_D$ accounts for the doorway decay to the open channels. We obtain from Eqs. (6.4) and (6.41) the

following form for $\langle \Delta\sigma_q \rangle_q$:

$$\langle \Delta\sigma_q \rangle_q = \left(\frac{\gamma^w_{Ds}}{\gamma_{Dp}}\right)\left(\frac{2D}{\pi\Gamma}\right)\left(\frac{1}{k^2}\right)\left[\frac{2\pi\gamma^2_{Dp}\Gamma_D}{(E^2_D + \Gamma^2_D/4)}\right] \tag{6.47}$$

Note that the factor $\frac{2D}{\pi\Gamma}$ refers to the fine structure compound resonances, whose value for n+^{232}Th was found to be $\simeq$ 300. From Eq. (6.47) we find that $\langle \Delta\sigma_q \rangle_q$ is independent of energy. This is so since $\gamma^2_{Dp} \propto (kR)^3$, and $\gamma^w_{Ds}/\gamma_{Dp} \propto k^{-1}$. We choose $E_n = 1$ eV to evaluate the RHS of (6.47). In Ref. [29], γ_{Ds}/γ_{Dp} was identified with $< P_q >_q$, which, at this energy, $\simeq$ 0.08. Using for $\langle \Delta\sigma_q \rangle_q$ the value cited earlier, namely 85 mb, we find the following numerical value for the doorway factor inside the square brackets,

$$\left[\frac{2\pi\gamma^2_{Dp}\Gamma_D}{(E^2_D + \Gamma^2_D/4)}\right] \simeq 1.7 \times 10^{-7} \tag{6.48}$$

As in [29] we take $E_D \simeq \Gamma_D = 30$ keV, which then gives for the partial p-wave neutron width of the local 2p-1h doorway, $2\pi\gamma^2_{Dp} \simeq 6.3$ meV, several orders of magnitude larger than the average width of the compound p-wave neutron resonances, quite consistent with our doorway picture. At this point it is important to remind the reader of an interesting relation involving the doorway strength function and that of the compound nucleus [21]. This relation reads:

$$2\pi\frac{\Gamma^{\uparrow}_D}{D_D} = 2\pi\langle\frac{\Gamma_q}{D_q}\rangle_q \tag{6.49}$$

For p-resonances in Th, $\langle \Gamma_q/D_q \rangle$, in the energy range of interest, is 2.1×10^{-3}. In Ref. [29] we have calculated $D_{Dp} \equiv 1/\rho_{Dp}$ which came out to be about 30 keV. Taking half this value for the negative parity states, therefore we get the following value for the average escape width of the p-wave 2p-1h doorway, $\Gamma^{\uparrow}_{Dp} \simeq 31$ eV . Within our model, the value of the total width of the doorway is assumed to be $\Gamma = 30keV$. Thus, most of this width is spreading.

Optical model calculation of Spin Polarization and Rotation.

Though difficult to measure, the final spin polarization and rotation of the ongoing neutrons are interesting quantities to investigate. Here we present the elements of our calculations using the optical potential of Eqs.(6.35) and (6.36) [42].

The results of our calculations are shown in Figs. (15) and (16) for the angle-independent parity conserving and parity non-conserving spin polarization and rotation quantities defined above, vs. E_n, in the range $10eV \leq E_n \leq 10keV$. At $10keV$, the S-matrix elements $s_1^{1/2} - 1$ and $s_1^{3/2} - 1$ are about 1% of the value of the element $s_0^{1/2} - 1$ and are increasing. We thus expect the deviations of the angular dependence of the spin polarization and rotation functions from the forms given in Eq.(6.34) to also be about 1% and increasing. From the figures we observe that $\frac{P_{PNC}^0}{P_{PC}^0}$ is about 7×10^{-3} at $E_n = 10eV$ and decreases to 1.3×10^{-4} at $E_n = 10keV$. The quantity $\frac{Q_{PNC}^0}{Q_{PC}^0}$, on the other hand, is 1.5×10^{-3} at $E_n = 10eV$ and decreasing to 6×10^{-5} $E_n = 10keV$. We now have to make contact with the longitudinal asymmetry anomaly discussed extensively in Section V, namely the extracted value of resonance-averaged $\frac{\sigma_T^{(+)}(p_{1/2}) - \sigma_T^{(-)}(p_{1/2})}{2\sigma_T(p_{1/2})}$, where $\sigma_T^{(\pm)}(p_{1/2})$ is the total cross-section for $\pm$ helicity neutron populating a $p_{1/2}$ resonance in ^{233}Th, was found to be positive and large, 0.08 ± 0.06. The optical model calculation performed required a vlue of ε_7 of 108 ± 81.

As emphasized above a more natural quantity to compare the data with is the optical model cross-section difference. Thus

$$\Delta\sigma_{opt} = \frac{8\pi}{k^2} Re s_{01}^{1/2} \quad . \tag{6.50}$$

Within the doorway model of Section V, $s_{10}^{1/2}$ acquires the following structure

$$s_{10}^{1/2} = \frac{-1}{2i} \frac{\gamma_{D_p} \gamma_{D_n}^W}{E - E_D + \frac{i\Gamma_D}{2}} \quad . \tag{6.51}$$

Clearly the same degree of enhancement of $\langle \Delta\sigma_T(P_{1/2}\rangle$ over the optical value, due to the doorway, would manifest itself in Q^0_{PNC} and P^0_{PNC} since all the quantities involve the same $s^{1/2}_{01}$, Eq.(6.34). To get an idea, the optical model value of $Res^{1/2}_{01}$ at $E_n = 1$ eV is 7×100^{-12}, to be compared to the doorway $Res^{1/2}_{01}$ (Eq.(6.51))$= 6 \times 10^{-9}$. We expect an enhancement of more than two orders of magnitude in P^0_{PNC} and Q^0_{PNC} over the values shown in Fig.(15).

VII. PARITY VIOLATION IN EXOTIC NUCLEI

In recent years the field of neutron- and proton rich nuclei has flourished into a worldwide experimental and theoretical activity. A natural question to ask is to what extent the r.m.s. value of the PNC matrix element extracted by the TRIPLE Collaboration compares with its value in these exotic nuclei.

The answer to the above question would shed light on the general properties of instability of the nuclear systems subjected to both strong and weak hadronic forces. Needless to say that the instability of drip-line nuclei arises from the diminishing intensity of the strong force at the larger radii where, e.g., halo or skin nucleons reside. The study of the weak force operating in this loose region is therefore very important in elucidating the full nature of the instability of unstable nuclei. To remind the reader, the extracted value of the single particle matrix element MM^w is $\simeq$ 1.0eV, which compares well with typical structure calculation [47] based on existing theory of the weak interaction or within the Standard Model [48].

In this section, we consider the Parity Nonconserving (PNC) mixing in the ground state of exotic (halo) nuclei caused by the PNC weak interaction between outer neutron and nucleons within nuclear interior. For the nucleus ^{11}Be as an example of typical nucleus with neutron halo, we use analytical model for the external neutron wave functions to estimate the scale of the PNC mixing. The amplitude of the PNC mixing in halo state is found to be an order of magnitude bigger than that of typical PNC mixing between the "normal" nuclear states in nearby nuclei. The enhanced PNC mixing in halo cloud is proportional to the neutron weak PNC potential constant g_n^W only.

So far, the PNC effects have been probed in "normal" nuclei. Physics of "exotic" nuclei

studied with unstable nuclear beams [49-60] appears to be one of the most promising modern nuclear areas. Due to their specific structure, exotic nuclei, e.g., halo nuclei can offer new possibilities to probe those aspects of nuclear interactions which are not accessible with normal nuclei. It is therefore interesting to examine possibilities of using exotic nuclei to investigate the effects of violation of fundamental symmetries, i.e., spatial parity and time reversal.

Some aspects of the Weak interactions in exotic nuclei have been discussed in literature [50],[51] in relation to the beta decay and to possibilities to study the parameters of the Cabibbo-Kobayashi-Mascawa matrix. To the best of our knowledge, however, the issue of the PNC effects in exotic nuclei has been addressed only recently [61].

The aim of this Section is to give an estimate of the magnitude of the PNC effects in halo nuclei. We confine ourselves to the case of nucleus ^{11}Be, the most well studied, both experimentally and theoretically [49,50,51,54,55]. We find that the ground state, the $2s_{1/2}$ halo configuration, acquires admixture of the closest in energy halo state of opposite parity, $1p_{1/2}$. This effect originates from the weak interaction of the external halo neutron with the core nucleons in the nuclear interior. As a result, the neutron halo cloud surrounding the nucleus acquires the wrong parity admixtures that may be tested in experiments which can probe the halo wave functions in the exterior.

The magnitude of the admixture is found to be $\sim 10^{-6} \times g_n^W$ that is an order of magnitude bigger than the PNC effects in normal spherical nuclei. What is important to notice is that the enhanced effect we have found here is proportional to the *neutron weak constant* g_n^W only. The value of this constant remains to be one of the most questionable points in modern theory of parity violation in nuclear forces [62]. The enhanced PNC mixing in halo

found here can be therefore useful in studies of the neutron weak constant.

Proton and neutron weak potential strengths

The knowledge about the proton and neutron constants g_p^W and g_n^W accumulated to date can be summarized as follows:

$$g_p^W = 4.5 \pm 2, \qquad g_n^W = 1 \pm 2 \tag{7.1}$$

These values correspond to the microscopic parameters of the DDH Hamiltonian [48] described above and they are found in reasonable agreement with the bulk experimental data on parity violation. The above relatively small absolute value of the neutron constant that follows from DDH analysis, results basically from cancellation between π- and ρ-meson contribution to g_n^W, while both terms contribute coherently to the proton constant g_p^W. One should mention that due to this difference between the absolute values of the proton and neutron constants, the proton constant tends to dominate most measurable PNC effects, especially when both g_p^W can g_n^W contribute, provided that DDH model gives correct estimates. In this sense, one usually measures the value of g_p^W, and it is difficult to probe g_n^W unless special suppression of the proton contribution occurs, and contribution of g_n^W is highlighted. By contrast, the case we consider in this work is sensitive to the value of the neutron constant only.

Halo structure effects on the PNC mixing

The basic specific properties of the halo nuclei are determined by the fact of existence of loosely bound nucleon in addition to the core composed by the rest of the nucleons [52]

(we will be interested here in the most well studied case of neutron halo). The matter distribution is shown schematically in Fig.(17) (part a).

In one-body halo nuclei like ^{11}Be, the ground state is particularly simple: it can be represented as direct product of the single-particle wave function of the external neutron, ψ_{halo}, and the wave function of the core. The residual interaction V_S^{res} can be neglected as the many-body effects related to the core excitations are generically weak in such nuclei [63]. The problem is then reduced to a single-particle problem for the external nucleon. The PNC potential matrix element between the ground state of halo nucleus and a state with opposite parity is

$$\langle \psi^+_{halo}|W^{PNC}|\psi^-_{halo}\rangle = g_n^W \frac{G}{2\sqrt{2}m}\langle \psi^+_{halo}|\{(\vec{\sigma}_n\vec{p}_n),\rho_c\}|\psi^-_{halo}\rangle, \tag{7.2}$$

where $\rho_c(r)$ is the core density. Due to relatively heavy core for $A \simeq 10$, difference between the center of mass coordinate and the center of core coordinate can also be neglected.

The effective potential that bounds the external neutron is rather shallow yielding small single-neutron separation energy, and one can expect small energy spacing between the opposite parity states. The PNC effects can therefore be considerably magnified. The spectrum of ^{11}Be is shown in Fig.(17)(part b). To evaluate the PNC mixing f^{HALO} in the ground state of this nucleus, it is enough to know the single-particle matrix element between the ground state 2s and the nearest opposite parity state 1p, and use their energy separation that is known experimentally.

The second effect of halo is that the value of the matrix element of the weak interaction operator between the halo states can be dramatically reduced as compared to its value in the case of "normal" nuclear states. The single-particle weak PNC potential in (7.2) originates

from the DDH Hamiltonian [48] which is a two-body operator. This fact is hidden in the nucleon density of the core $\rho_c(r)$. The external neutron spends most of its time away from the core region where only it can experience the PNC potential created by the rest of nucleons. Indeed, the dominant contribution to the matrix element (7.2) must come from the regions where the three functions can overlap coherently: $\psi^+_{halo}(r)$, $\psi^-_{halo}(r)$ and the core density $\rho_{core}(r)$. The latter one is essentially restricted by the region of nuclear interior, $r < r_c$ thus reducing the effective volume of required interference region to $\frac{4}{3}\pi r_c^3$. Normalization condition implies that the extended wave function of the bound state halo $\psi^{\pm}_{halo}(r)$ must be considerably reduced in the volume of coherent overlap $\frac{4}{3}\pi r_c^3$. By contrast, in "normal" nuclei the radii of localization of the wave functions with opposite parity that can be mixed by the weak interaction coincide generically with the core radius r_c. The resulting suppression for the PNC halo matrix element $\langle\psi^-_{halo}(r)|W_{sp}|\psi^+_{halo}(r)\rangle$ with respect to the matrix element for the normal nuclei can be extracted from the following simple estimate

$$\frac{\langle\psi^-_{halo}|W_{sp}|\psi^+_{halo}\rangle}{\langle\psi^-_{normal}|W_{sp}|\psi^+_{normal}\rangle} \sim \left(\frac{r_c}{r_{halo}}\right)^3 \sim \left(\frac{2fm}{6fm}\right)^3 \sim \frac{1}{25} - \frac{1}{30} \tag{7.3}$$

where we have used the mean square radii of halos from Ref. [51]. This suppression factor can cancel out the effect of the small energy separation between opposite parity levels which would suppress the PNC mixing. This simple estimate does not take into account the structure of the halo wave functions which can be quite substantial and may even lead to further suppression in the PNC mixing. In the following, we present a detailed analysis of the related effects. In particular, we find that the crude estimate (7.3) turns out rather pessimistic.

Halo Model and Evaluation of the PNC mixing in the ground state of ^{11}Be

The form of the single-particle wave functions of halo states can be deduced from their basic properties [55] and their quantum numbers [51]. The results of the Hartree-Fock calculations which reproduce the main halo properties (e.g., mean square radii) are also available [51]. We use the following ansatz for the model wave function of the $2s$ halo state:

$$\psi_{2s} = R_{2s}(r)\Omega^{l=0}_{j=1/2,m}, \quad R_{2s}(r) = C_0(1-(r/a)^2)exp(-r/r_0) \tag{7.4}$$

Here, $R_{2s}(r)$ is the radial part of the halo wave function and $\Omega^{l=0}_{j=1/2,m}$ is the spherical spinor. As we can neglect the center of mass effect for the heavy ($A = 10$) core, the halo neutron coordinate r in $R_{2s}(r) = \frac{1}{r}\chi_{2s}(r)$ is reckoned from the center of nucleus. The constant C_0 is determined from the normalization condition, $\int\limits_0^\infty dr[\chi_{2s}(r)]^2 = 1$ (we choose the radial wave functions to be real). We have

$$C_0 = \frac{2^{3/2}a^2}{r_0^{3/2}\sqrt{45r_0^4 + 2a^4 - 12a^2r_0^2}} \tag{7.5}$$

The parameters r_0 and the a are the corresponding lengths to fit the density distributions obtained in Ref. [51] and the mean square radius. The value of a is practically fixed to be $a = 2fm$ what corresponds to the position of the node. Recently, the node position have been restored from the analysis of the scattering process in work [55].

For the wave function $\psi_{1p} = R_{1p}(r)\Omega^{l=1}_{j=1/2,m}$ of the excited state $1p$, the following simplest form of the radial wave function turns out to be adequate

$$R_{1p}(r) = C_1 r exp(-r/r_1), \tag{7.6}$$

where C_1 is the normalization constant $C_1 = \frac{2}{\sqrt{3}}r_1^{-5/2}$ and the only tunable parameter r_1 is related to the $1p$ halo radius. The mean square root radii for the halo wave states (7.4) and (7.6) are given by

$$\sqrt{\langle r_{2s}^2\rangle} = r_0\left(\frac{6(45r_0^4+2a^4-12a^2r_0^2)}{105r_0^4+a^4-15a^2r_0^2}\right)^{1/2}, \quad \sqrt{\langle r_{1p}^2\rangle} = \left(\frac{15}{2}\right)^{1/2} r_1. \tag{7.7}$$

The matrix element of the weak interaction (7.2) between the ground state and the first excited state reads

$$\langle 2s|W_{sp}|1p\rangle = \tag{7.8}$$
$$ig_n^W \frac{G}{\sqrt{2}m}\int_0^\infty dr\chi_{2s}(r)\left(\rho_c(r)\frac{d}{dr}+\frac{\rho_c(r)}{r}+\frac{1}{2}\frac{d\rho_c(r)}{dr}\right)\chi_{1p}(r)$$

The core nucleon density $\rho_c(r)$ has been tuned to reproduce the data obtained from Ref. [51]. We found that their results are excellently reproduced by the Gaussian-shaped ansatz $\rho_c(r)$,

$$\rho_c(r) = \rho_0 e^{-(r/R_c)^2} \tag{7.9}$$

with the values of the parameters $\rho_0 = 0.2fm^{-3}$ and $R_c = 2fm$, as shown on Fig.(18).

Using the model wave functions (7.4),(7.4) and the core density (7.9), the required integrals can be done analytically, and we arrive with the result

$$\langle 2s|W|1p\rangle = ig_n^W \frac{G}{\sqrt{2}m}\mathcal{R} \tag{7.10}$$

where

$$\mathcal{R} = \rho_0 R_c^3 C_0 C_1\Big\{3I_2(y) - \left[3\left(\frac{R_c}{a}\right)^2+1\right]I_4(y) + \\ + \left(\frac{R_c}{a}\right)^2 I_6(y) - \frac{R_c}{r_1}\left[I_3(y) - \left(\frac{R_c}{a}\right)^2 I_5(y)\right]\Big\} \tag{7.11}$$

where $y = \frac{R_c(r_0+r_1)}{r_0 r_1}$ and the functions I_n are given by

$$I_n(y) = \int_0^\infty dx x^n e^{-x^2-yx} = (-1)^n\frac{\sqrt{\pi}}{2}\frac{d^n}{dy^n}e^{y^2/4}erfc(y/2),$$

where $erfc(y)$ is the error function

$$erfc(y) = 1 - \frac{2}{\sqrt{\pi}} \int_0^y dt exp(-t^2/2).$$

To obtain the results for the PNC weak interaction matrix element, we used the parameters r_0 and r_1 in the halo wave functions to fit the radial densities of the halos obtained by Sagawa [51].

The results for the best parameters are shown in Figs.(19) and (20) for the $2s$ and the $1p$ halos, respectively. One sees that the agreement for the densities is very good. Below, we use the values

$$r_0(best \quad value) = 1.45fm,$$

$$r_1(best \quad value) = 1.80fm, \tag{7.12}$$

to calculate the matrix elements in Eqs. (7.8,7.10,7.11). The radial wave functions χ are given in Fig.5. We used also deviations of the both r_0 and r_1 from (7.12) to check robustness of the results with respect to variations in the halo structure details. The values of the halo radii given by (7.7), $\sqrt{\langle r_{2s}^2 \rangle} = 5.9fm$ and $\sqrt{\langle r_{1p}^2 \rangle} = 4.9fm$ are close to the values of Ref. [51] $6.5fm$ and $5.9fm$ which agree with experimental matter radii.

Substituting the values (7.12) into our expressions for the matrix elements we obtain the following value of the matrix element $\langle 2s|W_{sp}|1p\rangle_{HALO}$

$$\langle 1p|W_{sp}|2s\rangle_{HALO} = -i0.2 \quad g_n^W \quad eV,$$

$$= -i0.2 \quad eV \quad (for \quad g_n^W \simeq 1 \quad). \tag{7.13}$$

It is seen that this value is only few times smaller than the standard value of the matrix element of the weak potential between the opposite parity states in spherical nuclei (see

e.g., [1]), that is typically about one eV. This results the wave function structure and comes basically from the facts that the $2s$ wave function crosses zero line near the core surface while the $1p$ radial wave function does not have nodes. Thus the functions χ_{1p} and $d\chi_{2s}/dr$ look similar and are folded constructively with $\rho_c(r)$ in the region of interaction (nuclear interior), see Figs.(21) and (22).

The matrix element of W_{sp} between the "normal" nuclear states can be evaluated for example, in the oscillator model. Taking the typical matrix element between the states $2s$ and $1p$ and using the same formula (7.8), one has

$$\langle 1p|W_{sp}|2s\rangle_{osc} = -ig_n^W G\rho_0 \left(\frac{\omega}{2m}\right)^{1/2} \tag{7.14}$$

where $\omega \simeq 40A^{-1/3}MeV$ is the oscillator frequency [64]. We used here the constant value of core nucleon density, $\rho_0 \simeq 0.138fm^{-1/3}$. This is very good approximation for the case of normal nucleus (see, e.g.[18]).

Recalling the energy difference between the ground state and the first excited state $1p$ that is known experimentally,

$$|\Delta E_{HALO}| = E_{p1/2} - E_{s1/2} = 0.32MeV \tag{7.15}$$

we obtain, using Eq.(7.13), the coefficient of mixing the opposite parity state ($1p$) to the halo ground state $2s$:

$$\begin{aligned} |f_{sp}^{HALO}| = \frac{|\langle 1p|W_{sp}|2s\rangle|}{|\Delta E_{HALO}|} &\simeq \frac{0.2eVg^W}{0.32MeV} \\ &\simeq 0.6\times 10^{-6} g_n^W \\ \simeq 0.6\times 10^{-6} \quad (for \quad g_n^W &\simeq 1) \end{aligned} \tag{7.16}$$

This PNC mixing is about one order of magnitude stronger than the scale of single-particle

PNC mixing in "normal" nuclear states that can be extracted from Eq.(7.14). In the case of normal $p-s$ mixing, we have

$$|f_{sp}^{normal}| = \frac{|\langle 1p|W_{sp}|2s\rangle|}{\omega} = \frac{G g_n^W \rho_0}{\sqrt{2}m}\left(\frac{m}{\omega}\right)^{1/2}$$
$$\simeq 0.7\times 10^{-7} g_n^W$$
$$\simeq 0.7\times 10^{-7} \quad (for \quad g_n^W \simeq 1) \tag{7.17}$$

in the same region of nuclei with $A \sim 11$. The above value (7.17) for the normal PNC mixing is rather universal and it is practically insensitive to variations of the details of the normal nuclear wave functions and core densities [18]. Comparing Eqs.(7.16) and (7.17), we obtain the halo enhancement factor to be

$$\frac{|f_{sp}^{HALO}|}{|f_{sp}^{normal}|} \simeq 9. \tag{7.18}$$

This result is quite remarkable in a number of respects. First, it is seen that in experiments when the halo wave functions in nuclear exterior are probed, the value of PNC mixing is even stronger than in "normal" nuclei. Secondly, this PNC mixing is dominated by the neutron weak constant g_n^W. Such experiments with neutron halo nuclei would therefore provide unique opportunity to probe the value of this constant. Usually, sensitivity of experiments to the value of this constant is "spoiled" by comparably large value of the proton weak constant g_p^W, cf. Eqs. (7.1).

In order to assess reliability of the results, we have studied stability of the enhancement factor against variations in the parameters of the halo wave functions. As one can see from the results presented in Table I, the matrix element (7.13) is changed by few per cent only when the wave functions are deformed. The enhancement factor (7.16) is therefore quite stable.

Having in mind to present a first estimate of the PNC effect in halo nuclei, we have chosen here the simplest possible case of one-body halo where the existing data allow one to rely on simple analytical model of halo structure. In this work, we confined ourselves to the case of exotic nucleus ^{11}Be for which we presented detailed consideration.

The analysis presented above rests basically on the most reliably known facts: the quantum numbers of the states involved, the halo radii which match the matter radii known from experiment, and the Hartree-Fock wave functions. With these input data, the further quantitative analysis is a straightforward analytical exercise which does not require any approximations. Stability of the results has been checked analytically. The PNC enhancement factor of one order of magnitude allows one to to speak about qualitative halo effect that should not be overlooked.

It is the matter of further studies to check universality of the effect while going along the table of exotic nuclei. One sees that other exotic nuclei with developed halo structure manifest similar properties (see, e.g., [51]). Indeed, the effect of PNC enhancement found here results basically from the two facts:

(i) small energy separation between the mixed opposite parity states

(ii) considerably strong overlap between the mixed wave functions and the core density, which saves part of suppression in the PNC weak matrix element.

The first of these points is rather common for nuclei with developed neutron halos. Systematics of separation energies for single neutron [52] shows that the ground states of halo nuclei can be distanced from the continuum by typical spacing $\varepsilon_{halo} \sim (2mr_{halo})^{-1/2} \sim$ few hundreds of KeV. Even in the cases when no bound states with parity opposite to that of the ground state occur, the PNC admixtures to the ground state wave functions must

exist. In these cases, the PNC admixtures can be evaluated by means of Green function method.

The second point (ii) is related to the wave function structure and requires further studies. It would be also interesting to study the PNC effects in proton rich nuclei 52],[53],[54].

One of possible experimental manifestations of the discussed effect is related to anapole moment [65] which is attracting much attention in current literature [66] in view of new experimental results (detection of anapole moment in nucleus ^{133}Cs [67]). Since the anapole moment is created by the toroidal electromagnetic currents which results from PNC, its value grows as the size of the system is increased [68]. In the case of a halo-type nucleus which we considered here, the value of the anapole moment can be therefore enhanced due to the extended halo cloud. We hope to address these issues in following publications.

VIII. TIME REVERSAL SYMMETRY BREAKING

The breaking of CP symmetry observed for neutral kaons [69] implies, because of CTP invariance, time reversal symmetry breaking (TRSB), which has never been demonstrated experimentally. Because of the results of tests looking for TRSB effects, expectations are that they will be small. We believe, however, that the amplification which occurs in low energy neutron reactions may make them visible - and in any event will provide limits [70,71]. In this Section we apply the results of section III to extract time symmetry breaking from both resonance and energy averaged experiments. In the following, we will discuss first, isolated resonances and then we turn our attention to the case of overlapping resonances regime.

We consider first the case of isolated resonances. This situation is usually encountered at neutron energies in the electron volt region. The parity non-conservation experiment of the TRIPLE Group was performed under these conditions. The study of TRBS in the isolated resonance regime has been discussed recently [72,73]. Here we present a different point of view concerning this matter. It is convenient for the discussion to use the K-matrix, which at a given isol ated resonance , we write, in the presence of TRSB, as:

$$K^q_{cc} = \frac{1}{2\pi}\frac{\gamma_{qc}\gamma^*_{qc}}{E - E_q} \tag{8.1}$$

K^q is hermitian but neither real, nor is it symmetric (see discussion in section II). Note that E_q in (37) is the real energy of the compound level, q. The T-matrix is obtained from the K-matrix through

$$T^q_{cc} = \frac{1}{2\pi}\frac{\gamma_{qc}\gamma^*_{qc}}{E - E_q + i\Gamma_q/2} \tag{8.2}$$

with Γ_q^γ being the radiative decay width of resonance q, which is the dominant piece of Γ_q. The above form of T_{cc}^q establishes the link with the discussion at the beginning of the paper, i.e. for the present case $\gamma_{qc}^0 = Re\gamma_{qc}$ and $\Delta\gamma_{qc} = iIm\gamma_{qc} \equiv i\gamma_{qc}^w$ Going back to Eq. (8.1), we introduce the eigenchannels that diagonalize K_{cc}^q, by the requirement $\gamma_{qc}\sum_{c'}\gamma_{qc'}^* f_{c'} = \lambda f_c$, which is solved by $\lambda = \sum_{c'}|\gamma_{qc'}|^2$ and $fc = \gamma_{qc}$. All other solutions have $\lambda = 0$. Thus there is only one physical eigenchannel for each level q. We thus write for K_q in operator form:

$$K^q = \frac{|\gamma_q|^2}{E - \varepsilon_q}|\hat{\gamma}_q\rangle\langle\hat{\gamma}_q|$$

where $|\hat{\gamma}_q\rangle$ is a unit vector with components $\frac{\gamma_{qc}}{\sqrt{\sum_c|\gamma_{qc}|^2}}$. Note that this eigenchannel also diagonalizes T^q:

$$T^q = \frac{|\gamma_q|^2}{E - \varepsilon_q + i\Gamma_q/2}|\hat{\gamma}_q\rangle\langle\hat{\gamma}_q| \tag{8.3}$$

If we represent the TRSB measurement operator by θ_T, then the difference in total cross-sections with two different neutron helicities and a polarized nuclear target is:

$$\Delta\sigma_q = \frac{2\pi}{k^2}Im\frac{1}{E - \varepsilon_q + i\Gamma_q/2}\sum_{c,c'}\langle\gamma_{qc}|\theta_T|\gamma_{qc'}\rangle \tag{8.4}$$

where c denotes the entrance channel, and c' the channel that θ_T couples. Since θ_T is by definition Hermitian and antisymmetric, $\langle\gamma_{qc}|\theta_T|\gamma_{qc'}\rangle$ must be purely imaginary. Accordingly, we have at the $q-$th resonance,

$$\Delta\sigma_q = \frac{2\pi}{k^2}\frac{2}{\Gamma_q}\sum_{c,c'}\left[\gamma_{qc'}^*\gamma_{qc} - \gamma_{qc'}\gamma_{qc}^*\right](\theta_T)_{cc'} \tag{8.5}$$

As noted above we have $\gamma_{qc} = \gamma_{qc}^o + i\gamma_q^w$, where γ_{qc}^o is the (real) strong T-even amplitude. Thus to first order in γ^W, and defining $(\theta_T)_{cc'} = i\theta_{cc'}$ where $\theta_{cc'}$ is antisymmetric:

$$\Delta\sigma_q = \frac{2\pi}{k^2}\frac{4}{\Gamma_q}\sum_{c,c'}\left[\gamma_{qc}^w\gamma_{qc'}^o\right]\theta_{cc'} \tag{8.6}$$

For the special case of two channels, one (c_1) coupled weakly and the other (c_0) coupled strongly:

$$\Delta\sigma_q = \frac{2\pi}{k^2}\frac{4}{\Gamma_q}\gamma^w_{qc_1}\gamma^o_{qc_0} \tag{8.7}$$

The asymmetry, $P_q \equiv \frac{\Delta\sigma_q}{2\sigma_q}$ is then given by (ignoring the background contribution):

$$P_q = \frac{2\gamma^w_{qc_1}}{\gamma^o_{qc_0}} \tag{8.8}$$

Generally, P_q will have a vanishing average value because of the random nature of γ^w_{qc} , and $\gamma^o_{qc_o}$. This situation changes if a local 2p-1h doorway dominates the TRSB mixing. Just as in th PNC case, discussed extensively in the previous sections, the P_q, Eq. (3.8), will have a definite sign.

We mention here that the detailed nature of the T-violation experiment depends on the T-violating operator θ_T. Several forms may be cited. For parity non-conserving, time reversal violating, these are:

$$\theta_{TP,1} = (\vec{\sigma}\cdot\vec{q}) \tag{8.9}$$

$$\theta_{TP,2} = \left(\vec{\sigma}\times\vec{I}\right)\cdot\vec{p} \tag{8.10}$$

The time reversal violating P-even interactions are more complicated. We list these operators in terms of the unit vectors $\hat{q} = \hat{k'} - \hat{k}$, $\hat{p} = \hat{k} + \hat{k'}$ and $\hat{n} = \hat{p}\times\hat{q}$:

$$\theta_{T,1} = i\left[\vec{\sigma}\times\vec{I}\cdot\hat{n}\right] \tag{8.11}$$

$$\theta_{T,2} = i\left[\vec{\sigma}\times\vec{I}\cdot\hat{q}\right]\left(\vec{I}\cdot\hat{q}\right) \tag{8.12}$$

$$\theta_{T,3} = i\left[\vec{\sigma}\times\vec{I}\cdot\hat{p}\right]\left(\vec{I}\cdot\hat{p}\right) \tag{8.13}$$

where $\frac{\vec{\sigma}}{2}$ is the spin of the nucleon, $\vec{I}$ the spin of the target nucleus. In a neutron transmission experiment where the total cross sections are measured, only $\theta_{TP,2}$ and $\theta_{T,3}$ survive. It is clear that in order to see time reversal violation both for P-odd and P-even, we must have at least two channel spins coupled by the violating interaction. As examples we mention the transition caused by the T-odd, P-odd interaction and the transition ${}^1P_1 \rightarrow {}^3P_1$ caused by a P-even, T-odd interaction. In particular, the transition ${}^1P_1 \rightarrow {}^3S_1$ mentioned above, which could occur in the neutron scattering from a spin 1/2 nucleus, is particularly interesting as it resembles the P-odd T-even case studied in Ref. by the TRIPLE Group except for the change in channel spin. We suggest that to get a measurable P_q, Eq. (8.8), one comes in a ${}^1P_1$ state in a nucleus where the single particle P-wave strength function exhibits a minimum and comes out in a centrifugal barrier uninhibited ${}^3S_1$-state sitting at a maximum in the corresponding s-wave strength function. In the $A \simeq 180$ and 140 region one encounters such a situation [46]. The nucleus ^{130}La considered in Ref. [74] seems to be a good candidate to study TRSB.

We now turn to the case of overlapping (statistical) resonances. For this purpose we use the methods employed by Kawai, Kerman and McVoy (KKM) [22] to obtain the average fluctuation cross-section. Because of time symmetry breaking the S matrix is not symmetric, $S_{ab} \neq S_{ba}$ (Eq.(3.9)). We write $\tilde{\gamma} = \gamma^0 + \Delta\gamma$, and $\gamma = \gamma^- \Delta\gamma$

The energy averaged fluctuation cross-section is given by:

$$\langle \sigma_{ab}^{fl} \rangle = \langle S_{ab}^{fl} S_{ab}^{fl*} \rangle \tag{8.14}$$

which, with the usual random phase assumption, gives:

$$\langle \sigma_{ab}^{fl} \rangle = x_0^2 \langle \gamma_{qa}^* \tilde{\gamma}_{qb}^* \gamma_{qa} \tilde{\gamma}_{qb} \rangle_q \tag{8.15}$$

We now introduce the following quantities obtained by applying the KKM analysis [22]:

$$X = x_0\langle\gamma\gamma^*\rangle, \qquad \bar{\bar{X}} = x_0\langle\tilde{\gamma}\tilde{\gamma}^*\rangle, \qquad \bar{X} = x_0\langle\gamma\tilde{\gamma}^*\rangle, \tag{8.16}$$

In Eq. (8.16) $x_0 = \sqrt{\frac{2\pi}{\Gamma D}}$, where Γ and D are the average width and spacing of the resonance. This constant will drop out in our final expressions. The average on the RHS of Eqs. (8.15) and (8.16) is carried out over the compound nuclear states as indicated by the subscript q. In terms of this quantities, the energy average fluctuation cross section is given by:

$$\langle\sigma_{ab}^{fl}\rangle = X_{aa}\bar{\bar{X}}_{bb} + \bar{X}_{ab}\bar{X}_{ba}^{+} \tag{8.17}$$

and

$$\langle\sigma_{ab}^{fl}\rangle = \bar{\bar{X}}_{aa}X_{bb} + \bar{X}_{ba}\bar{X}_{ab}^{+} \tag{8.18}$$

As in the KKM example the above quantities can be related to the transmission coefficients which are given by the optical model:

$$\begin{aligned} T_{ab} \equiv \delta_{ab} - \left(\bar{S}\bar{S}^{+}\right)_{ab} &= \langle\left(S^{fl}S^{fl+}\right)_{ab}\rangle \\ &= XTr\bar{\bar{X}} + |\bar{X}|^2 \end{aligned} \tag{8.19}$$

where $\bar{S}$ is the optical model S matrix. In principle three other transmission coefficients can be defined:

$$\bar{\bar{T}} = \bar{\bar{X}}TrX + |\bar{X}|^2 \tag{8.20}$$

$$\bar{T} = \bar{X}Tr\bar{X}^{+} + X\bar{\bar{X}} \tag{8.21}$$

$$\bar{\bar{T}} = \bar{X}^{+}Tr\bar{X} + \bar{\bar{X}}X \tag{8.22}$$

Assuming pair correlations among the γ's and the random independence of γ^0 and $\Delta\gamma$ we find (it is assumed that the number of levels is large),

$$X = \bar{\bar{X}} = X^o + x \tag{8.23}$$

where

$$X^o_{ab} = x_0 \langle \gamma^0_{qa} \gamma^{0*}_{qb} \rangle_q, \qquad x_{ab} = x_0 \langle \Delta\gamma_{qa} \Delta\gamma^*_{qb} \rangle_q$$

We can now formulate the consequences of the above analysis. First note that according to Eq. (8.23), $\langle \sigma^{fl}_{ab} \rangle = \langle \sigma^{fl}_{ba} \rangle$. Thus it is not possible to detect time reversal symmetry breaking by comparing the energy averaged cross sections for $a \to b$ with that for $b \to a$. Detailed balance holds in the presence of symmetry breaking. An early experimental test of this was reported in [75]. Figure (23) summarizes this results for $p + {}^{27}Al \to \alpha_0 + {}^{24}Mg$. To observe symmetry breaking we have to analyze the appropriate cross-section correlation function C_{ab}:

$$C_{ab} = \frac{\langle \sigma^{fl}_{ab} \sigma^{fl}_{ba} \rangle - \langle \sigma^{fl}_{ab} \sigma^{fl}_{ab} \rangle}{\langle \sigma^{fl}_{ab} \sigma^{fl}_{ab} \rangle} \tag{8.24}$$

It can be shown using the pair correlation assumption that to first order in N, where N is the number of open channels,

$$C_{ab} = \frac{\langle \tilde{\sigma}^{fl}_{ab} \rangle^2 - \langle \bar{\sigma}^{fl}_{ab} \rangle^2}{\langle \bar{\sigma}^{fl}_{ba} \rangle^2} \tag{8.25}$$

where we have introduced the pseudofluctuation cross-section $\langle \tilde{\sigma}^{fl}_{ab} \rangle$

$$\begin{aligned} \langle \tilde{\sigma}^{fl}_{ab} \rangle &= \langle S_{ab} S^*_{ba} \rangle = \bar{X}_{aq} \bar{X}_{bb} + X_{ab} X^+_{bq} \\ &= (X^o - x)_{aa} (X^o - x)_{bb} + (X^o + x)^2_{ab} \end{aligned} \tag{8.26}$$

From Refs.[22], we know that the non-diagonal term in (8.26) is N^{-1} smaller than the first, diagonal one.

From Eq. (8.17), Eq. (8.23) and Eq. (8.26), and neglecting the non-diagonal terms ($X_{ab} = 0 = x_{ab}$), one finds, to leading order in the TRSB matrix element, the following form for C_{ab}:

$$C_{ab} \simeq -4 \frac{x_{aa} X_{bb} + X_{aa} x_{bb}}{X_{aa} X_{bb}} \quad . \tag{8.27}$$

When written in terms of the transmission coefficient, we find:

$$C_{ab} \simeq -4 \left(\frac{t_{aa}}{T^o_{aa}} + \frac{t_{bb}}{T^o_{bb}} \right) \tag{8.28}$$

where T_{aa} is the optical transmission matrix element in channel a without TRSB, and t_{aa} is just the difference $(T_{aa} - T^o_{bb})$.

Equation (8.28) clearly shows that C_{ab} depends on the channels. This is in contrast to the result of Refs. [75],[76] and [77]. In particular Ref. [77] calculated $|C_{ab}|^2 = \frac{[\langle \sigma^{fl}_{ab} \sigma^{fl}_{ba} \rangle - \langle \sigma^{fl}_{ab} \rangle^2]}{\langle \sigma^{fl}_{ab} \rangle^2}$ using the theory of random matrices and claimed that is does not depend on a and b. The reason for this is that the authors of [77] consider TRSB to be entirely in Hqq and do not consider its effect on H_{pq}. Thus, if treated as purely internal mixing, the TRSB is channel independent (in C_{ab}). In fact to first order C does not depend on the symmetry breaking as contained in H_{qq}.

The use of symmetry breaking one-body potentials to treat energy-averaged observables has already been discussed in Section VII in the case of parity non-conservation following the procedure suggested by Michel [37]. An optical model description of TRSB has been presented recently [78]. It would be profitable to calculate C_{ab}, Eq.(8.28), using one-body models of TRSB.

IX. CONCLUSIONS AND DISCUSSION

In this review we have discussed fundamental symmetry violation in nuclear reactions. The unified theory of nuclear reactions is used for the purpose. The problem of parity nonconservation in epithermal neutron scattering is discussed. The data seem to follow nicely the prediction of the statistical model except for ^{232}Th. The role of simple $2p-1h$ doorway states is poinrted out as a possible cause of the sign correlation in the longitudinal asymmetries of the n+^{232}Th system.

The optical model description of the PNC is fully developed and several observables are calculated. The optical cross-section difference $\sigma^{(+)} - \sigma^{(-)}$, where + and − refer to positive and negative helicity neutrons, is compared to the available data involving several target nuclei. In particular, we found that the data on n+^{238}U can be nicely accountewd for by the optical model calculation, while the same is not true for n+^{232}Th, where the calculation understimates the data by about two orders of magnitude. This discrepancy is attributed to shortcoming of the optical potential in this case which should contain explicit refernce to the $2p-1h$ doorways which is needed to explain the sign correlation. It would be imprtant to extend the optical modelanalysis to other systems and to establish possible general correlation between the avaergage longitudinal asymmetry and the average cross-section difference. Such a study would be useful to further elucidate the reaction dynamics involved in PNC.

Another important conclusion reached in this review concerns Time Reversal Symmetry Breaking (TRSB). It is emphasised that in studies of deviations for detailed balance, the

cross-section correlation function is channel-dependent, contrary to the findings of other authors. This conclusion warrants further theoretical scrutiny and eventually should be put to the, understandably very difficult , experimantal test. The problem of TRSB is also considered in the case of isolated resonance. Several options for observables aer available her. A short account for the fundamental theory of symmetry violation in the nucleon-nucleon system is presented.

Before ending, it is useful to hit the highlight of our conclusions and point out future directions.

1. In the analysis of the longitudinal asymmetry, $P_{|mu}$, one usually uses the expression

$$P_\mu = \sum_\nu A_{\mu\nu}\langle\mu|V^{PNC}|\nu\rangle, \tag{9.1}$$

$$A_{\mu\nu} = \frac{2}{E_\mu - E_\nu}\left(\frac{\Gamma_\nu}{\Gamma_\mu}\right)^{1/2} \equiv \frac{2}{s_{\nu\mu}}\left(\frac{\Gamma_\nu}{\Gamma_\mu}\right)^{1/2} \tag{9.2}$$

where μ and ν refer to compound nuclear levels with opposite parities. Randomness of the weak matrix element guarantees that the ensemble average of P_μ is zero. The average of P_μ^2 is calculated by considering $A_{\mu\nu}$ and $\langle\mu|V^{PNC}|\nu\rangle$ as uncorrelated

$$\langle P_\mu^2\rangle = \left(\sum_\nu A_{\mu\nu}^2\right)\langle\langle\mu|V^{PNC}|\nu\rangle^2\rangle = \sum_\nu A_{\mu\nu}^2 M^2. \tag{9.3}$$

Now the average of $\langle P_\mu^2\rangle$ over all the μ resonances gives

$$\frac{1}{N}\sum_\mu\langle P_\mu^2\rangle = \langle\sum_\nu A_{\mu\nu}^2\rangle M^2 = A^2 M^2, \tag{9.4}$$

from which M^2 is extracted since A^2 can be calculated from the known energies and widths.

We point out that A^2 can be confronted directly with the assumed random matrix ensemble that represents the compound nucleus. In fact, we can write

$$A^2 = \langle\frac{4}{s_{\nu\mu}^2}\frac{\Gamma_\nu}{\Gamma_\mu}\rangle \tag{9.5}$$

Statistically, the s and Γ distributions are independent which should allow a detailed statistical analysis of A^2 independent on the system. This should furnish another test of the statistical theory and would allow the extraction of M^2 from the data more directly.

2. The recent extended data of the TRIPLE Collaboration indicated that at about $E_n \sim 300$ eV the asymmetry becomes negative in $n+^{232}$Th. Presently a more careful analysis of these negative asymmetries in Thorium are being performed using our suggestion of looking at $\sigma_\mu^{(+)} - \sigma_\mu^{(-)}$ rather than P_μ. If confirmed, the dip of P_μ to predominantly negative values at $E_n > 30$ eV in Th, would supply a very important test of the **statistical** nature of the $2p-1h$ doorways: An average of P_μ over resonances in a **wider** energy interval may end up being zero after all even in ^{232}Th.

3. The weak spreading width deserves more investigation, especially with regards to its mass-dependence. The analysis of the TRIPLE data indicated a rather weak dependence on the mass number of the compound states. However, once A^2 is known apriori, following the proposal above, and if knowledge of $\langle \sigma_\mu^{(+)} - \sigma_\mu^{(-)} \rangle$ from the global optical model calculation reported in this review can be transformed into knowledge of cross-section variance analysis, $\langle \left(\sigma_\mu^{(+)} - \sigma_\mu^{(-)} \right)^2 \rangle$, one would be able to obtain the mass dependence of the PNC spreading width more precisely.

4. At a more fundamental level, we have found in Section VI, that the optical potential appropriate for systems that exhibit the sign correlation effect contains a PNC term which is manifestly complex. Thus we propose that analysis of epithermal neutron scattering data should be performed with a real Michel-type PNC potential added to it a doorway inspired imaginary part.

5. The r.m.s. value of the PNC matrix element extracted by the TRIPLE Collaboration

are consistent with those expected for stable nuclei. There is ongoing great effort in the field of neutron- and proton-rich nuclei. Certainly, important change may be inflicted on the strength of the weak matrix element due to the loose nature of the excess nucleons. We have calculated such a change in the case of the light halo nucleus ^{11}Be. We found that the strength of PNC mixing in the halo nucleus is almost ten times larger than in stable nuclei. A not-so-trivial fact since the instability of halo nuclei stems from the strong force and not the weak one. Our finding shows an enhanced β-decay of these nuclei which contributes further to their instability. Similar effect should be manifested in proton-rich nuclei such as ^{8}B. Further, stronger PNC admixture in the halo wave function combined with its extended range would result in an appreciable enhancement of the anapole moment, an object of great importance in the physics community.

6. The Time Reversal Symmetry Breaking is also investigated. We have found that the deviation from detailed balance symmetry can be quantitatively studied by looking at an appropriate correlation function. We found that in the overlapping resonance region this correlation function is channel-dependent contrary to the findings of other authors. This finding certainly deserves further theortical scrutiny to understand the differences cited above and warrant a careful , thogh understandably difficult, experimantal test.

We have also looked into TRSB in the case of isolated resonance. We point out that, as in PNC, one may encounter a sign correlation "problem", not necessarily in ^{232}Th.

REFERENCES

[1] E.G. Adelberger and W.C. Haxton, Annu. Rev. Nucl. Pat. Sci. 35 (1985) 50.

[2] J.D. Bowman, G.T. Garvey, M. Johnson and G.E. Mitchell, Annu. Rev. Nucl. Part. Sci. 43 (1993) 829.

[3] V.V. Flambaum and G.F. Gribakin, Prog. Part. Nucl. Phys. 35 (1996) 423.

[4] B. Desplanques, Phys. Reports 297 (1998) 1.

[5] G.E. Mitchell, J.D. Bowman and H.A. Weidenmüller, Rev. Mod. Phys. 71 (1999) 435.

[6] G.E. Mitchell et al., "Applications of Accelerators in Research and Industry" edited by J.L. Duggan and I.L. Morgan, AIP (1999) 219.

[7] C.M. et al., Phys. Rev. Lett. 67 (1991) 564: C.M. Frankle et al. Phys. Rev. C46 (1992) 778; X. Zhu et al. Phys. Rev. C46 (1992) 768.

[8] J.D. Bowman et al., Phys. Rev. C48 (1993) 116.

[9] S,L. Stephenson, Ph.D. Thesis, North Carolina State University, 1996; S.L. Stephenson, Phys. Rev. C58 (1998) 1236.

[10] B.E. Crawford, Ph.D. Thesis, Duke University, 1997; B.E. Crawford et al., Phys. Rev. C58 (1998) 1225.

[11] J.D. Bowman, L.Y. Lowie, G.E. Mitchell, E.I. Sharapov and Yi-Fen Yen, Phys. Rev. C59 (1996) 285.

[12] L.Y. Lowie et al., Phys. Rev. C59 (1999) 1331.

[13] L.Y. Lowie et al., Phys. Rev. C59 (1999) 119.

[14] E.I. Shaparov et al., Phys. Rev. C59 (1999) 1772.

[15] B.E. Crawford et al., Phys. Rev. C58 (1998) 729; B.E. Crawford et al., TRIPLE preprint (1999).

[16] D.A. Smith et al., "Parity Violation in Neutron Resonances or ^{103}Rh", TRIPLE preprint (1999); D.A. Smith et al.,"Neutron resonance spectroscopy of ^{103}Rh from 30eV to 2keV", TRIPLE preprint (1999).

[17] V.P. Alfimenkov et al., Nucl. Phys. A398 (1983) 93; O.P. Sushkov and V.V. Flambaum, Sov. Phys. Usp. 25 (1982) 1.

[18] V.V. Flambaum and O.K. Vorov, Phys. Rev. Lett 70 (1993) 4051.

[19] G.E. Mitchell and S.L. Stephenson, private communications.

[20] See, e.g., N. Auerbach and O.K. Vorov, Phys. Lett. B391 (1997) 249.

[21] H. Feshbach, Theoretical Nuclear Physics: Nuclear Reactions (John Wiley and Sons. New York, 1992).

[22] M. Kawai, A.K. Kerman and K.M. McVoy, Ann. Phys. (NY) 75 (1973) 156.

[23] H. Feshbach, A.K. Kerman and R.M. Lemmer, Ann. Phys. (NY) 41 (1967) 280.

[24] B.Block and H. Feshbach, Ann. Phys. 28 (1963) 47; A.K. Kerman, L.S. Rodberg and J.E. Young, Phys. Rev. Lett. 11 (1963) 422.

[25] See, e.g., N. Auerbach, Proceedings of the "5^{th} Conference on Intersections of Particle and Nuclear Physics", St. Petersburg, Florida, AIP, 1995, pp. 279-284.

[26] V. Spevak and N. Auerbach, Phys. Lett. B359 (1995) 254; N. Auerbach, J.D. Bowman

and V. Spevak, Phys. Rev. Lett. 74 (1995) 2638; V. Spevak, N. Auerbach and V.V. Flambaum, Phys. Rev. C56 (1997) 1357.

[27] V.V. Flambaum and V. Zelevinsky, Phys. Lett. B350 (1995) 8.

[28] Proceedings of "Parity and Time Reversal Violation in Compound Nuclear States and Related Topics", editors: N. Auerbach and J.D. Bowman (World Scientific; Singapore, 1996).

[29] M.S. Hussein, A.K. Kerman and C.-Y. Lin, Z. Phys. A351 (1995) 301.

[30] See, e.g., R. Bonetti, M. Chadwick, P.E. Hodgson, B.V. Carlson and M.S. Hussein, Phys. Rep. 202 (1991) 171.

[31] T. Ericson, Phil. Mag. Suppl. 9 (1960) 425.

[32] F. Garcia, O. Rodriguez, F. Guzman, H. Dias, M.S. Hussein and A.K. Kerman, Nucl-th/9907108. Submitted for publication in Phys. Rev. C.

[33] M. Herman and G. Reffo, Phys. Rev. C36 (1987) 1546: ibid C37 (1988) 797: F. Garcia et al., J. Phys. G19 (1993) 2165.

[34] S. Bjornholm, A. Bohr and B.R. Mottelson, Proceedings of the "Third IAEA Symposium on the Physics and Chemistry of Fission ", IAEA, Vol. I (1973) 367.

[35] A. Hayes, private communication.

[36] A. Krasznahorkay et al., Phys. Rev. Lett. 80 (1998) 2073.

[37] F.C. Michel, Phys. Rev. 133 (1964) B329.

[38] S.E. Koonin, C.W. Johnson and P. Vogel, Phys. Rev. Lett. 69 (1992) 1163.

[39] C.H. Lewenkopf and H.A. Weidenmüller, Phys. Rev. C46 (1992) 2601.

[40] B.V. Carlson and M.S. Hussein, Phys. Rev. C47 (1993) 376.

[41] B. Desplanques and S. Noguéra, Nucl. Phys. A598 (1993) 189.

[42] B.V. Carlson and M.S. Hussein, Phys. Rev. C56 (1997) 292.

[43] D.G. Madland and P.G. Young, Los Alamos Report nº LA7533-mb (1978) (unpublished).

[44] P.R. Bevington, "Data Reduction and Error Analysis for the Physical Sciences" (McGrwaw-Hill, New York 1969) pp. 66-71.

[45] B.V. Carlson, M.S. Hussein, A.K. Kerman and C.-Y. Lin, Phys. Rev. C52 (1995) R11.

[46] S.K. Mughabghab, "Neutron Cross Sections" (Academic Orlando, 1984) Vol. I.

[47] See, e.g., A.C. Hayes and I.S. Tower, Phys. Lett. B302 (1993) 157.

[48] B. Desplanques, J.F. Donoghue and B. Holstein, Ann. Phys. (NY) 124 (1980) 449.

[49] J.S. Al-Khalili, J.A. Tostevin, Phys. Rev. Lett. 76 (1996) 3903.

[50] R.C. Johnson, J.S. al-Khalili, J.A. Tostevin, Phys. Rev. Lett. 79 (1997) 2771.

[51] H. Sagawa, Phys. Lett. B286 (1992) 7.

[52] C.A. Bertulani, L.F. Canto and M.S. Hussein, Phys. Rep. 226 (1993) 281.

[53] C.A. Bertulani, L.F. Canto and M.S. Hussein, Phys. Lett. B353 (1995) 413.

[54] K. Hencken, G. Bertsch and H. Esbensen, Phys. Rev. C54 (1996) 3043.

[55] A. Mengoni, T. Otsuka, T. Nakamura, M. Ishihara, Contribution to the 4^{th} International Seminar on Interaction of Neutrons with Nuclei, Dubna (Russia), April 1996, Preprint nucl-th/9607023.

[56] J. Hardy, talk given at International Workshop on Physics of Unstable Nuclear Beams, Serra Negra, 1996 (unplublished).

[57] T. Suzuki, In Physics of Unstable Nuclear Beams, C.A. Bertulani, L.F. Canto and M.S. Hussein ed., World Scientific, Singapore, 1997, p. 157.

[58] B.A. Brown and P.G. Hansen, Phys. Lett. B381 (1996) 391.

[59] S. Karataglidis and C. Bennhold, Phys. Rev. Lett. 80 (1998) 1614.

[60] Z.Z. Ren, A. Faessler and A. Bobyk, Phys. Rev. C57 (1998) 2752.

[61] M.S. Hussein, A.F.R. de Toledo Piza, O.K. Vorov and A.K. Kerman, "Enhancement of parity violating mixing in halo nuclei and the problem of neutron weak PNC potential" (submitted to Phys. Rev. C).

[62] O.P. Sushkov and V.B. Telitsin, Phys. Rev. C48 (1993) 1069.

[63] T.T.S. Kuo, F. Krmpotic and Y. Tzeng, Phys. Rev. Lett. 78 (1997) 2708.

[64] A. Bohr and B.R. Mottelson, Nuclear Structure (Benjamin, New York, 1969), Vol. I.

[65] Ya. B. Zel'dovich, Zh. Exp. Teor. Fiz. 33 (1957) 1531 [Soviet Phys. JETP 6 (1957) 1184].

[66] W.C. Haxton, Science 275 (1997) 1753.

[67] C.S. Wood, S.C. Bennet, D. Cho, B.P. Masterson, J.L. Roberts, C.E. Tanner and C.E. Wieman, Science 275 (1997) 1759.

[68] V.V. Flambaum and L.B. Khriplovich, Zh. Eksp. Teor. Fiz. 79 (1980) 1656 [Sov. Phys. JETP 52 (1980) 835]; V.V. Flambaum and I.B. Khriplovich and O.P. Sushkov, Phys. Lett. B146 (1984) 367.

[69] J.H. Cristenson, J.W. Cronin, v.L. Fitch and R. Turlay, Phys. Rev. Lett. 13 (1964) 138.

[70] E.M. Henley and B.A. Jacobson, Phys. Rev. 113 (1959) 225.

[71] For a recent review, see: W.C. Haxton and A. Höring, Nucl. Phys. A560 (1993) 469: P. Herczeg in Proceedings on "Parity and Time Reversal Violation in Compound Nuclear States and Related Topics", Editors: N. Aurbach and J.D. Bowman (World Scientific, Singapore 1996) pp. 214-230.

[72] V.E. Bunakov, Phys. Rev. Lett. 60 (1988) 2250.

[73] V.E. Bunakov, E.D. Davis and H.A. Weidenmüller, Phys. Rev. C42 (1990) 1718.

[74] Y. Takahashi, H.M. Shimizu, T. Maekawa and T. Yabuzaki, Phys. Lett. B326 (1994) 27.

[75] E. Blanke, H. Driller, W. Glöckle, H. Genz, A. Richter and G. Schreider, Phys. Rev. Lett. 51 (1983) 355.

[76] T.E.O. Ericson, Phys. Lett. 23 (1966) 97.

[77] D. Boosé, H.L. Harney and H.A. Weidenmüller, Phys. Rev. Lett. 19 (1986) 2012: E.D. Davis and U. Hartmann, Ann. Phys. (NY) 211 (1991) 334.

[78] V. Hnizdo and C.R. Gould, Phys. Rev. C49 (1994) R612.

Figure Captions

Figure 1. The s- and p-wave neutron strength functions plotted against mass number (A) [2].

Figure 2. The TRIPLE experimental system [7-16].

Figure 3. Transmission spectra for the two helicity states near the 63-eV resonance in ^{238}U. The resonance appears as a dip in the transmission curve. Since the transmission at the resonance is significantly different for the two helicity states, the parity violation is apparent by inspection [2].

Figure 4. Parity violating asymmetries P versus neutron energy E_n for ^{232}Th [9].

Figure 5. Parity violating asymmetries P versus neutron energy E_n for ^{238}U [10].

Figure 6. The $2p-1h$ level density for ^{239}U and ^{233}Th. The Microscopic Combinatorial Method results are compared with the equidistant Ericson formula. See text and Ref.[32] for details.

Figure 7. Same as Fig.6 but with no deformation.

Figure 8. The parity distribution of levels obtained using the Microscopic Combinatorial Method [32].

Fig.9. The singlet, S_0 , and triplet, S_1, strength functions vs the mass number A, obtained with the Madland-Young optical potential.

Fig.10. The optical asymmetry calculated with the Madland-Young potential vs. the mass number at $E_n = 1\text{eV}$. The parameter ε_7 was set equal to unity. See text for details.

Figure 11. Cross-section difference for ^{232}Th resonances. See text for details.

Figure 12. Cross-section difference for ^{238}U resonances. See text for details.

Figure 13. Optical model calculation of $\Delta\sigma$ for n+^{232}Th.

Figure 14. Optical model calculation of $\Delta\sigma$ for n+^{238}U.

Fig.15. The optical model angle-independent parity conserving spin polarization and spin rotation quantities vs. E_n, for n+^{232}Th. See text for details.

Fig 16. Same as Fig.15 for parity non-conseving quantities.

Fig.17. a) Schematic plot of matter distribution in halo nuclei. The dark region corresponds to the nuclear core, the grey region shows the halo neutron cloud.

b) The spectrum of the bound states ^{11}Be.

c) Illustration of the single-particle PNC mixing in the ground state of ^{11}Be.

Fig.18. The core density distribution (logarithmic scale). The dashed line corresponds to Ref. [51], the solid line gives parametrization (7.9).

Fig. 19. The halo density in the ground state, $\rho_{2s1/2}(r) = \frac{1}{4\pi}\left(R_{2s1/2}(r)\right)^2$. The dashed line corresponds to the Hartree-Fock calculations of Ref. [51], the solid line gives parametrization (7.4),(7.12).

Fig.20. The halo density in the first excited state, $\rho_{1p1/2}(r) = \frac{1}{4\pi}\left(R_{1p1/2}(r)\right)^2$. The dashed line corresponds to the Hartree-Fock calculations of Ref. [51], the solid line gives parametrization (7.6),(7.12).

Fig.21. Plot of the radial wave functions of the states $|2s1/2\rangle$ and $|1p1/2\rangle$, $\chi_{2s1/2}(r) = rR_{2s1/2}(r)$ and $\chi_{1p1/2}(r) = rR_{1p1/2}(r)$.

Fig.22. Plot of the functions contributing to the weak PNC matrix element. The function $s(r) = \frac{d}{dr}\chi_{1p1/2}(r) + \frac{\chi_{1p1/2}(r)}{r} + \frac{d\rho_c/dr}{2\rho_c}\chi_{1p1/2}(r)$ (dot-dashed line) depends on r in the way similar to $\chi_{2s1/2}(r)$ (dashed line). The combination $\chi_{2s1/2}(r)\rho_c s(r)$ that enters the PNC matrix element in Eq.(7.8) is shown by the solid line. It contributes coherently to $\langle 2s|W_{sp}|1p\rangle$.

Figure 23. Left-hand side: Excitation function of the reaction $^{27}\mathrm{Al}(p,\alpha_0)^{24}\mathrm{Mg}$ folded with an energy spread of $\Delta E = 2\mathrm{keV}$ and a mean energy loss $t_E = 4\mathrm{keV}$ (solid curve) plotted together with the excitation function of the reaction $^{24}\mathrm{Mg}(\alpha,p_0)^{27}\mathrm{Al}$ (open circles,

not all measured points shown normmalized to the (p, α_0) excitation function. The quantities ΔE and t_E result from a computer search minimizing x^2. These fit parameters can be determined precisely because of the steep slopes left and right of the maximum. Middle part: a comparison of the forward and backward reaction cross-sections near and at a deep minimum with same procedure and normalization factor as at the maximum. Right-hand side: The region around the minimum displayed on an enlarged scale. This figure demonstrates the validity of detailed balance for the cross sections measured [75].

Table Captions

Table.I.

Relative signs of parity violations observed by the TRIPLE Collaboration. "Total number" is the number of parity-violating asymmetries observed in each nuclide; only asymmetries with statistical significance greater than three standard deviations are included. The columns labeled "positive" and "negative" are the number of asymmetries with + or − sign relative to the sign of the effect at 0.74eV in ^{139}Lu [7-16].

Table.II.

Weak spreading widths $\Gamma^{\downarrow} = 2\pi\bar{v^2}/D$ obtained by the TRIPLE Collaboration [7-16].

Table.III.

Stability analysis for the matrix element of W_{sp} between the halo states $2s_{1/2}$ and $1p_{1/2}$. The results for the values of the parameters r_0 and r_1 differing from the best values are shown. The central entry in the table corresponds to the best value. It is seen that variations in r_0 and r_1 do not affect $\langle 2s_{1/2}|W_{sp}|1p_{1/2}\rangle$ any considerably [61].

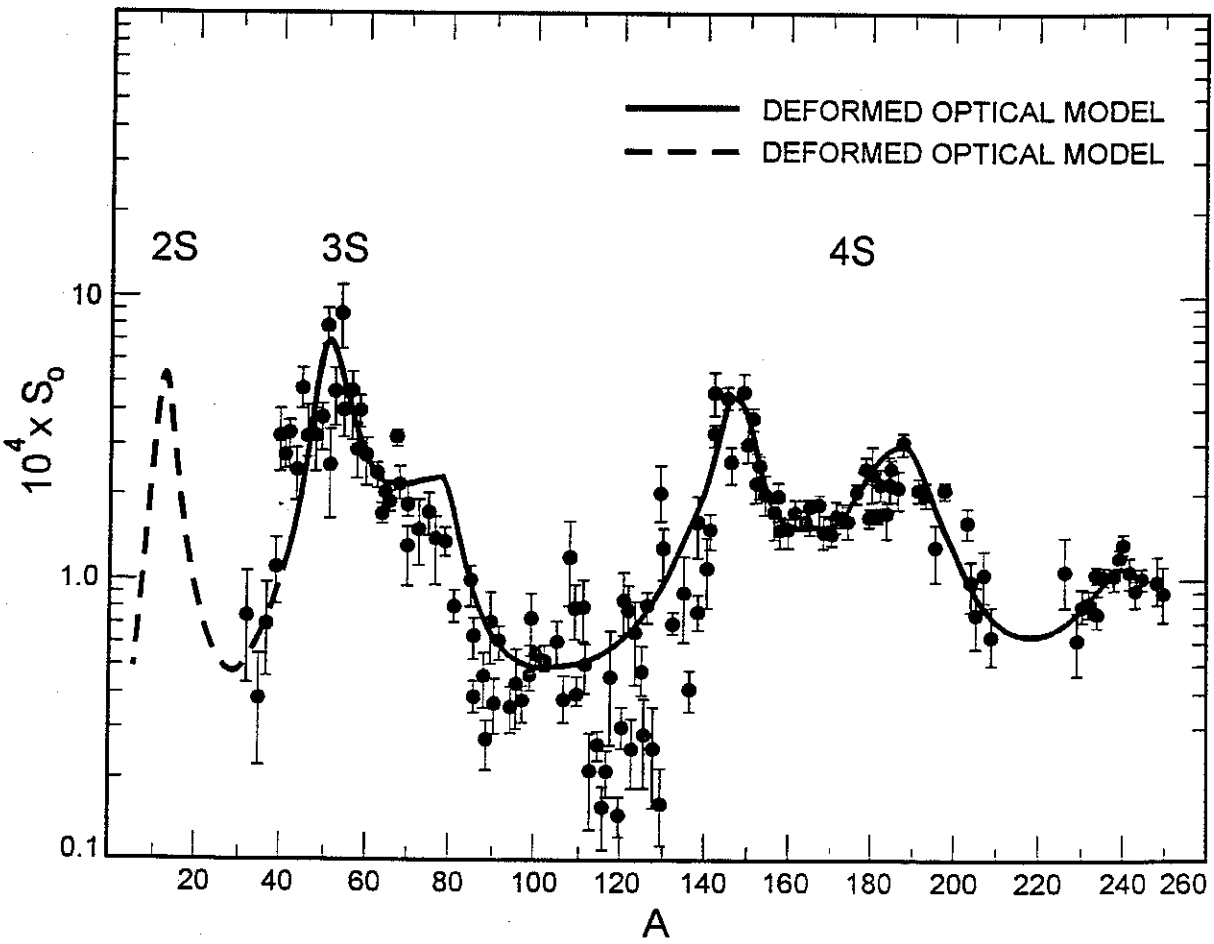
DEFORMED OPTICAL MODEL
DEFORMED OPTICAL MODEL
2S
3S
4S
10
1.0
0.1
$10^4 \times S_o$
20
40
60
80
100
120
140
160
180
200
220
240
260
A

Figure 1a

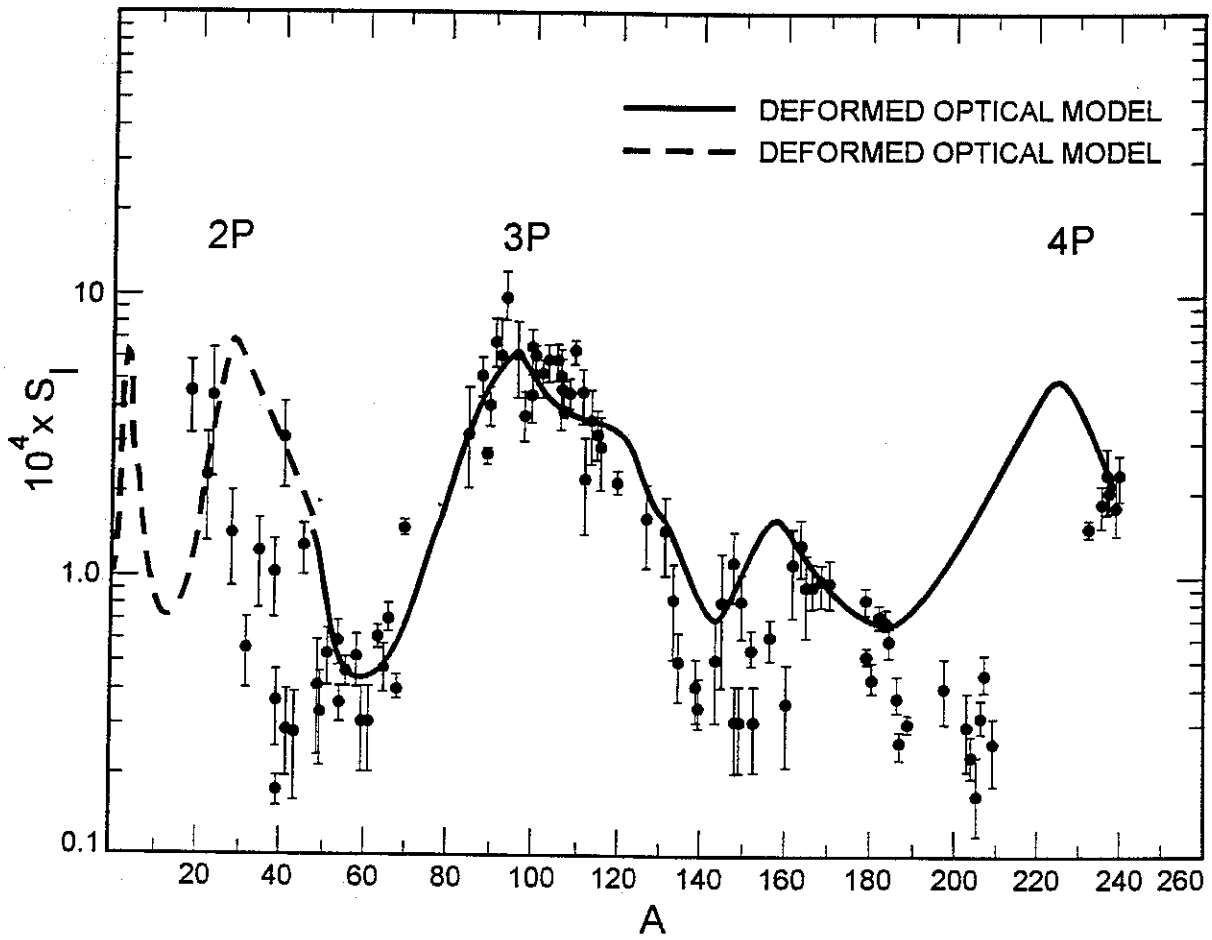
DEFORMED OPTICAL MODEL
DEFORMED OPTICAL MODEL
2P
3P
4P
10
1.0
0.1
$10^4 \times S_l$
20
40
60
80
100
120
140
160
180
200
220
240
260
A

Figure 1b

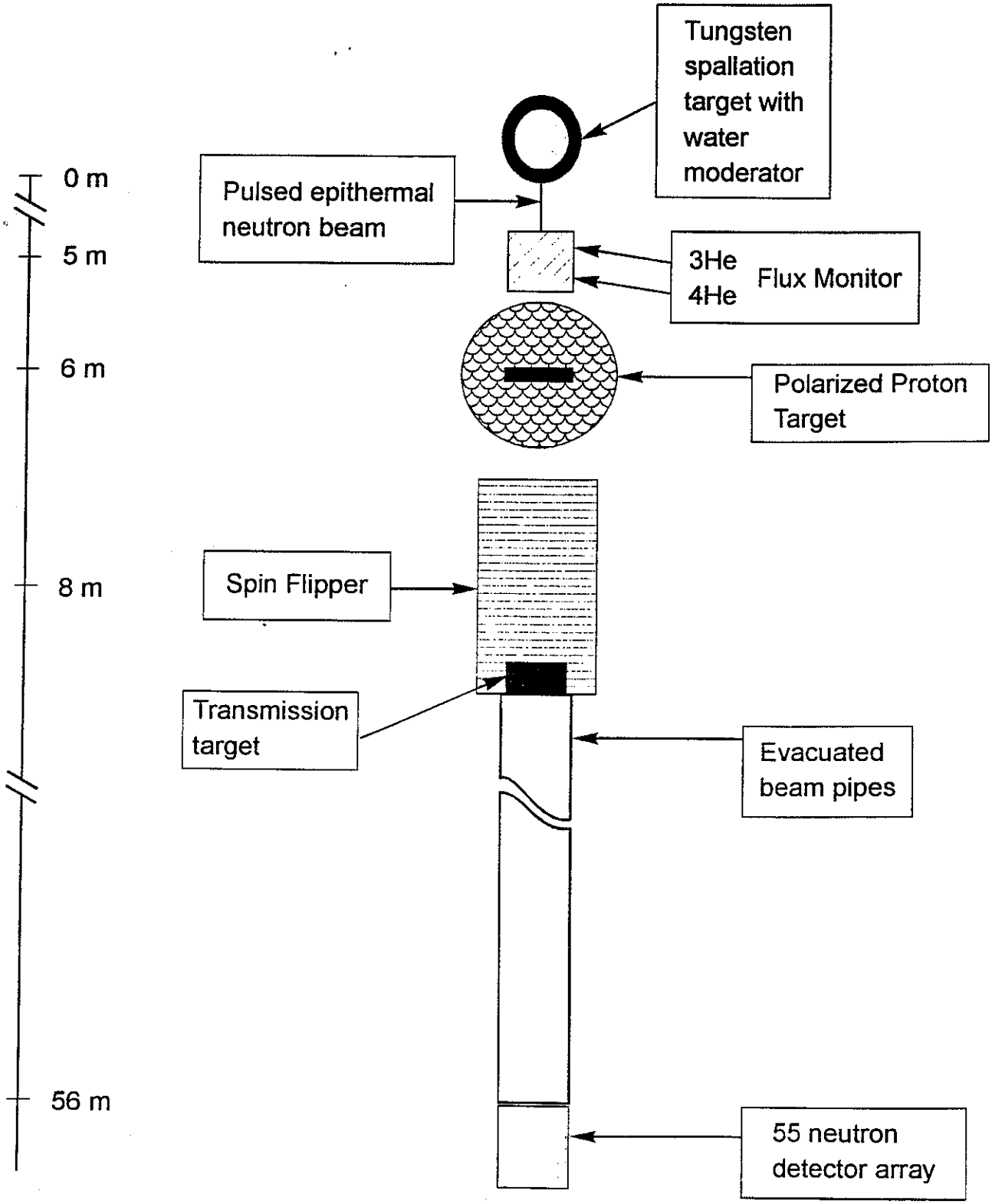
Tungsten spallation target with water moderator
Pulsed epithermal neutron beam
3He
4He
Flux Monitor
Polarized Proton Target
Spin Flipper
Transmission target
Evacuated beam pipes
55 neutron detector array
0 m
5 m
6 m
8 m
56 m

Figure 2

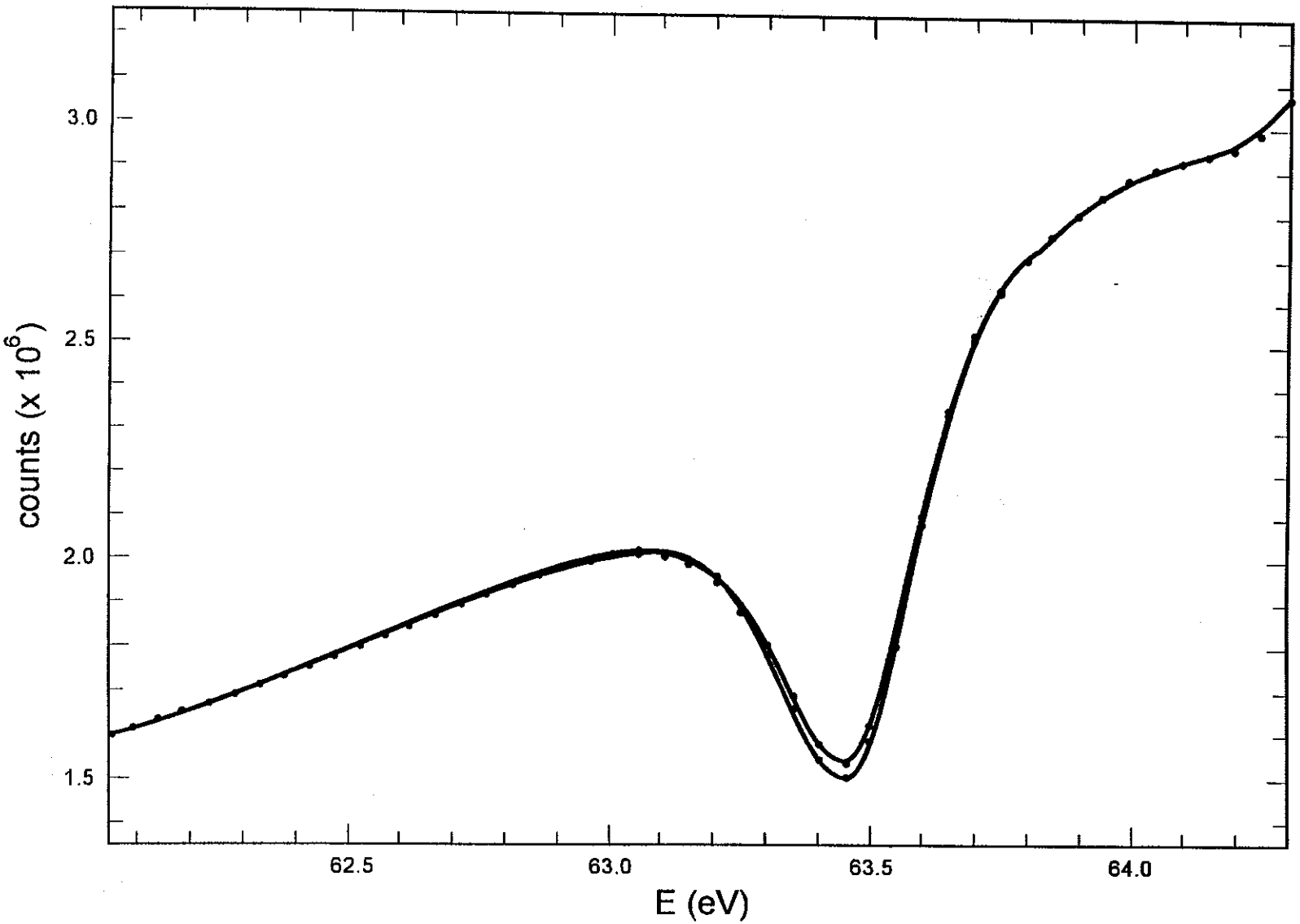

Figure 3

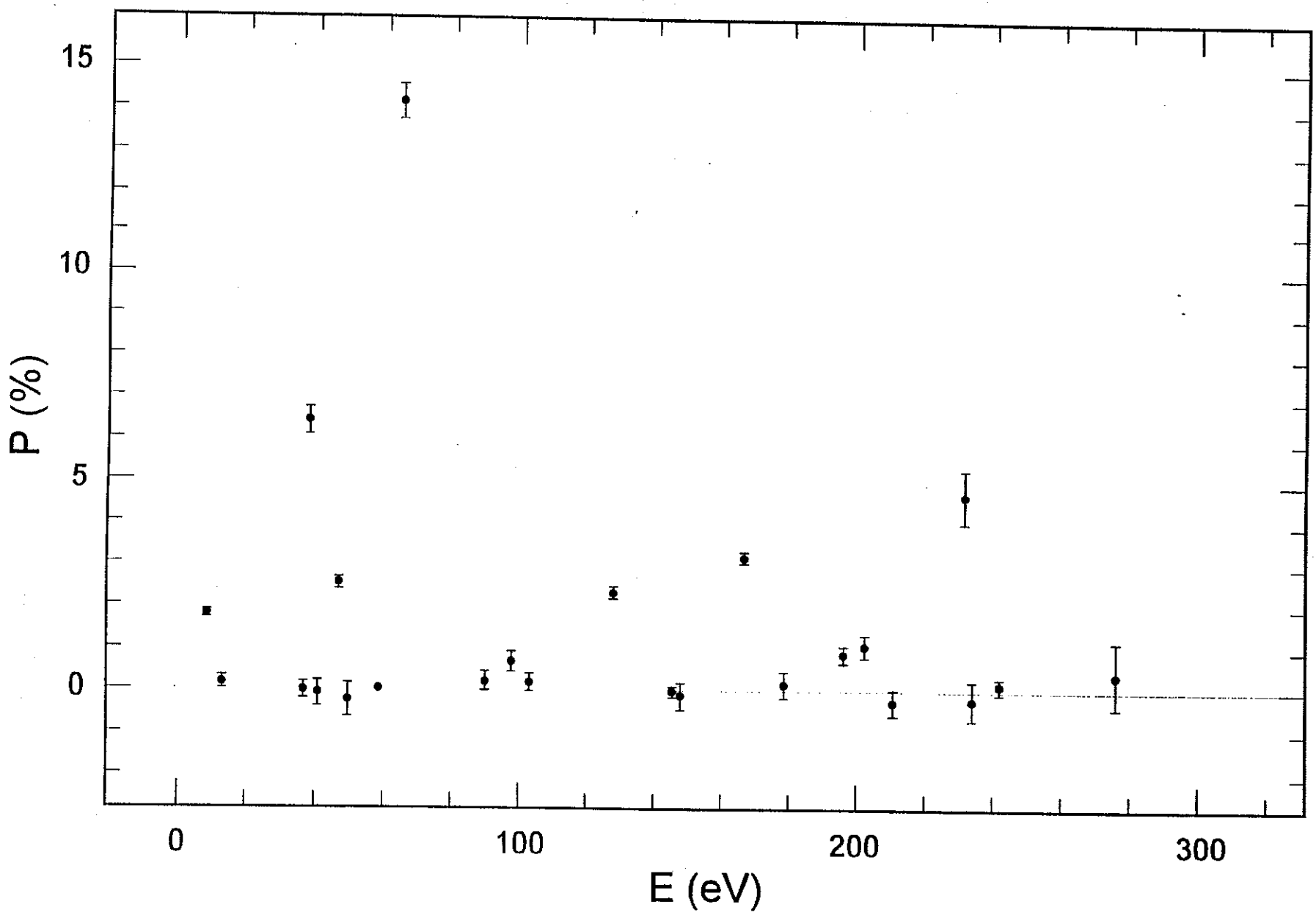

Figure 4

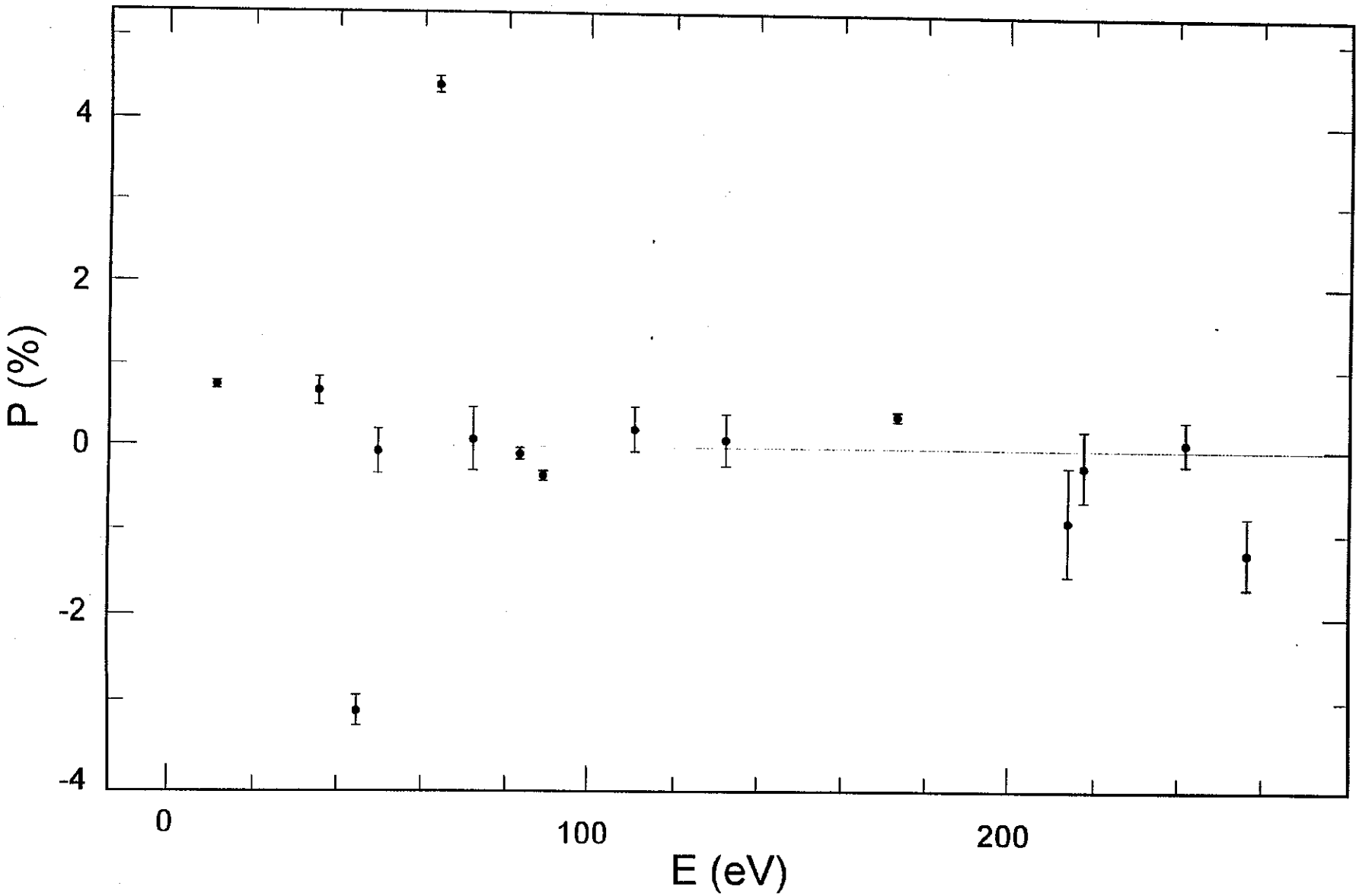

Figure 5

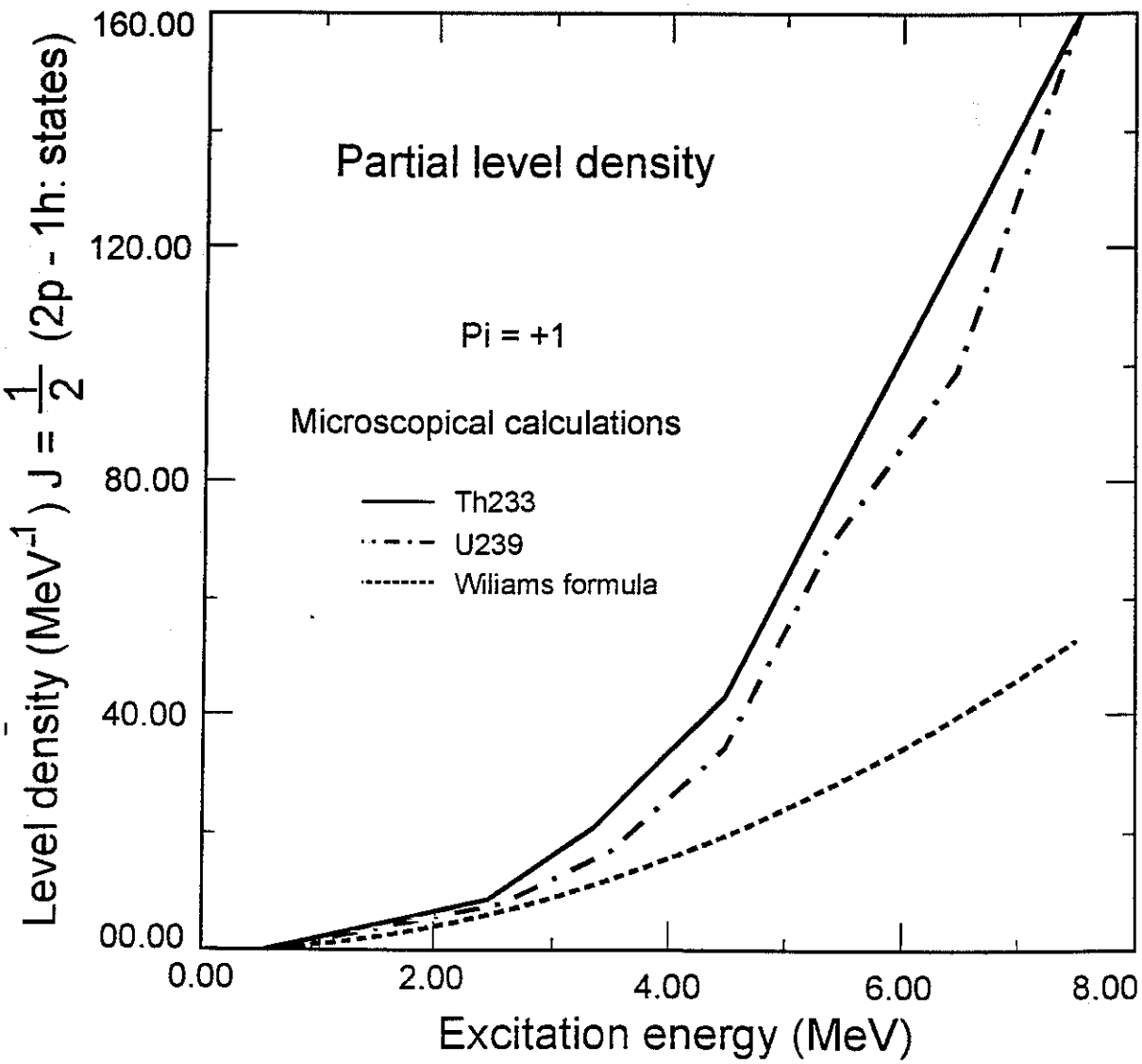
Partial level density
Pi = +1
Microscopical calculations
Th233
U239
Wiliams formula
Level density (MeV-1) J = 1/2 (2p - 1h: states)
160.00
120.00
80.00
40.00
00.00
0.00
2.00
4.00
6.00
8.00
Excitation energy (MeV)

Figure 6

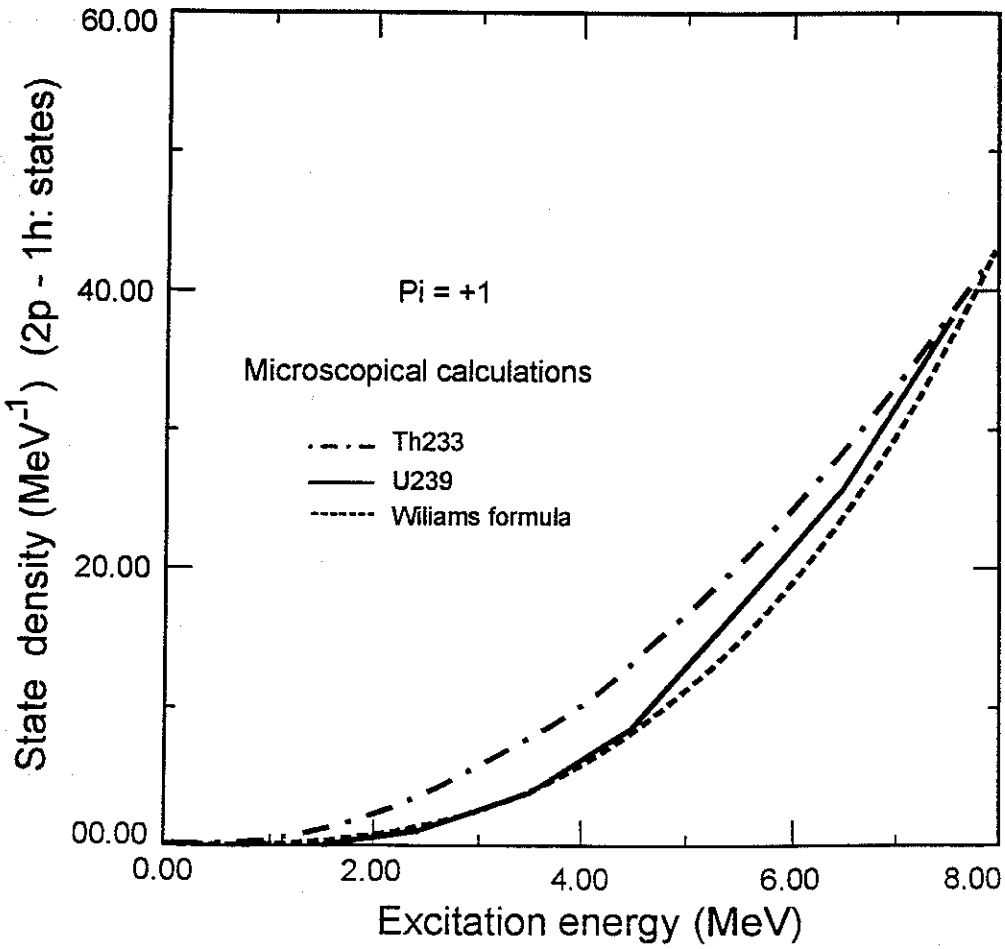
60.00
40.00
20.00
00.00
State density (MeV-1) (2p - 1h: states)
Pi = +1
Microscopical calculations
Th233
U239
Wiliams formula
0.00
2.00
4.00
6.00
8.00
Excitation energy (MeV)

Figure 7

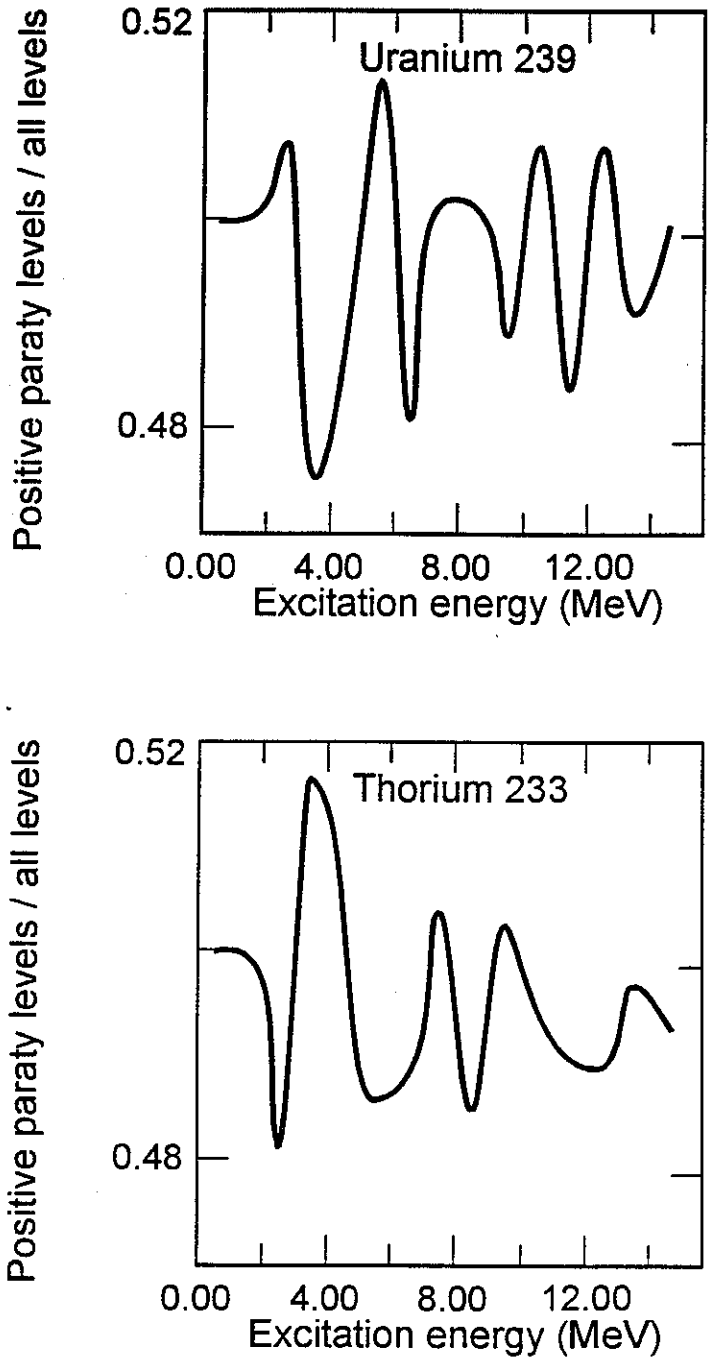
Positive paraty levels / all levels
0.52
0.48
Uranium 239
0.00
4.00
8.00
12.00
Excitation energy (MeV)
Positive paraty levels / all levels
0.52
0.48
Thorium 233
0.00
4.00
8.00
12.00
Excitation energy (MeV)

Figure 8

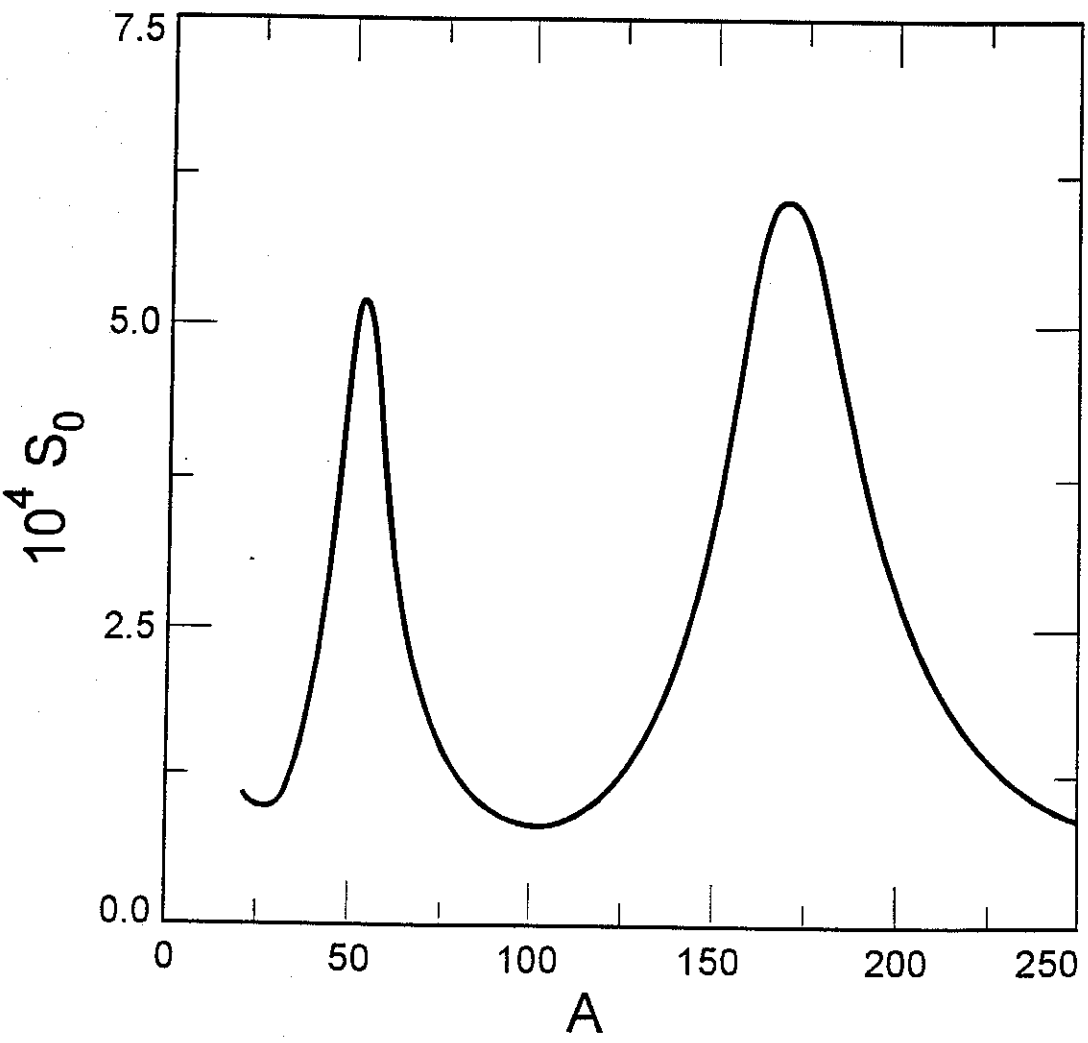

Figure 9a

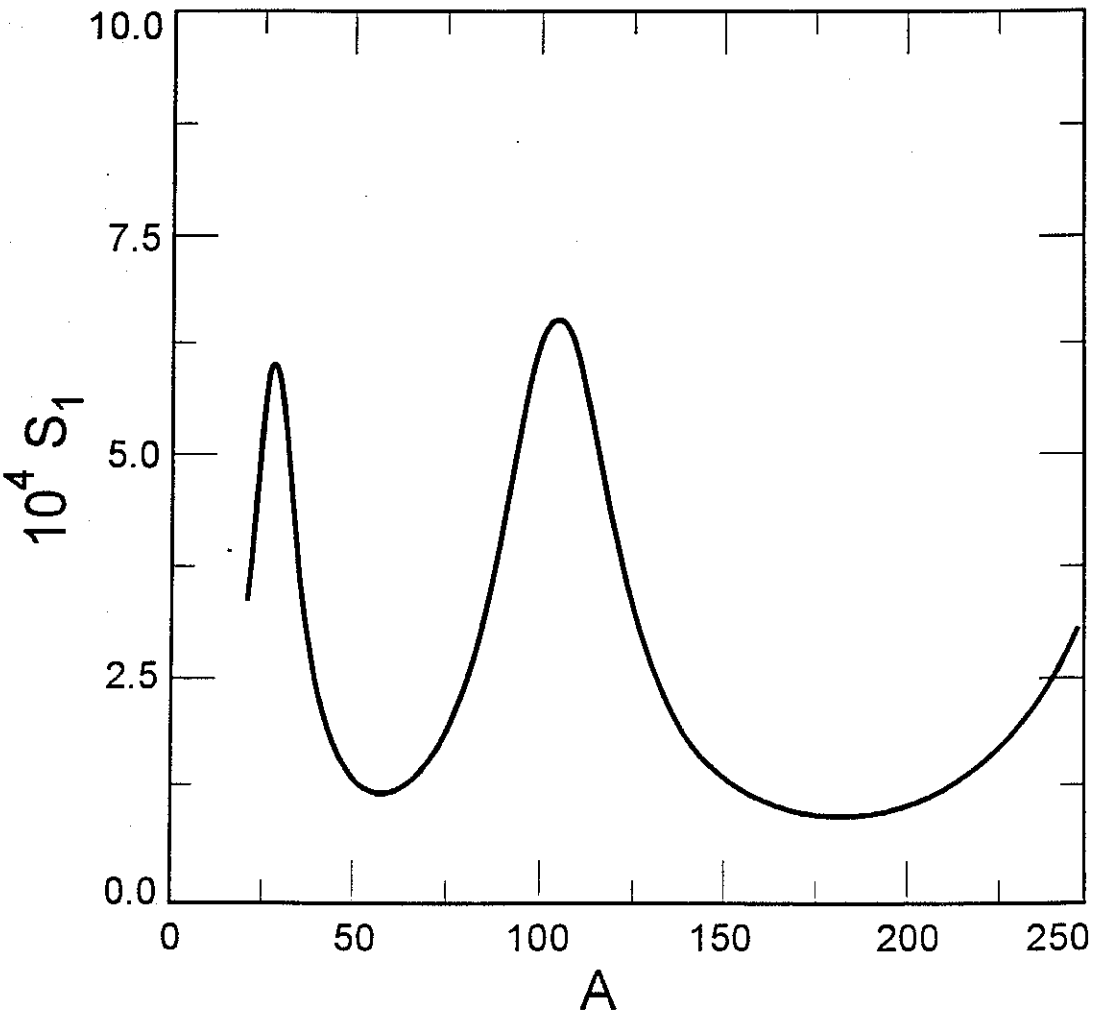

Figure 9b

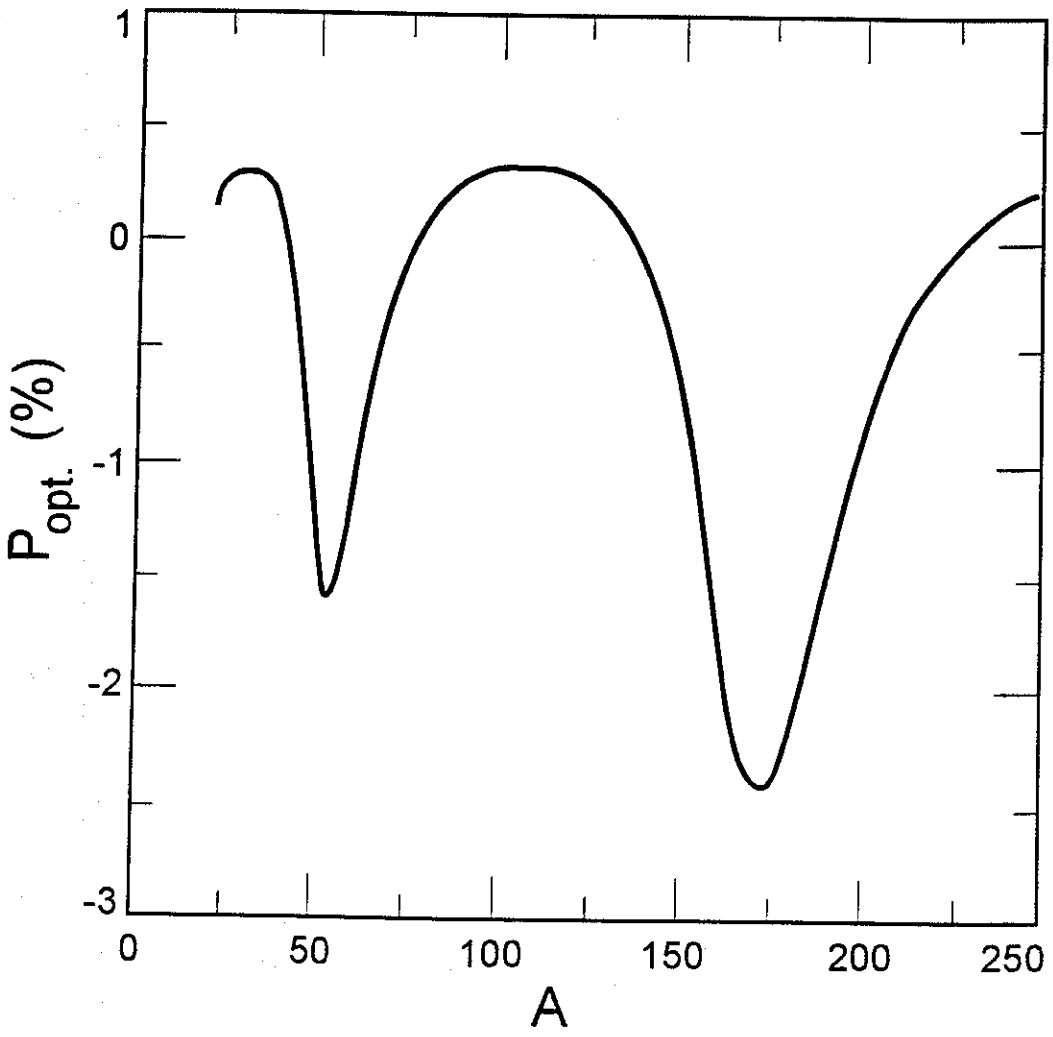

Figure 10

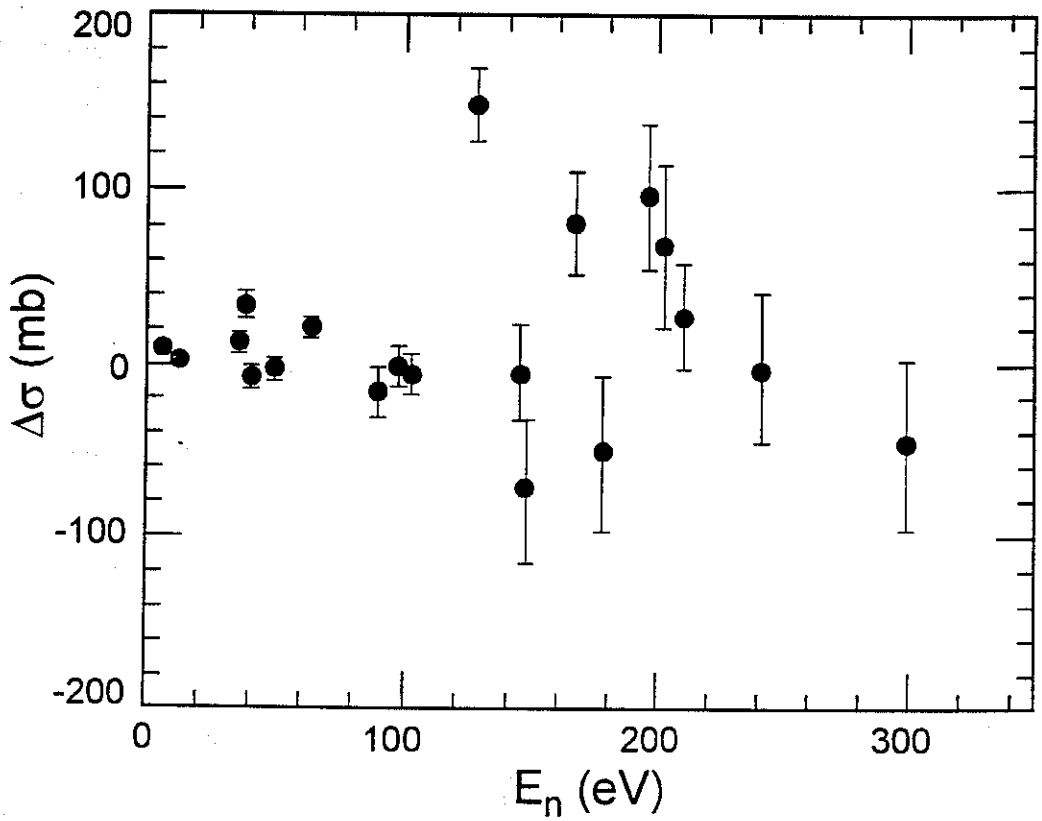

Figure 11

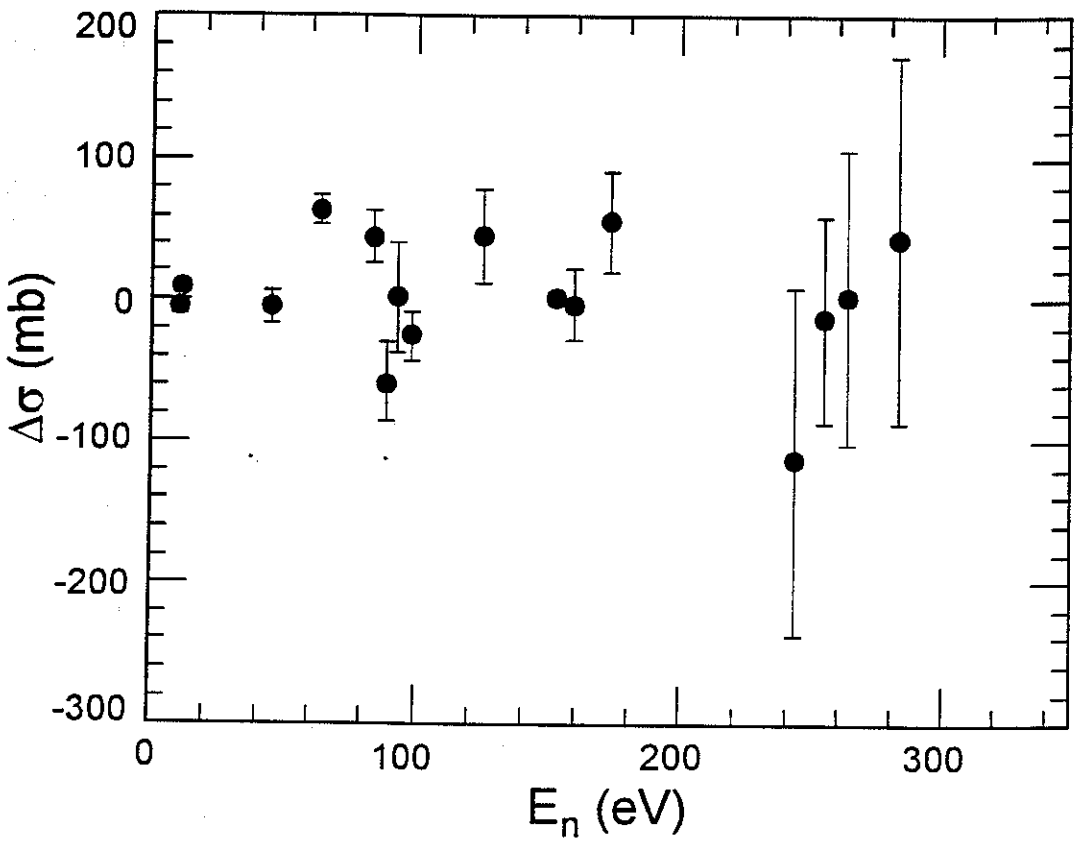

Figure 12

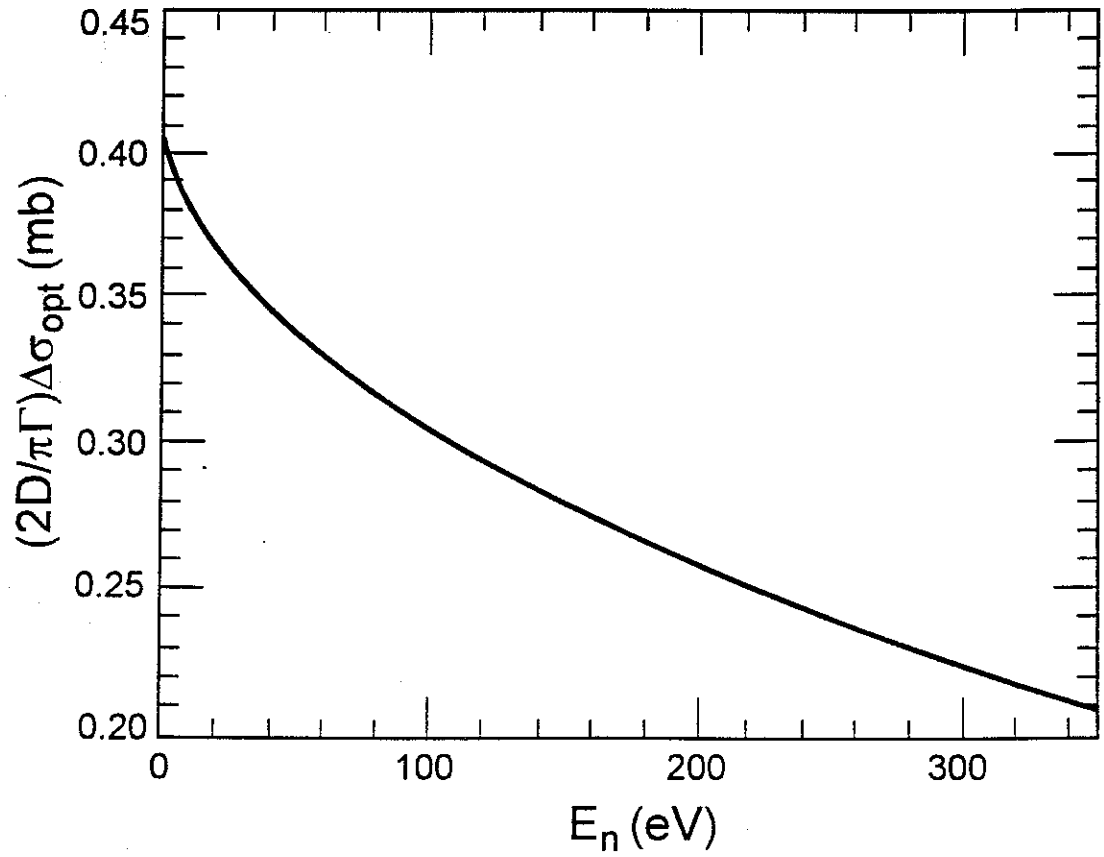
0.45
0.40
0.35
0.30
0.25
0.20
$(2D/\pi\Gamma)\Delta\sigma_{opt}$ (mb)
0
100
200
300
E_n (eV)

Figure 13

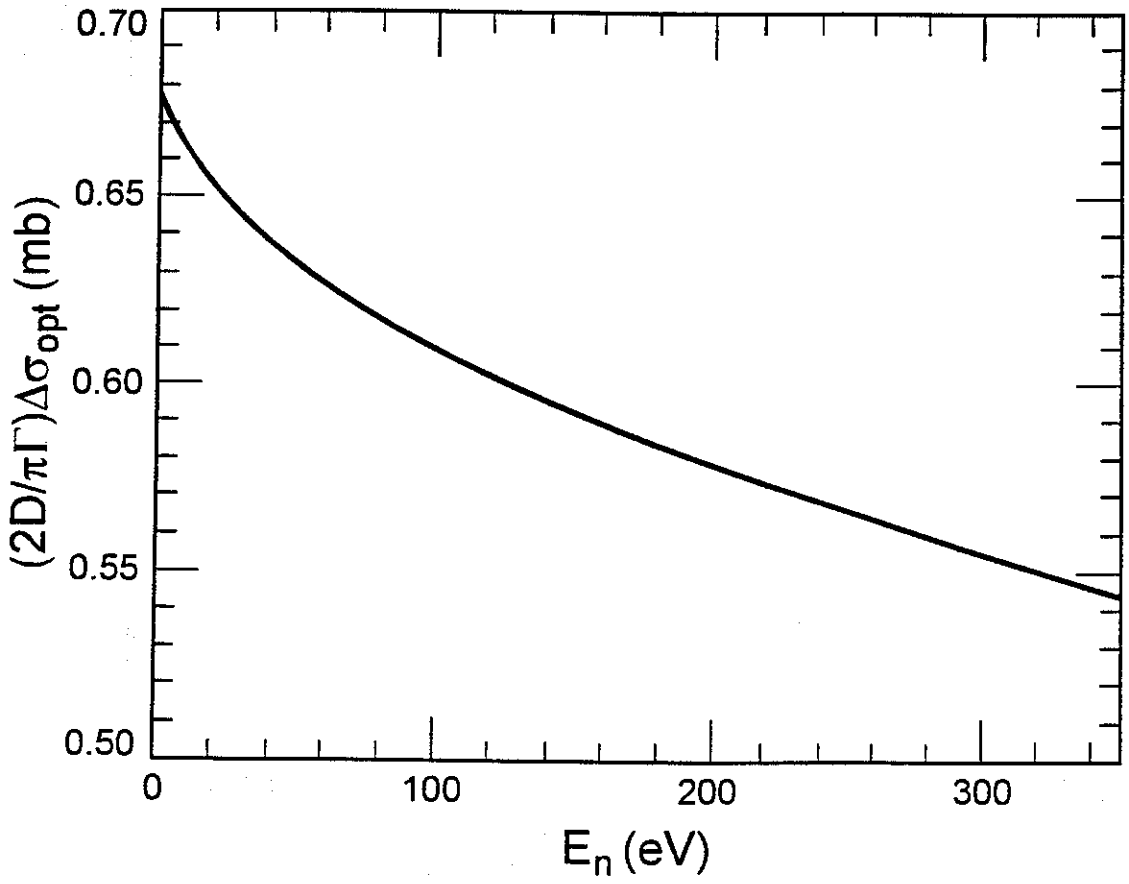
0.70
0.65
0.60
0.55
0.50
0
100
200
300
$(2D/\pi\Gamma)\Delta\sigma_{opt}$ (mb)
E_n (eV)

Figure 14

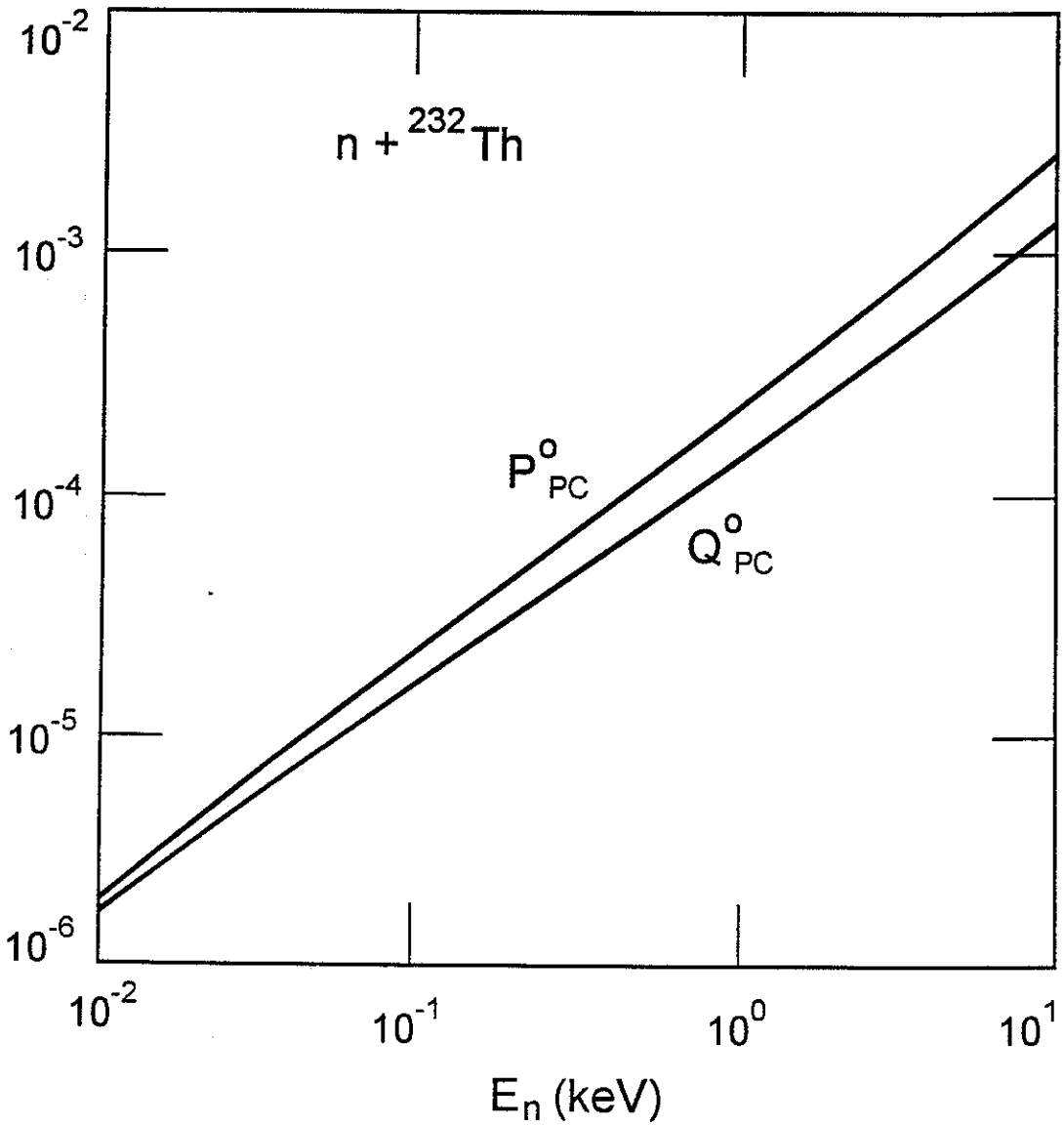

Figure 15

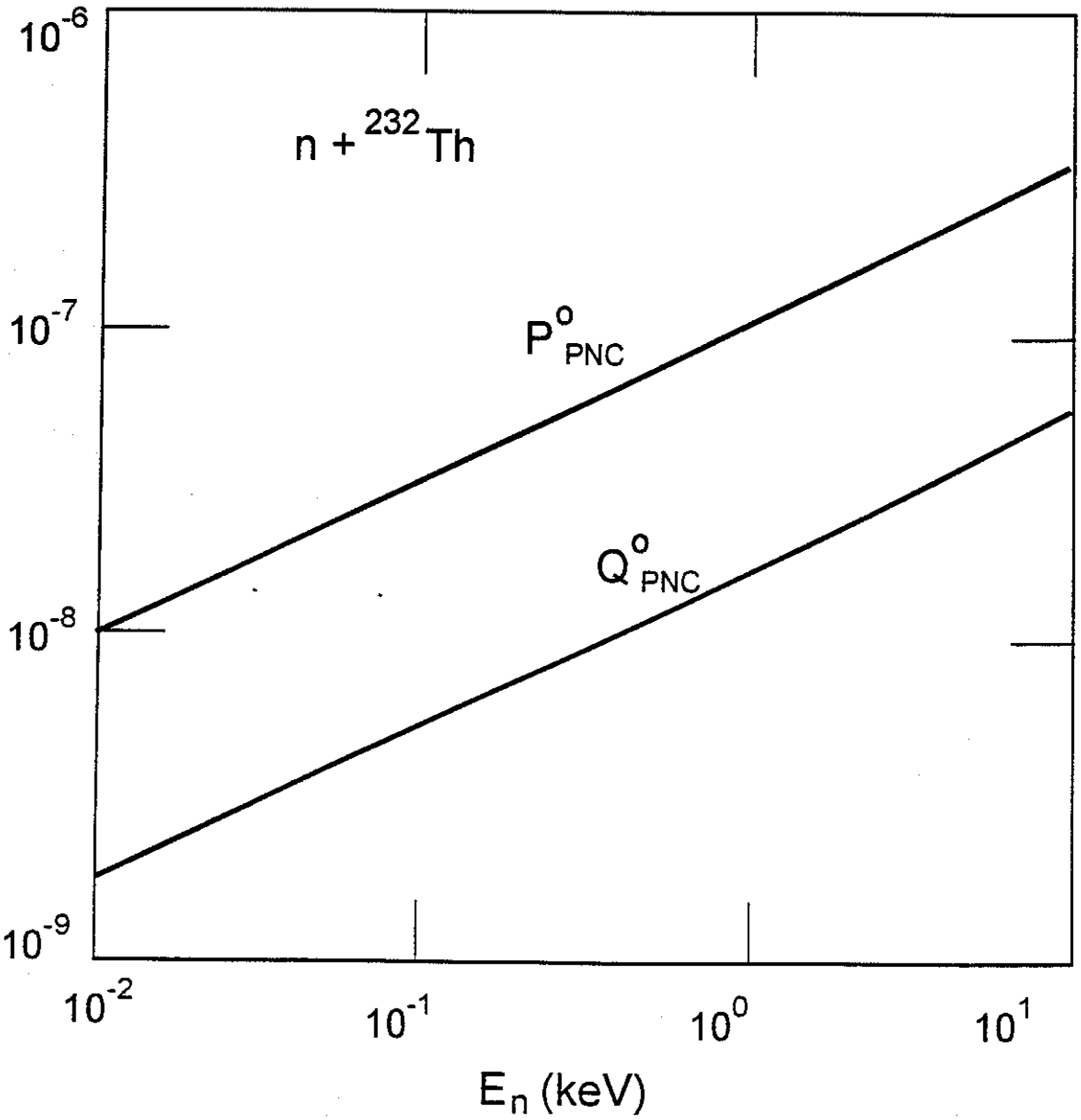

Figure 16

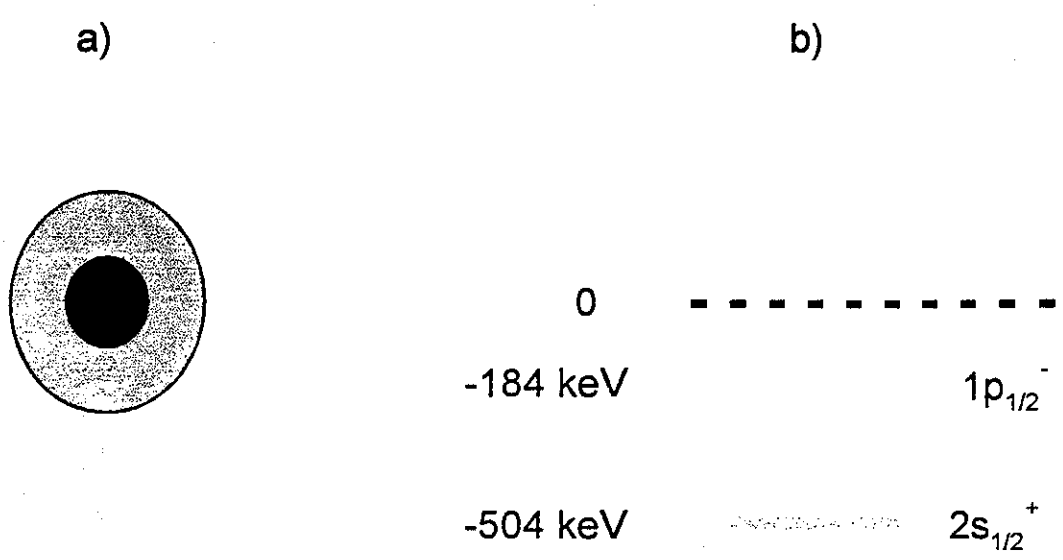

Figure 17

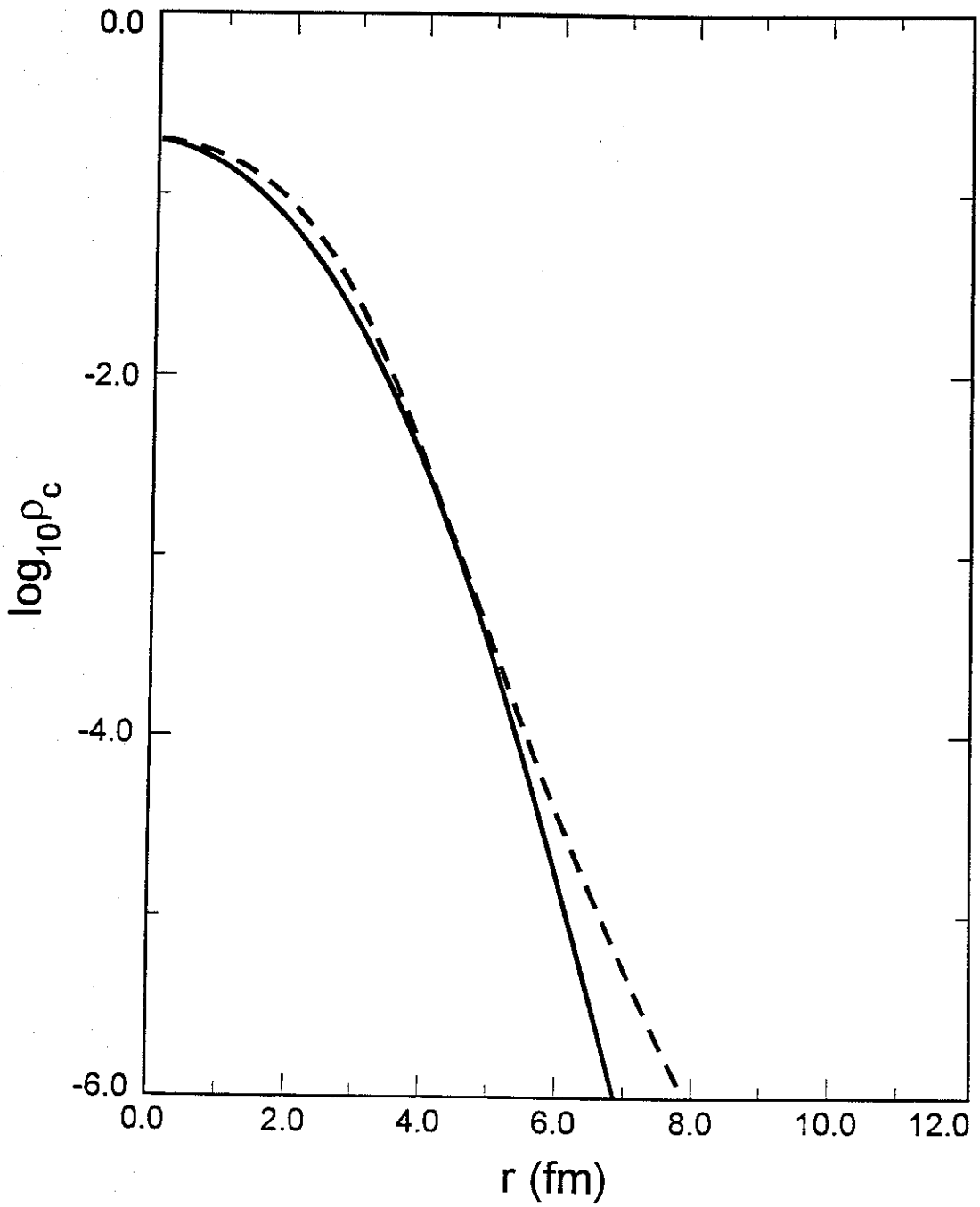

Figure 18

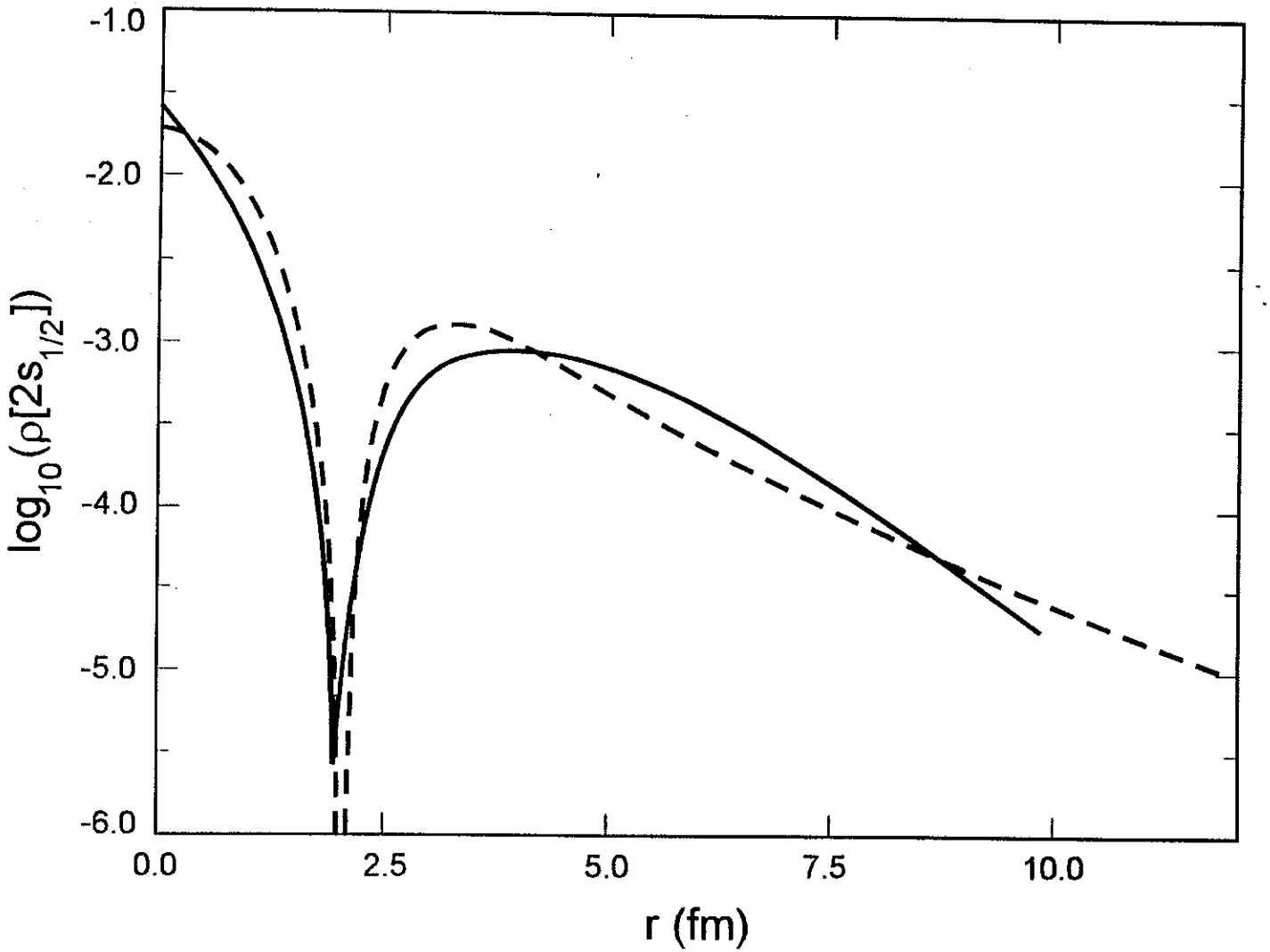

Figure 19

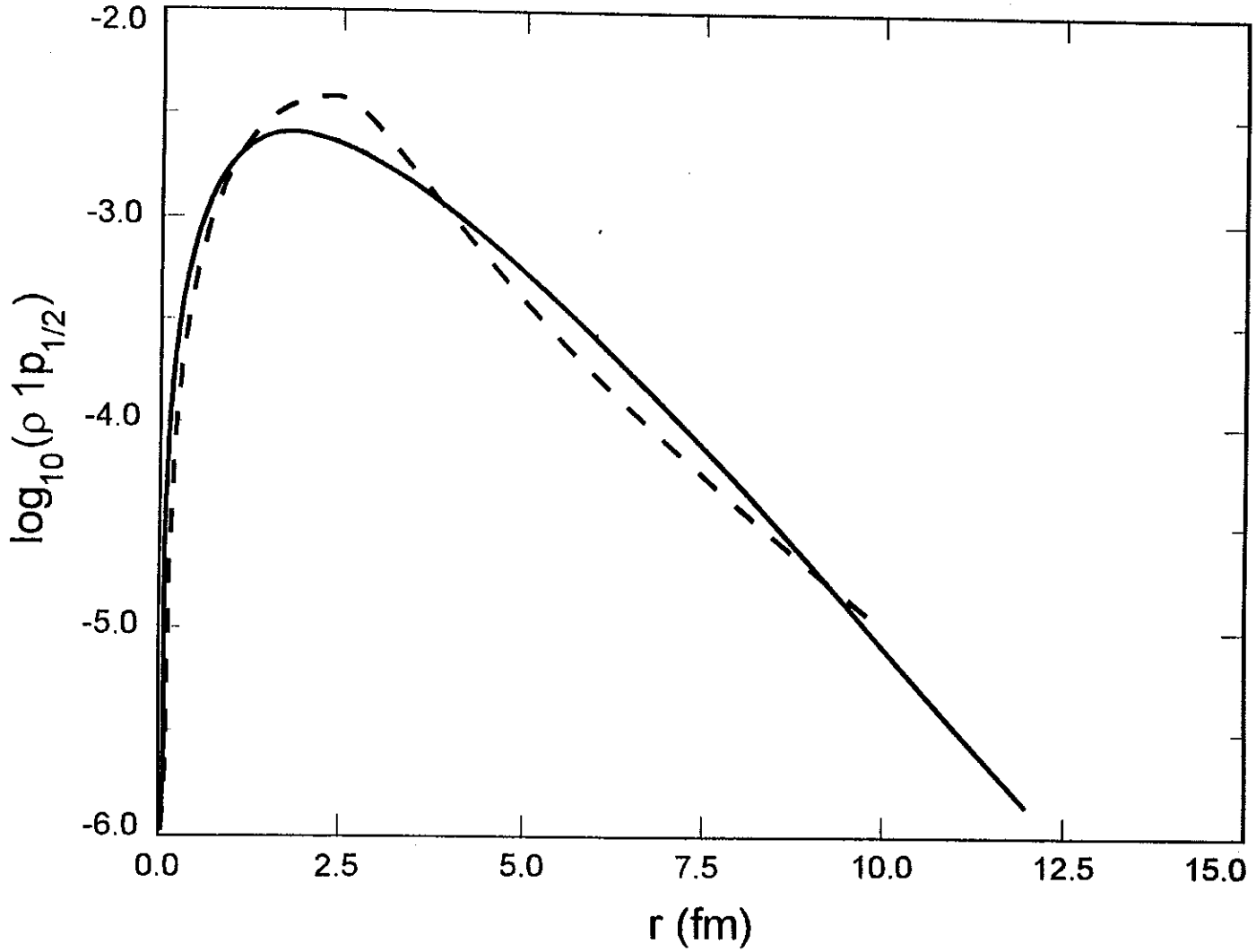

Figure 20

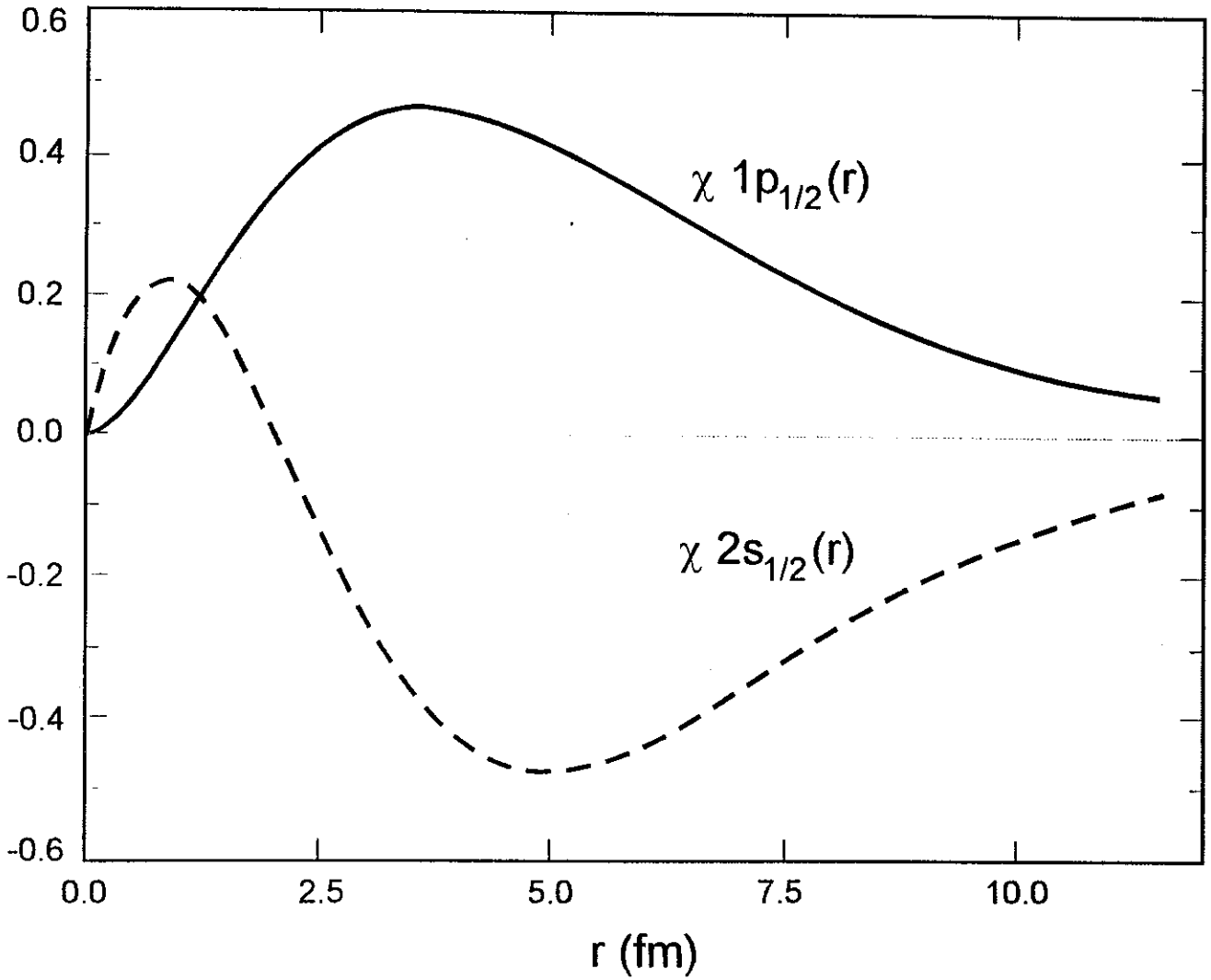

Figure 21

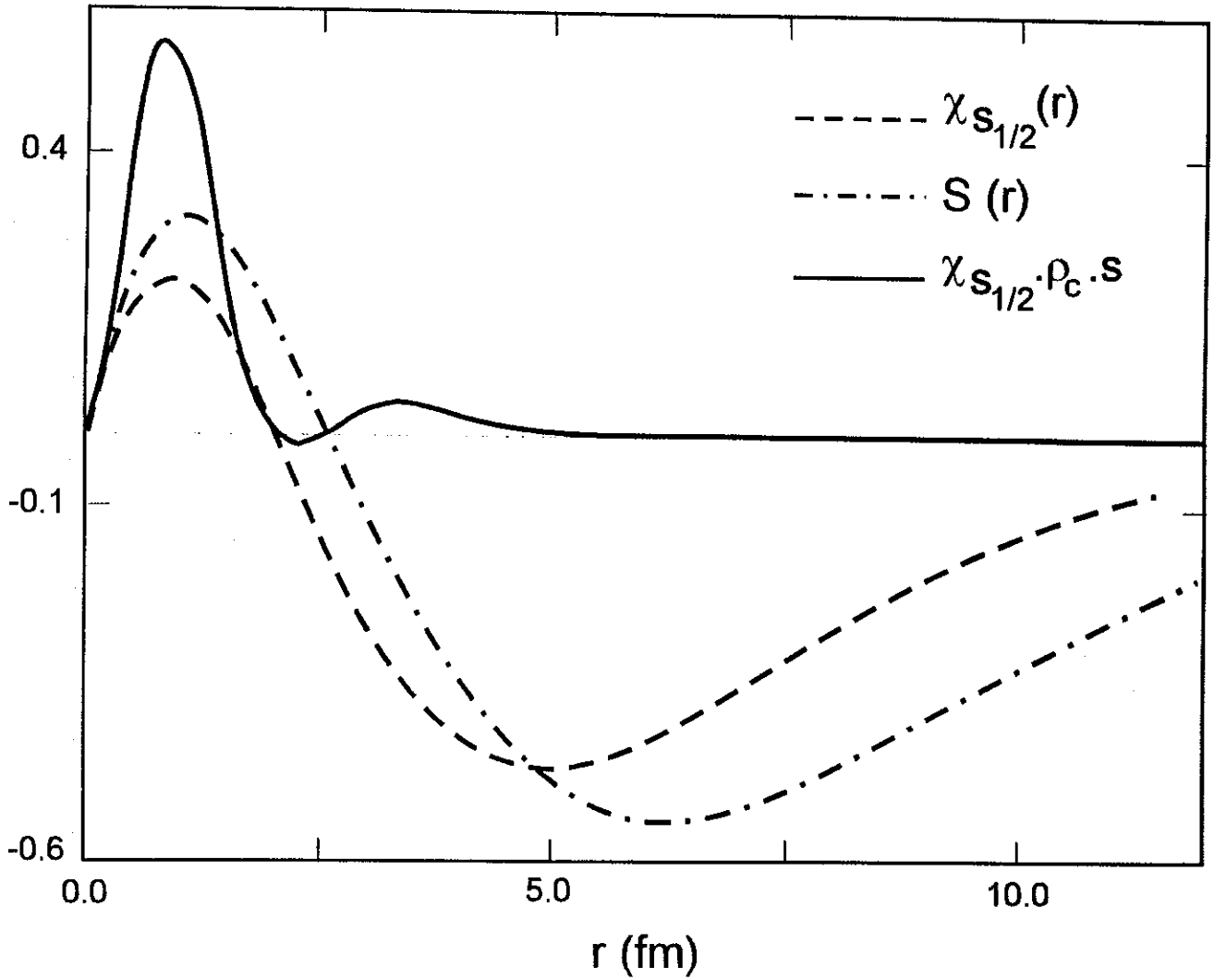

Figure 22

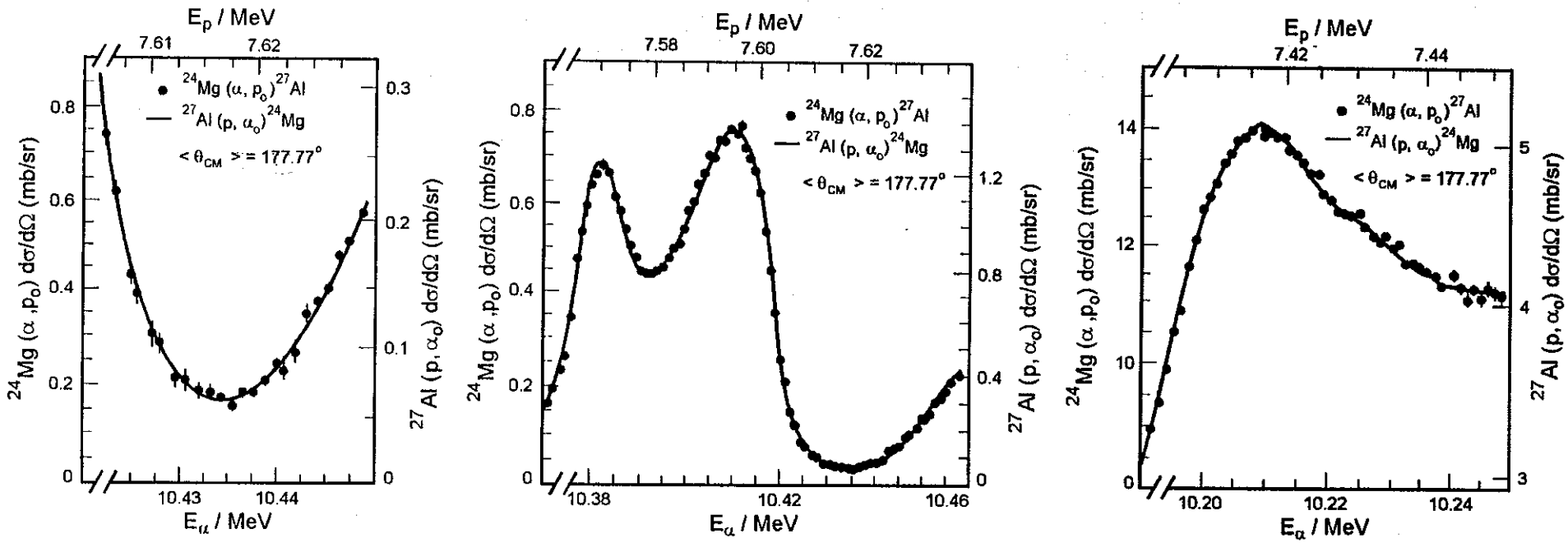
E_p / MeV
7.61
7.62
^{24}Mg (α, p$_o$)^{27}Al
^{27}Al (p, α$_o$)^{24}Mg
< θ$_{CM}$ > = 177.77°
^{24}Mg (α, p$_o$) dσ/dΩ (mb/sr)
^{27}Al (p, α$_o$) dσ/dΩ (mb/sr)
0.8
0.6
0.4
0.2
0
0.3
0.2
0.1
0
10.43
10.44
E$_α$ / MeV
E$_p$ / MeV
7.58
7.60
7.62
^{24}Mg (α, p$_o$)^{27}Al
^{27}Al (p, α$_o$)^{24}Mg
< θ$_{CM}$ > = 177.77°
^{24}Mg (α, p$_o$) dσ/dΩ (mb/sr)
^{27}Al (p, α$_o$) dσ/dΩ (mb/sr)
0.8
0.6
0.4
0.2
0
1.2
0.8
0.4
0
10.38
10.42
10.46
E$_α$ / MeV
E$_p$ / MeV
7.42
7.44
^{24}Mg (α, p$_o$)^{27}Al
^{27}Al (p, α$_o$)^{24}Mg
< θ$_{CM}$ > = 177.77°
^{24}Mg (α, p$_o$) dσ/dΩ (mb/sr)
^{27}Al (p, α$_o$) dσ/dΩ (mb/sr)
14
12
10
0
5
4
3
10.20
10.22
10.24
E$_α$ / MeV

Figure 23

TARGET	TOTAL NUMBER	POSITIVE	NEGATIVE
^{81}Br	1	1	0
^{93}Nb	0	0	0
^{103}Rh	4	3	1
^{107}Ag	8	5	3
^{109}Ag	4	2	2
^{104}Pd	1	1	0
^{105}Pd	7	4	3
^{106}Pd	1	0	1
^{108}Pd	0	0	0
^{113}Cd	3	2	1
^{115}In	6	3	3
^{117}Sn	6	3	3
^{121}Sb	5	3	2
^{123}Sb	1	0	1
^{127}I	7	5	2
^{131}Xe	1	0	1
^{133}Cs	1	1	0
^{139}La	1	1	0
^{232}Th	10	10	0
^{238}U	5	3	2

Br	C.M. Fvanble et at, Physical Review C 46, 1542 (1992)
Nb	E.I. Sharapov et al, Physical Review C 59, 1131 (1999)
Rh	D.A. Smith et al, Physical Review, to be published
Ag	L.Y. Loure et al, Physical Review C 59, 1119 (1999)
^{104,105}Pd	D.A. Smith et al, unpublished
^{106,108}Pd	B.E. Crawford et al, Physical Review, submited
^{113}Cd	S.J. Seestrom et al, Physical Review C 58, 2977 (1998)
^{115}In	L.Y.Loure et al, PhD Theis, NCSU 1996 (in progress)
^{117}Sn	D.A. Smith et al, unpublished
Sb, I	Y. Matsuda et al, PhD Thesis, Kioto 1998
Xe	J.J. Symanski et al, Physical Review C 53, R2576 (1996)
Cs	E.I. Sharapov et al. Physical Review C 59, 1772 (1999)
La	V.Y. Ynon et al, Physical Review C 44, 2187 (1991)
Th	S.L. Stephenson et al, Physical Review C 58, 1236 (1999)
U	B.E. Crawford et al, Physical Review C 58, 1225 (1998)

Table I

NUCLEUS	$\Gamma\downarrow$ (10^{-7} eV) unless noted
^{93}Nb	< 1,0
^{103}Rh	1,42 + 1,4 - 0,59
^{107}Ag	2,67 + 2,65 - 1,21
^{109}Ag	1,30 + 2,44 - 0,74
^{104}Pd	2,53 + 10,4 preliminary (very) - 1,7
^{106}Pd	3,6 + 5,1 x 10^{-6} - 2,4
^{108}Pd	< 1,2 x 10^{-6}
^{113}Cd	16,4 + 18,0 - 8,4
^{115}In	0,94 + 0,94 preliminary - 0,34
^{113}Sn	0,86 + 1,94 preliminary - 0,54
^{121}Sb	6,45 + 9,72 preliminary - 3,66
^{123}Sb	1,2 + 15,0 preliminary - 0,96
^{127}I	2,05 + 1,91 preliminary - 0,43
^{133}Cs	0,006 + 0,154 x 10^{-7} - 0,003
^{232}Th	9,7 + 2,7 - 1,8
^{238}U	1,35 + 0,97 - 0,64

Table II

	$r_0 = 1.40$	$r_0 = 1.45$	$r_0 = 1.50$
$r_1 = 1.75$	1.168	1.052	0.950
$r_1 = 1.80$	1.110	1.000	0.903
$r_1 = 1.85$	1.056	0.952	0.860

Table III